THE INFLUENCE OF STRENGTH PROPERTIES OF THE ROCK MASS ON THE SEISMIC RESPONSE AT AN ULTRA-DEEP LEVEL MINE

LOURENS JOHANNES SCHEEPERS

PROJECT REPORT FOR THE DEGREE

MSc (Applied Science)

IN THE FACULTY OF ENGINEERING, BUILT ENVIRONMENT AND INFORMATION TECHNOLOGY

DEPARTMENT OF MINING ENGINEERING

UNIVERSITY OF PRETORIA

DECEMBER 2020

ABSTRACT

Keywords: Rockburst, seismic event, seismicity, lithology, Witwatersrand Basin, closure volume, strength, stress

Rockbursts, associated with mining induced seismic events, is the biggest risk in ultra-deep level tabular hard rock mines. The high seismic response to production in these mines is a function of the high stress levels owing to the great depth below surface and the rockmass properties. Some rock types are more prone to seismic damage than other rock types. Current risk mitigation strategies are focussed on managing the stress redistribution on stope faces and mining abutments by partial extraction and controlling the maximum mining spans, placing mine-wide backfill and managing the overall mining face shapes and inter-panel lead-lag distances. Whilst these strategies can be accommodated in mine design and implementation, information regarding the rockmass properties is generally sparse, especially in terms of local variations in strength. Typically, the strata in which mining activities occur are composed of successive layers of different rock types with varying strength properties as well as geological structures. The seismic response can be expected to differ according to these different rock types and structural domains.

Mponeng Mine is the deepest mine in the world. The deepest stopes are on 127 Level at a depth of approximately 3700 m below surface. For the Ventersdorp Contact Reef (VCR) at the mine, two distinct areas based on footwall lithology can be identified. In the eastern side of the mine the footwall is shale and on the western side the footwall is quartzite. A simplified model of the shale illustrates that this layer dips at a shallow angle underneath the quartzite towards the west. The quartzite footwall is absent or starts off thin in the east and gradually increases in thickness towards the west.

In this dissertation, the seismic response to mining on the eastern side of the mine where the footwall is a siltstone (metamorphosed shale rock that is generally referred to as shale on the mine and in the rest of this document) is quantified and compared to the seismic response on the western side of the mine where the footwall is a strong quartzite. Careful data selection was done to investigate the effect of the footwall rock type on the measured seismic response to mining. The objective was that all other factors that may influence the seismic response to mining varied as little as possible between the two areas of comparison. It is shown that the seismic response to mining in the area with a shale footwall is different to the seismic

response in an area with a quartzite footwall. The number of large events is higher on the shale footwall compared to the quartzite footwall while the number of smaller events is higher on the quartzite footwall compared to the shale footwall.

By comparing the normalised seismic response to mining for the shale footwall area with the quartzite footwall area in terms of cumulative annual potency for the annual production (potency per m^2 mined), it is shown that the normalised seismic response is higher on the shale footwall than on the quartzite footwall.

Comparing the seismic hazard in terms of the b-slope of the Gutenberg-Richter (GR) graph confirms that the seismic hazard associated with mining on the shale footwall is higher than for mining on the quartzite footwall as more events in the large magnitude range can be expected in the shale footwall area. A comparison of the seismic hazard in terms of the M_{Max} from the GR graphs further supports the interpretation that the seismic hazard associated with mining on the shale footwall is higher than for mining on the quartzite footwall.

Map3D numerical modelling was used to quantify the modelled closure volume for a conceptual mining area at a depth of 3500 m below surface for two different rock strengths. Young's modulus is the elastic parameter used in Map3D to control the elastic response of the host rock. Map3D does not support the modelling of different layers of rock with different material properties and a single approximation of Young's Modulus must be used. For this preliminary modelling, the laboratory-determined Young's modulus of the quartzite footwall (77 GPa) and for the shale footwall (63 GPa) was used as input in two models where all other parameters and the mining geometry were kept constant. As expected, the simulated closure volume for the shale footwall is higher than for the quartzite footwall for the same mining geometry, providing a possible explanation for the observed seismic response. The higher seismic response associated with mining on the shale footwall is associated with the higher closure volume compared to mining on the quartzite footwall. This conclusion is supported by the traditional ERR design criterion. The computed ERR value increases for an increase in closure and this has been shown to indicate a higher risk of rockbursts. The predicted increase in closure for the shale footwall should nevertheless be confirmed by underground measurements in future research.

Moment-tensor analyses are often used to interpret the possible mechanism of a seismic

event. The isotropic component can be associated with implosion or volumetric deformation in the rockmass towards the source of the event. This is often interpreted as bursting at the skin of a mining excavation. The Compensated Linear Vector Dipole component can be associated with uniaxial deformation at the source, potentially associated with pillar failure and the Double Couple component potentially describes a planar slip mechanism where the orientation of the slip plane is also interpreted. The location of an event and the moment tensor decomposition can be used to identify the most likely source of a seismic event.

In this study it was found that the majority of the large magnitude events recorded at Mponeng Mine were face related (based on the moment-tensor analysis). This indicates shear failure through intact rock ahead of the mining front when the shear stress exceeds the shear strength of the rock. One of the factors to be considered is the fact that the virgin stress orientation (with σ_1 orthogonal to the reef plane, σ_2 in the direction of dip and σ_3 in the direction of strike) is such that it promotes fracture orientation in the direction of dip (σ_1-σ_2 plane). The orientation of the overall mining fronts (overhand and underhand) are approximately 15° from this orientation. It is possible that the similarity in the overall face orientation and the most likely fracture orientation (based on the virgin stress orientation) promotes face related seismicity. Alternative mining configurations can be considered where the overall face orientation is not similar to the orientation of the most likely fracture orientation associated with the orientation of the virgin stress field.

LIST OF ABBREVIATIONS

AGA	AngloGold Ashanti
SAR	South Africa Region
VCR	Ventersdorp Contact Reef
CFC	Chlorofluorocarbons
SAG	Semi-Autonomous Grinding
ISRM	International Society of Rock Mechanics
MPa	Mega Pascal
M_L	Magnitude on the local magnitude scale
CLVD	Compensated Linear Vector Dipole
UCS	Uniaxial Compressive Strength
MT	Moment Tensor
LSS	Loading System Stiffness
ERR	Energy Release Rate
LERR	Local Energy Release Rate
GR	Gutenberg-Richter
DC	Double Couple
ESS	Excess Shear Stress
RAW	Return Airway
ER	Extraction Ratio

TABLE OF CONTENTS

CHAPTER 1 INTRODUCTION 1

1.1 PROBLEM STATEMENT 1

1.1.1 Context of the problem 1

1.1.2 Mponeng Mine 2

1.1.3 Footwall lithology 6

1.1.4 Research gap 9

1.2 RESEARCH OBJECTIVE AND QUESTIONS 10

1.3 METHODOLOGY 12

1.4 OVERVIEW OF CHAPTERS 15

CHAPTER 2 LITERATURE STUDY 17

2.1 CHAPTER OBJECTIVES 17

2.2 THE HISTORY OF ROCKBURSTS ASSOCIATED WITH MINING 17

2.3 TERMINOLOGY USED IN ROCKBURST DISCUSSIONS 18

2.4 MOMENT TENSOR INVERSION 23

2.5 MECHANICAL PROPERTIES OF ROCK 28

2.6 MODELLING INPUT PARAMETERS 36

2.7 CLOSURE AS A DESIGN CRITERION AT MPONENG MINE 44

CHAPTER 3 DATA SELECTION FOR DIFFERENT FOOTWALL LITHOLOGIES 49

3.1 SEISIMC DATA SELECTION BASED ON THE MAGNITUDE DISTRIBUTION ASSOCIATED WITH DIFFERENT FOOTWALL LITHOLOGIES (SHALE FOOTWALL AND QUARTZITE FOOTWALL) 50

3.1.1 Seismic data selection based on appropriate magnitude range 50

3.2 SEISMIC DATA SELECTION FOR THE DIFFERENT FOOTWALL LITHOLOGIES (SHALE FOOTWALL AND QUARTZITE FOOTWALL) BASED ON SIMILARITY OF MINING DEPTH 53

3.3 SEISMIC DATA SELECTION BASED ON MODELLED ERR TO TEST FOR SIMILAR STRESS CONDITIONS 60

3.3.1 ERR modelling rationale 60

3.3.2 ERR modelling results 61

3.4 SEISMIC DATA SELECTION BASED ON CLOSURE MODELLING FOR SIMILARITY OF STRESS AND MINING SPANS 63
3.4.1 Closure modelling rationale 63
3.4.2 Closure modelling results 65
3.5 SEISIMIC DATA SELECTION: EVENT SOURCE MECHANISMS 68
3.6 SEISMIC DATA SELECTION: NORMALISED SEISMIC RESPONSE TO MINING 82

CHAPTER 4 SEISMIC DATA ANALYSIS 86
4.1.1 Analysis of magnitude distribution for the different footwall lithologies (shale footwall and quartzite footwall) 86
4.1.2 Analysis of number of events in different magnitude bins for the different footwall lithologies (shale footwall and quartzite footwall) based on similarity of mining depth 88
4.1.3 Seismic data analysis: normalised seismic response to mining 89
4.2 SEISMIC HAZARD COMPARISON BASED ON FREQUENCY MAGNITUDE GRAPHS 91
4.3 SEISMIC DATA ANALYSIS RESULTS: EVENT SOURCE MECHANISMS . 95

CHAPTER 5 DISCUSSION 99

CHAPTER 6 CONCLUSIONS 109

CHAPTER 7 RECOMENDATIONS AND FUTURE WORK 112

REFERENCES 114

APPENDICES 118
A.1 APPENDIX 1 118
DESCRIPTION OF THE SEISMIC HAZARD MANAGEMENT PRACTICE IN ANGLOGOLD ASHANTI SOUTH AFRICA REGION 118

CHAPTER 1 INTRODUCTION

1.1 PROBLEM STATEMENT

1.1.1 Context of the problem

The major hazard in the ultra-deep level mines of the Witwatersrand Basin in South Africa is rockbursts associated with the high seismic response to mining (a rockburst is loosely defined as a seismic event that causes damage to mining excavations). McGarr and Wiebols (1977) proposed that the overall seismic deformation or integrated seismicity is measured by the summation of all seismic moments of tremors in a given region and time period, that is, mining areas where the closure volume is high will experience more and larger events compared to mining areas where the closure volume is low (for similar rockmass properties).

Closure volume is proportional to stress (depth underground) and mining span; that is, a mining area at great depth (high stress) will experience a larger volume of closure (and experience more and larger events) compared to a mining area with a similar mining span and rockmass properties, but at shallow depth (lower stress). Alternatively, a mining area at similar depth and rockmass properties to another, but with increased mining span, will experience a larger closure volume (and experience more and larger seismic events) compared to a mining area with a smaller mining span.

Additional factors that may influence the seismic response include the strength, elastic modulus (stiffness) and brittleness of the rock mass as this may also impact on the closure volume and failure typical or likely mechanism of failure. Current seismic risk mitigation

strategies that are incorporated in the mine design at Mponeng Mine do not distinguish between areas with different rock mass properties.

The current seismic hazard management strategies at Mponeng Mine are based on managing the stress levels near mining excavations through partial extraction, limited mining spans and mine-wide placement of backfill. The same strategies are implemented in all the mining areas on the mine and do not take cognisance of the lithology (specifically the different footwall rock types) near the reef horizon. If it is proven that the footwall lithology impacts on the seismic response to mining, then additional seismic hazard management practices that take cognisance of the impact of the footwall lithology on the seismic response, should be implemented.

1.1.2 Mponeng Mine

Mponeng Mine of AngloGold Ashanti South Africa Region (AGA SAR) (recently sold to Harmony Gold) is situated approximately 70 km southwest of Johannesburg, near the town of Carletonville, and mines reefs associated with the Witwatersrand Basin (Figure 1). The Witwatersrand Basin comprises a sequence of interbedded argillaceous and arenaceous sediments that extend laterally for some 300 km northeast-southwest and 100 km northwest-southeast on the Kaapvaal Craton (McCarthy, 2006; AngloGold Ashanti Country Report, South Africa, 2006).

The upper portion of the basin, which contains the orebodies, outcrops at its northern extent near Johannesburg. Further west, south and east, the basin is overlain by up to 4 km of Archaean, Proterozoic and Mesozoic volcanic and sedimentary rocks. The Witwatersrand Basin is late Archaean in age and is considered to be around 2.7 to 2.8 billion years old. Gold occurs in laterally extensive quartz pebble conglomerate horizons or reefs, which are generally less than 2 m thick and are widely considered to represent laterally extensive braided fluvial deposits. Separate fan systems were developed at different entry points and these are preserved as distinct goldfields (Figure 1).

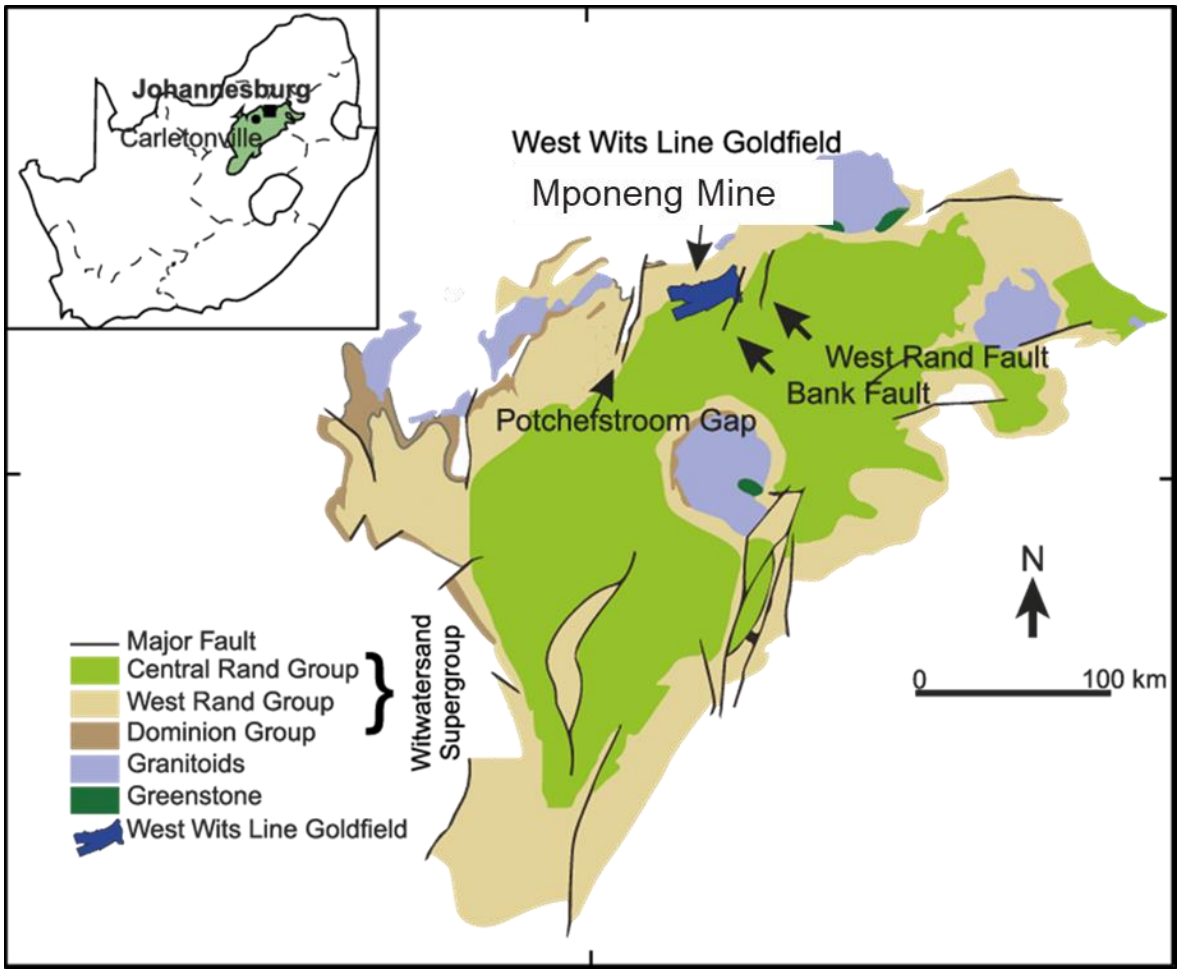

Figure 1. The Witwatersrand Basin and location of Mponeng Mine at the West Wits Line Goldfield.

Currently only one reef horizon is exploited at Mponeng Mine: the Ventersdorp Contact Reef (VCR), located at the top of the Central Rand Group and being exploited at an average mining depth in excess of 3000 m. The deepest mining is taking place on 126 Level; approximately 3700 m below surface. The structure is relatively simple with rare instances of faults with throws greater than 70 m. Regionally, the VCR dips at approximately 21°, but may vary between 5° and 50°, accompanied by changes in thickness of the conglomerate units. Where the conglomerate has the attitude of the regional dip, it tends to be thick, well-developed and accompanied by higher gold accumulations. Where the attitude departs

significantly from the regional dip, the reef is thin, varying from several centimetres to more than 3 m in thickness.

Shaft-sinking at Mponeng began in 1981 with the twin shafts commissioned along with the gold plant complex in 1986, the sub shaft followed seven years later when it was commissioned in 1993 (Mponeng Mine Key, 2011). Mining at a current depth of up to 3700 m below collar, and with infrastructure almost reaching 4000 m underground, Mponeng is the deepest operational mine in the world.

Mponeng commenced operations utilising the long wall method of mining. In 1995, a decision was taken to convert to the sequential grid method. This allows for selective mining of the VCR, with its inherently high-grade variability. Current production is approximately 14 000 m^2/month, which yields about 78 000 tonnes for milling at the plant.

The mining method implemented at Mponeng Mine is primarily sequential grid mining; that is, the development grid from where the reef is accessed, is established, and it leads the mining (refer to Figure 2). Reef raises are spaced 220 m apart. This allows for partial extraction, leaving 30 m wide regional dip stability pillars between mining blocks spanning 180 m on strike and several hundreds of metres on dip. More recently, 30 m wide strike pillars were also left in addition to the dip pillars. This is to further reduce the extraction ratio and reduce mining spans with the aim of reducing the closure volume and hence the seismic response. An active mining level will typically have development end crews that develop the haulage and RAW (return airway) pairs further east or west towards the edge of the mining operation to establish access to new ground. From the haulage, crosscuts are developed (south in the case of Mponeng Mine) to intersect the reef horizon. From the crosscut-reef intersection, a raise is developed on reef to establish the on-reef access. The raise typically holes into the raise of the level above (raises are aligned to form a raiseline). The raise is ledged on reef to establish the stoping section. The stoping can commence when the raise is fully ledged. In a sequential grid mine one will typically find the current raise line in an advanced extraction stage approaching the designed stopping position (dip pillar position) with spans nearing the maximum. The next raise line further away from the shaft

location will be fully ledged with stoping operations in a beginning phase and mining spans still small. The next raise line will be in the ledging phase, with the next line still being raised and at the last (planned) raise line, the crosscut will be in the process of being developed.

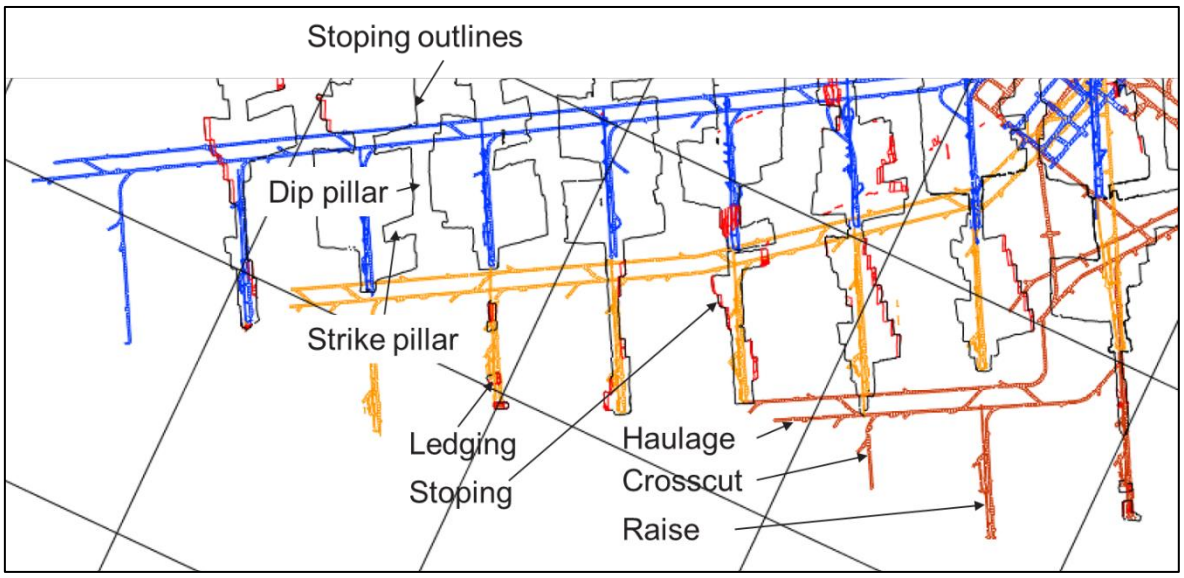

Figure 2. A typical sequential grid layout in a small portion of the mine. The coloured lines are the development grid tunnels developed ahead of the stoping operations.

Owing to the mining depth (currently in excess of 3500 m), the stress levels in the mine are high and mining related seismicity (and the associated potential for rockburst damage) is the biggest risk at the mine. Careful mine design with the aim of managing the seismic hazard is required to ensure safe mining. Over the years a number of seismic hazard management strategies have been included in the mine design strategy for Mponeng Mine (McGill, 2007). Most of these strategies aim at reducing excess shear stress on the seismically active geological structures and minimising volumetric closure in the stopes. The current seismic risk management strategies are:

- Partial extraction with low extraction ratio (ER < 60 %)
- Sequential grid mining with limited mining spans (180 m maximum on strike)
- Large regional stability pillars (30 m minimum width) on dip and strike (Tanton et al., 1984; Handley et al., 1997)

- Bracket pillars on major geological structures (20 m wide both sides of the structure) (Napier, 1987)
- Overhand face configuration with controlled lead/lag (7 m to 10 m)
- 35° approach angle onto minor structures to be mined through
- Preconditioning (face-perpendicular) (Blake, 1984; Toper, 2007)
- good local face shape
- Mine-wide backfill (classified tailings > 70% area filled), to reduce convergence (Gay et al., 1988, Spottiswoode and Churcher, 1988)
- Rockburst-resistant support (pre-stressed yielding elongates in stopes) (Wagner, 1984; Roberts, 1999, Stacey and Ortlepp, 2007)

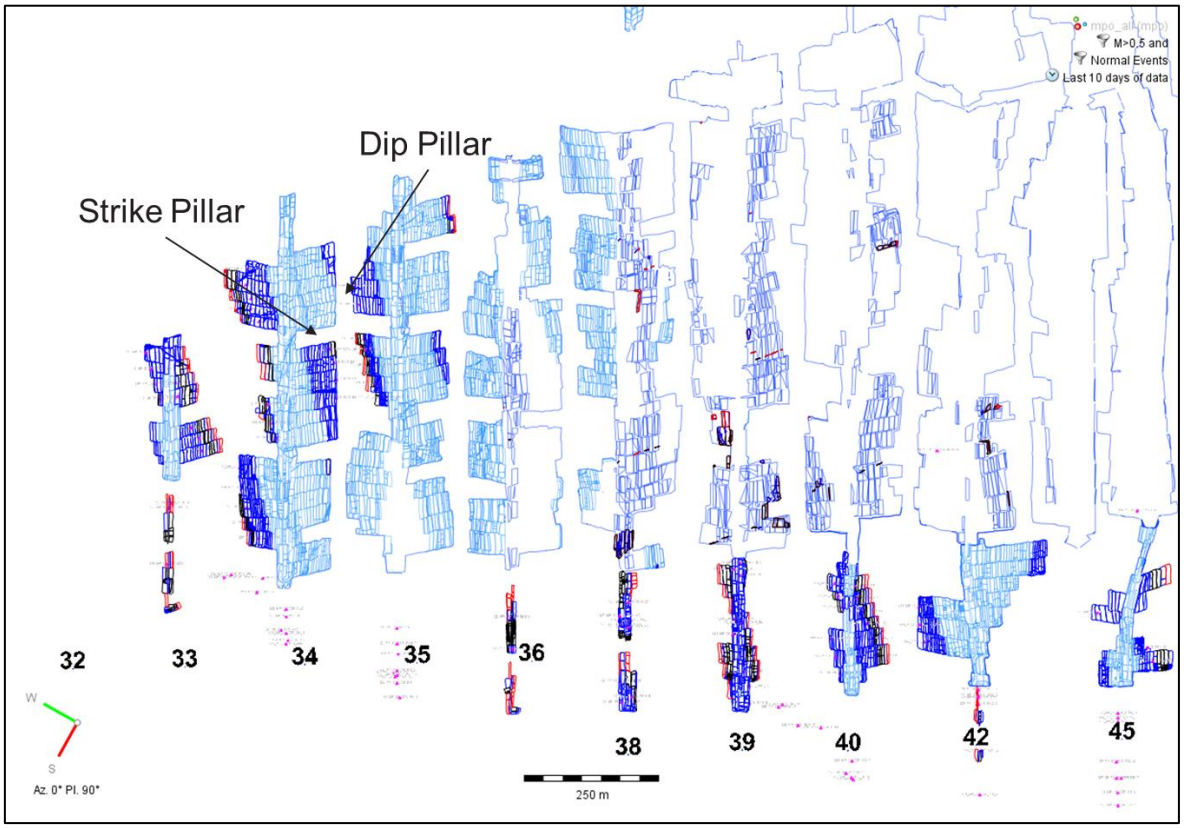

Figure 3. Rotated plan view of the western side of Mponeng Mine to show partial extraction and examples of dip and strike pillars.

1.1.3 Footwall lithology

The near-reef lithology associated with the current mining at Mponeng Mine on the VCR is described as a thick strong lava hangingwall, conglomerate reef, and either shale or quartzite footwall. On the western side of the mine the footwall is quartzite of the Elsburg series. On the eastern side of the mine the footwall is a thick shale of the Booysens series. This shale at Mponeng Mine must not be confused with the weak and soft shale associated with some of the reefs in the Welkom area. The shale at Mponeng Mine is a siltstone that is of shale origin, but metamorphosed to relatively high strength and is a brittle rock. The strength of the shale ranges between 155 MPa and 195 MPa (UCS) with an average of 173MPa. This is significantly lower than the strength of the quartzite that range between 160 MPa and 332 MPa with an average of 252 MPa (Mponeng rock strength database). This is an important consideration in this study as the influence of the footwall lithology on the seismic response to mining is investigated; i.e. the seismic response to mining on the shale footwall is compared to the seismic response to mining on the quartzite footwall (for similar mining depth, span and geometry) to confirm the influence of rock mass properties associated with the footwall lithology on the seismic response.

In Figure 4, a plan of the footwall lithology transition lines is overlain with the Mponeng mining outlines. The Booysens zone refers to the Booysens shale that forms the direct footwall to the VCR in that area. All the other zones refer to quartzite as the direct footwall to the VCR. In Figure 5, a simplified section view of a model of the footwall lithology associated with the VCR is shown to further clarify the identification of mining areas on the shale footwall and mining areas on the quartzite footwall.

It is clear that only the far eastern zone of mining on Mponeng Mine is in the area with the shale footwall. To the far west, the footwall is thick quartzite (and then shale followed by quartzite again). The thickness of quartzite in the footwall gradually increase from east to west. A zone can be identified where the quartzite in the footwall is thin, followed by the shale layer. This can be interpreted as the transition zone where the seismic response may be influenced by both the shale and the quartzite footwall. In this study, the seismic response in the area with thick shale footwall is compared with the seismic response in the area with thick quartzite footwall, therefor the data from the transition zone is not used or discussed

further in this dissertation. It is clear that a section to the far east can be chosen to represent the mining area with a shale footwall and to the far west to represent the mining area with a quartzite footwall.

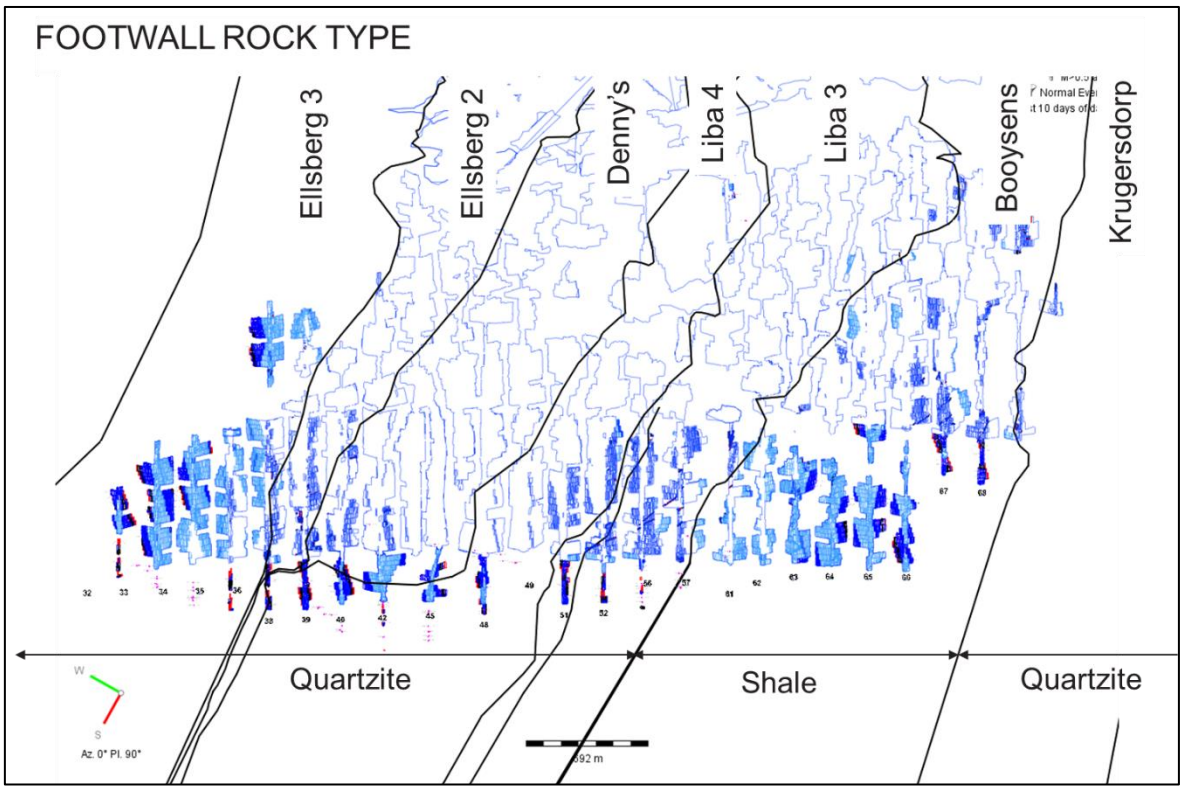

Figure 4. Schematic (plan view) of the footwall lithology found below the VCR at Mponeng Mine.

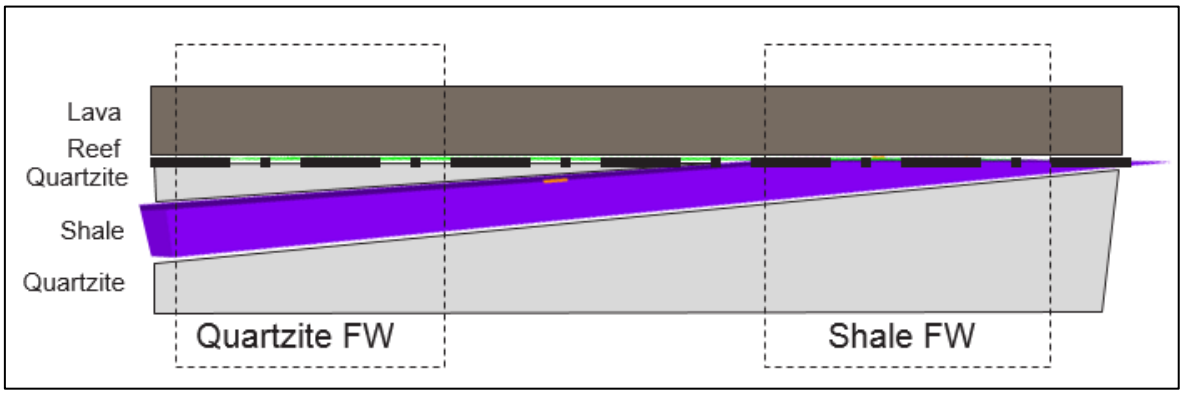

Figure 5. West-East section, showing the hangingwall, reef and footwall lithology succession (simplified model). The zones where quartzite or shale is thin can be identified and excluded from the study.

1.1.4 Research gap

The influence of the footwall rock type at Mponeng Mine on the seismic response to mining is not defined or quantified, therefore footwall lithology is not used as a parameter to assist in the mine design for mitigating the seismic hazard.

> If it can be shown that the rock mass properties associated with different footwall lithology do impact on the seismic response to mining, then it can be considered in mine design towards managing the seismic hazard.

The source mechanisms of large events on Mponeng Mine are poorly understood in general, hence it is not clear if the large events are typically related to geological structures or related to high stress ahead of mining faces.

> It is important to distinguish between events controlled by the footwall lithology (and associated rock mass properties) and events controlled by the properties of a specific geological structure. When a large magnitude seismic event occurs, it is not always clear if the event is associated with slip on a geological structure or shear through intact rock (Ortlepp shear, Ortlepp, 1997) at a mining abutment (face related or pillar related).
>
> The seismic hazard management strategies at Mponeng Mine include the implementation of bracket pillars on major geological structures and on all geological structures believed to be seismically active. In order to update the appropriate seismic hazard management practice, it is important to better understand the event source mechanism. If it is shown that most of the large events are geological structure related, then the bracket pillar design for geological structures needs to be reviewed. If it is shown that the large events are mining face related, then the mining strategies

must be reviewed and updated accordingly and similarly for pillars if it is shown that the events are associated with the regional stability pillars.

The influence of the orientation of the virgin stress field on the seismic response to mining is not properly quantified for Mponeng Mine.

The orientation of the field stress is determined by the orientation of the virgin stress and changes associated with mining and mining abutments. This impact on the orientation of the most likely failure plane orientations of shear-slip face related seismic events. This can have a major impact on mine design. The seismic hazard may be reduced if the overall mining abutments are not orientated parallel to the most likely failure plane based on the orientation of the virgin stress field.

1.2 RESEARCH OBJECTIVE AND QUESTIONS

The key focus of this research work was to quantify the difference in seismic response to production in the shale footwall area versus the quartzite footwall area at Mponeng Mine. It needs to be determined if the rock mass properties associated with a different footwall lithology can impact on the seismic response so that it can be considered in mine design towards managing the seismic hazard. The associated research questions are:

What is the difference in the seismic response to mining when mining in the shale footwall area compared to mining on the quartzite footwall?

In order to make appropriate changes to the mining strategies to mitigate the seismic hazard, it is important to understand the technical factors resulting in the difference in seismic response to mining on the shale footwall compared to the quartzite footwall. This leads to the research question:

> Why is there a difference in the seismic response between the shale footwall area and the quartzite footwall area?

It is important to distinguish between events controlled by the general lithology and rock mass properties and events controlled by the properties of a specific geological structure. The associated research question is:

> Are the majority of large events that occur on Mponeng Mine related to geological structures or related to mining faces?

When shear through intact rock occurs, the orientation of the most likely failure plane is determined by the orientation of the maximum excess shear stress in the rock mass. This in turn is determined by the orientation of the virgin stress field and the induced stress caused by the mining excavations. Where the orientation of the maximum excess shear stress is similar to the overall mining face shape orientation, the likelihood of face related seismic events is increased. The appropriate research question is:

> Are the orientations of the overall mining face configurations similar to the orientation of maximum excess shear stress associated with the virgin stress field, resulting in an increased likelihood of mining face related seismicity?

In summary, the objective is to quantify the influence of the footwall lithology (shale and quartzite), overall mining face shape and orientation of the most likely failure plane (based on the orientation of the virgin stress field) on the seismic response to mining at Mponeng Mine. The feasibility additional design parameters to be included in the list of parameters or strategies implemented on Mponeng Mine to mitigate the rockburst risk on the mine will be explored.

Furthermore, it is aimed to better understand the most common seismic event source mechanism in order to confirm the influence of geological structures on the majority of

seismic events and to identify the optimum overall mining face configuration orientation that will reduce the likelihood of face related seismicity.

1.3 METHODOLOGY

In order to show the difference in seismic behaviour for a different lithology, the seismic response to production for different areas on the mine with different lithology were quantified and compared. For Mponeng Mine, the VCR is a conglomerate and the hangingwall of the reef is a thick strong lava over the full extent of the mining lease area. From the footwall lithology plan provided by the geology department, it was found that for most of the Mponeng Mine lease area, the footwall is a strong quartzite, but in an area on the eastern side of the mine the footwall is shale with significantly lower strength compared to the quartzite.

Appropriate polygons for seismic data collection were established; that is a polygon on the eastern side of the mine in the area with the shale footwall and a polygon on the western side of the mine in the area with the quartzite footwall. All the seismic events that occurred in the shale footwall polygon as well as the quartzite footwall polygon were collected for the time period from the beginning of 2011 to the end of 2018.

With several different parameters or factors that generally impact on the seismic response to production, careful data selection and analysis were required to ensure the impact of footwall lithology on the seismic response to mining was considered in isolation when comparing the seismic response in the shale footwall area with the seismic response in the quartzite footwall area.

In order to identify the appropriate magnitude range to be used in the comparison that would eliminate possible differences in network coverage, and more specifically the sensitivity of the network in the identified areas (shale footwall and quartzite footwall), seismic event magnitude – frequency graphs, or so-called Gutenberg-Richter (GR) graphs were generated

for each of the two areas (shale footwall and quartzite footwall) from where the sensitivity of the network in each area was identified. The appropriate magnitude range for comparison was based on the worst sensitivity of the two areas; that is the minimum magnitude used in the comparison is larger than the worst sensitivity of the network in the identified areas.

The seismic response to production was plotted annually from 2011 to 2018 and inspected to identify annual data sets where the mining on the shale footwall and on the quartzite footwall were similar in terms of depth underground and mining spans.

Numerical modelling was used to confirm if the areas under comparison are similar from a stress and closure perspective. Modelled closure volume and maximum closure in stopes in the shale footwall area was compared to the modelled closure volume and maximum closure in the quartzite footwall area. When using the same rock mass properties for all areas on the mine as input in the model, stress (and redistribution of stress associated with mining abutments, mining spans and mining geometry) is isolated as the only parameter influencing the modelled closure. If the seismic response to mining in areas of the mine where the modelled closure volume (or other stress-related modelled parameter) is the same for both areas, the difference is associated with something other than stress; that is, for such areas the difference in the seismic response is associated with the rock mass properties. In the case of Mponeng mine, as described before, the difference in rockmass properties is associate with the footwall lithology (shale versus quartzite footwall). The reef and hangingwall strata remain constant over the full extend of the mining area.

This corresponds with ERR (Energy Release Rate) modelling in that the annual average modelled ERR for the shale footwall mining area was compared to that of the quartzite footwall mining area. Still using the same rock mass properties as input in the model, the modelled ERR is determined by stress and closure and correlate well with the influence of mining geometry on stress redistribution. This enables comparison of mining depth, mining span and mining geometry for the shale footwall area and the quartzite footwall area. Where the modelled average ERR for the shale footwall area and the quartzite footwall area are

similar, but the seismic response is different, the rock properties (footwall lithology) is identified as the parameter influencing the difference in seismic response to mining.

An important factor that needs to be considered in terms of understanding the influence of the footwall lithology on the seismic response to mining, is the influence of geological structures on the seismic response to production. The orientation and dip of geological structures compared to the orientation of the stress field impacting on the geological structures as well as the shear strength of these structures (compared to the shear stress) determine the likelihood of shear slip type events on these structures. Therefore the orientation, dip and shear strength properties of the individual structures must be known in detail in order to quantify the influence of these structures on the seismic response to mining. This detailed information in terms of the dip, strike and shear strength properties of the individual geological structures is not readily available in sufficient detail and it may make comparison of the seismic response on the areas under comparison unreliable. It was therefore important to do an analysis on the source mechanisms of seismic events in both the shale footwall area and the quartzite footwall area in order to identify the influence of geological structures on the occurrence of seismic events in these areas. Moment-tensor analyses were used to determine the event mechanisms for a large number of seismic events in the areas under investigation. Where it can be proven that most evens are mining face related, rather than geological structure related, the influence of individual geological structures can be ignored in the comparison of the seismic response to mining in the areas under comparison.

A refinement on the comparison of the seismic response to mining is to normalise the seismic response with production area or production volume. PvP (Potency versus Production) is a reliable normalised seismic parameter where the annual cumulative seismic potency of all the events in the magnitude range under comparison is divided by the annual production volume in that area.

Additional statistical seismic hazard assessment tools were used to compare the seismic hazard in the shale footwall area with the seismic hazard in the quartzite footwall area. From

the Gutenberg-Richter graphs for the different areas, it is possible to determine the statistical maximum magnitude seismic event for each area as well as the hazard magnitude for each area (with appropriate data collected in seismic polygons). These statistical hazard parameters provide insight into the likelihood of the occurrence of large magnitude events in the different areas.

After quantifying the difference in seismic response in the shale footwall area compared to the quartzite footwall area, numerical modelling is used to add insight into the potential impact of the rock mass properties on the likely seismic response to mining. In the model, the input parameters in terms of the elastic properties of the shale area is changed to highlight the difference between the shale and the quartzite in order to confirm if this would result in higher maximum closure and ERR. This indicate that the difference in elastic properties of the shale compared to the quartzite potentially explain the difference in seismic response to mining for these areas.

1.4 OVERVIEW OF CHAPTERS

In Chapter 2 a literature study is described. From literature the terminology and definitions, appropriate to the research described in this dissertation, is listed as a reference.

In Chapter 3 the data collection for the research project is described. The importance of data selection and data integrity is emphasised; Care must be taken to use appropriate data where the parameter under investigation can be singled out and other parameters do not affect the interpretation of the data. For this study, the key parameter under investigation is the influence of the footwall type, either shale or quartzite, on the seismic response to mining. Other potential parameters that may influence the seismic response include mining depth, mining span and geological structures. In this chapter it is illustrated how the data was selected to ensure that the influence of the footwall type is singled out for the study.

In Chapter 4 the results from the seismic data analysis are described. The annual number of events in different magnitude ranges for the shale footwall area and the quartzite footwall area is compared. The normalised seismic response in terms of annual potency divided by production is compared for the shale footwall area and quartzite footwall area. The seismic hazard derived from appropriate Gutenberg Richter graphs are described for the comparison areas. The event source mechanism investigation is discussed and the typical mechanism orientation compared to the most likely fracture orientation based on the virgin stress field.

In Chapter 5 the results are discussed with specific reference to the objectives of the study; that is, to understand the influence of the different footwall rock types (shale versus quartzite) on the seismic response to mining. The supporting studies, that assist in isolating the footwall rock type as the controlling parameter for the seismic response to mining, are also discussed.

In Chapter 6 concluding remarks are made in terms of the objective of the study; that is, the influence of the footwall rock type on the seismic response to mining. Conclusions from the study into typical event mechanisms and the virgin stress orientation are made in support of the primary objective of the study.

In Chapter 7 recommendations are made in terms of potential new strategies to include in the mining strategies to mitigate the high seismic hazard associated with the ultra-deep mining at Mponeng Mine. Mining strategies with specific reference to the footwall rock type (shale or quartzite) are recommended. I addition, mining strategies with specific reference to the orientation of the virgin stress field, are recommended.

CHAPTER 2 LITERATURE STUDY

2.1 CHAPTER OBJECTIVES

The objectives of the literature study are to identify applicable research that was done previously, as this will enrich the planned research into the topic of the influence of lithology on the seismic response to mining.

2.2 THE HISTORY OF ROCKBURSTS ASSOCIATED WITH MINING

It is of interest to describe the history of mining and the history of rockbursts associated with mining based on literature in this study field. Major gold production commenced in 1886 in the central Witwatersrand area, on the East Rand in 1914, the Klerksdorp and far West Rand area in 1937, in the Orange Free State in 1946 and the Kinross area in 1955 (Cook et al, 1966). Tremors and rockbursts were experienced from the early days of mining and by the time mining in the Central Rand area reached depths of several hundreds of feet below surface, earth tremors had become fairly common. As early as 1908, the Ophirton Earth Tremors Committee concluded that the tremors were due to the shattering of support pillars (Cook et al, 1966, Durrheim, 2010). Even though rockburst data was not available for the whole industry, on six large rockburst prone mines, 281 rockbursts occurred in 1963 alone.

During the first half of the twentieth century, even though isolated cases of fundamental research was carried out, most of the attempts to counter rockbursts were made by mining engineers most closely involved with the problem and were based on practical experience (Jeppe, 1946; Cook et at, 1966, Jooste and Malan, 2020). It was apparent by 1948 that attempts to solve the problem of rockbursts based on practical experience were inadequate.

Proper research was necessary to obtain an adequate fundamental understanding of the rockburst problem. The early observations from data analysis confirmed that, where hard brittle rock was being mined, an increase in the stress in the abutment ahead of the face increased its proneness to bursting (Cook et al, 1966). The following variables were found to be of importance:

- Excavation size; Rockburst incidents increased with increased span up to a point from where no further increase was observed.
- Abutment size; Rockburst incidents increased with decrease in abutment size until the remnant was mined out.
- Depth below surface; Rockburst incidents increased linearly with increased depth.
- Dykes; Rockburst incidents increased at mining abutments in proximity to dykes.
- Faults; Rockburst incidents increased at small mining abutments exposed to faults, not so with large abutments.
- Stoping width; Rockburst incidents increased with increased stoping width
- Rate of face advance; Beyond a certain rate of face advance, rockburst incidents increased with increased rate of face advance.

2.3 TERMINOLOGY USED IN ROCKBURST DISCUSSIONS

To support the discussion, important terminology used in rockburst descriptions need to be quoted from the literature. Several definitions for a seismic event can be offered, but only the most common definitions used in the field of rock mechanics and rock engineering, and stated in the rock engineering text books by Ryder and Jager (after the definitions developed by the Rockburst Commission Working Group of the International Society of Rock Mechanics (ISRM)) are described here:

A seismic event is a transient earth motion caused by a sudden failure of the earth's crust. The resulting emission and radiation of kinetic energy in the form of ground vibrations causes a sensible shock or tremor. Depending on many factors, this energy may or may not result in damage to underground or surface structures (Mendecki, 1997; Jager and Ryder,

1999).

A seismic event is a sudden inelastic deformation within a given volume of rock whereby a source radiates detectable seismic waves. The amplitude and frequency of radiated waves depend, in general, on the size of the source, and on the magnitude and rate at which the strain in the rock is relaxed during the fracturing process (Ryder and Jager, 2002). Rockbursts are commonly and pragmatically defined as seismic events that cause damage. This definition may be inadequate as it fails to cover the whole spectrum of phenomena that cause rockbursts.

A rockburst is the sudden and violent disruption of rock or disturbance of excavation walls in mines, which is caused by, or accompanied by, a shock or tremor (seismic event) of sufficient magnitude to cause obvious damage to excavations and support, or widespread simultaneous falls of rock. A rockburst is a consequence of mining activity (Ortlepp, 1984; Gay et al., 1984; Hedley, 1992; Jager and Ryder, 1999).

Types of rockbursts classified in terms of the source mechanism (Jager and Ryder, 1999): Strain bursts are triggered by small changes in the stress field which cause the strength of highly stressed rock to be exceeded, and strain energy stored in the rock mass to be released. The explosive failure of a hard rock specimen in a “soft” testing machine forms a very close analogy of the mechanism involved. The triggering agent may be a transient stress change associated with a (distant) seismic event, a stress change brought about by the advance of a nearby face, or the result of a time-dependant stress redistribution; but this causative activity only account for a fraction of the energy associated with the rockburst. In this type of rockburst the association between the rockburst and the seismic event is direct – the mechanism of the seismic event is the rockburst and vice versa.

Strainbursts are characterised by the violent failure of intact wall rock of excavations. The effect is usually localised to an area of less than a few square metres and occurs in the immediate wall rock. On occasions, up to a few cubic metres of intact rock, located outside the fracture zone of an excavation may become over-stressed and fail violently, ejecting the

previously fractured rock between the excavation and the newly failed rock. Strainbursts associated with stress redistribution usually occur in the vicinity of newly exposed rock surfaces (Jager and Ryder, 1999).

At Mponeng Mine, the primary risk mitigation strategy to combat strain bursts is preconditioning; i.e. face-perpendicular preconditioning is implemented, integrated into the drilling and blasting cycle. All stoping faces and certain development ends are preconditioned.

Face-parallel bursts mainly affect the rock in the immediate vicinity of stope faces. The source mechanism of the seismic event associated with this type of rockburst is usually a shear rupture ahead of the stope face, and probably initiates in intact rock beyond the periphery of the fractured ground surrounding the stope (Ortlepp, 1984). Such a shear fracture in the hangingwall typically propagates downwards in en echelon segments towards the stope, dips towards the back area, and has a normal sense of displacement. This displacement causes wedging and crushing of the fractured rock ahead of the stope face, stress redistribution than may cause local strain bursts, and on occasion, secondary low-angle fractures are formed which dip up and away from the face. Similar ruptures and deformations in a mirror-image sense occur in the footwall.

The violent compression of already fractured rock results in rapid dilation of the rock ahead of the face causing ejection or buckling of slabs in the face, violent peeling off of rock from new fracture surfaces in the hangingwall and severe shake down of fractured rock from the hangingwall due to the proximity of the seismic event, which can be of magnitude of up to M = 3, but usually less. Footwall heave into the stope is often experienced due to shearing on bedding planes or pre-existing fractures in the footwall which causes buckling of the immediate footwall beds (Ortlepp, 1984; Jager and Ryder, 1999).

At Mponeng Mine the primary risk mitigation strategies to combat face parallel bursts are: controlled mining spans to manage face stress levels and creating lead-lag distances between adjacent mining panels of a minimum 7 m to prevent the formation of long continuous

mining faces that promote face parallel bursting.

Pillar or remnant bursts. Pillars or remnants are loaded by mining in their vicinity. If such blocks of ground are of critical dimensions, they can become over-stressed and fail violently, either totally or in part (Cook et al., 1966). The damage occurs peripheral to the pillar; and dynamic closure of 100 mm or more can be expected in the immediate vicinity, the closure dying away concentrically from the focus area. Similar to the case with strain bursts, the failure of the pillar is the rockburst and causes a seismic event of magnitude ranging from about M = 0.5 to M = 2.5.

The underlying cause of the failure is a transfer of induced stress to the core of the pillar which become over-stressed and fails. The final additional stress which overloads the pillar can be due to time dependent fracturing of the edges of the pillar transferring load to the core, or due to seismic stress waves from a distant event impinging on a pillar in a state of unstable equilibrium (Jager and Ryder, 1999).

At Mponeng Mine, the primary risk mitigation strategies to combat pillar or remnant bursts are: not leaving remnants as far as possible and not mining remnants that have been created. Mponeng Mine do not implement pillars as local support, but sometimes leaves crush pillars between an abandoned stoping panel and the re-establishment of that panel face from a raise development directly ahead of the abandoned face. In this case the pillars are left sufficiently small to be crush pillars; i.e. that are fractured through to the core of the pillar so that it cannot become burst-prone (3 m maximum pillar width).

Pillar foundation failures. In deep longwall mines, a system of systematic strike-aligned stabilising pillars has been implemented for regional support. Rockbursts have occurred where the seismic events locate beneath the pillar. This has been interpreted to indicate the ‘punching’ of the pillar into the softer footwall strata, creating new shear ruptures, and resulting in stope closure and shakedown damage. The seismic events associated with pillar foundation failures do not generally exceed M = 3.5 (Lenhardt and Hagan, 1990; Jager and Ryder, 1999).

At Mponeng Mine, the primary risk mitigation strategies to combat pillar foundation failure is leaving sufficiently large regional stability pillars to prevent foundation failure; i.e. minimum 30 m wide continuous pillars on dip and strike.

Slip on geological structures. Geological structures such as faults and dykes represent zones of potential weakness in the rock mass. The redistribution of stress associated with mining may trigger slip along one of these pre-existing structures (Ortlepp, 1984). As these features may extend for hundreds of metres or even kilometres, a large volume of stressed rock may be involved and the magnitude of the event can be very large (up to M = 5, Durrheim, 2010). Any excavation in the near-field may suffer severe damage, while shakedown may affect stopes and tunnels over a large area; strain bursts may also be triggered.

A useful 'rule of thumb' relating the magnitude M and source dimension L_s, (the linear distance over which slip occurs) of a seismic event is:
$Log_{10}L_s$ (in metres) $\equiv 1 + M/2$
Or L_s (in metres) $\equiv 10^{(1+M/2)}$
For example, for M = 2, L_s = 100 m, For M = 5, L_s = 3000 m approximately.
Any point located at a distance less than $\frac{1}{2}L_s$ from the seismic source is said to be in the near-field; sites further away are in the far-field.

Near-field deformations decay rapidly with distance from the source, and thus the rockburst potential in the near-field is highest near the source rupture plane. A preliminary estimate of the width, normal to the rupture plane, of maximal rockburst damage potential is about $^1/_{10}L_s$. The size and shape of this potentially damaging "near-field" zone, in which ground velocities exceeding 1 m/s are likely, is probably dependant on the magnitude and nature of the stress-drop on the rupturing plane, and on the radiation pattern from the source (Jager and Ryder, 1999).

At Mponeng Mine, the primary risk mitigation strategies to combat large seismic events associated with slip on geological structures is leaving sufficiently large bracket pillars

(minimum 20 m) on both sides of large or significant structures as well as minimising the mining in major geological structures (where required) as far as possible by doing only the minimum required ledging of raises through structures to ensure their long-term stability. Minor structures that are planned to be negotiated (mined through) are approached with an angle between the overall mining front (formed by several adjacent panels) and the geological feature, of minimum 35°.

Further definitions to support rockburst discussion:

Location: The three-dimensional location of the origin of a seismic event, indicated in the mine coordinate system (x, y and z).

Hypocentre: The three-dimensional point within the earth where the seismic event occurred. This is similar to the location of the seismic event in the mine coordinate system.

Epicentre: The two-dimensional location on plan (on the earth's surface) vertically above the hypocentre of a seismic event.

2.4 MOMENT TENSOR INVERSION

Moment tensor inversion is a numerical technique aimed at giving a more general and more accurate description of the seismic source than provided by traditional P-wave first motion analyses (Andersen, 2001; Andersen and Spottiswoode, 2001).

With full generality in terms of its remote effects, a seismic source can be regarded as a collection of averaged strains in the source volume; specifically a symmetric tensor V_{ij} whose components are volumes of ride and closure. The corresponding moment tensor M_{ij} is functionally very similar to a 3D stress tensor since it is defined as the result of Hooke's law operating on the V_{ij} strain tensor (Ryder and Jager, 2002):

$$M_{ij} = \lambda \delta_{ij} V_{kk} + 2GV_{ij} \quad (2.1)$$

Where λ and G are the usual Lame parameters of linear elasticity. The shear components in V_{ij} are analogous to the tensor shear strain components $\Gamma_{ij} = ½\lambda_{ij}$ and so are one half of the corresponding volumes of ride.

The moment tensor M_{ij} is defined by a combination of equivalent forces:

$$M_{ij} = \begin{bmatrix} M_{11} & M_{12} & M_{13} \\ M_{21} & M_{22} & M_{23} \\ M_{31} & M_{32} & M_{33} \end{bmatrix} \quad (2.2)$$

Where each element of the tensor represents a force couple or dipole as illustrated in Figure 6. There are nine possible combinations of force and arm directions. When i and j are the same, the couple is known as a vector dipole or as a couple without moment. All other couples have a non-zero moment equivalent to the torque they exert about the axis perpendicular to their plane of action. From considerations of equilibrant torques, it emerges that $M_{ij} = M_{ji}$ for $i \neq j$ so that the moment tensor consists of only six independent components (Ryder and Jager, 2002). The six components can be combined in different ways to describe a wide range of seismic sources.

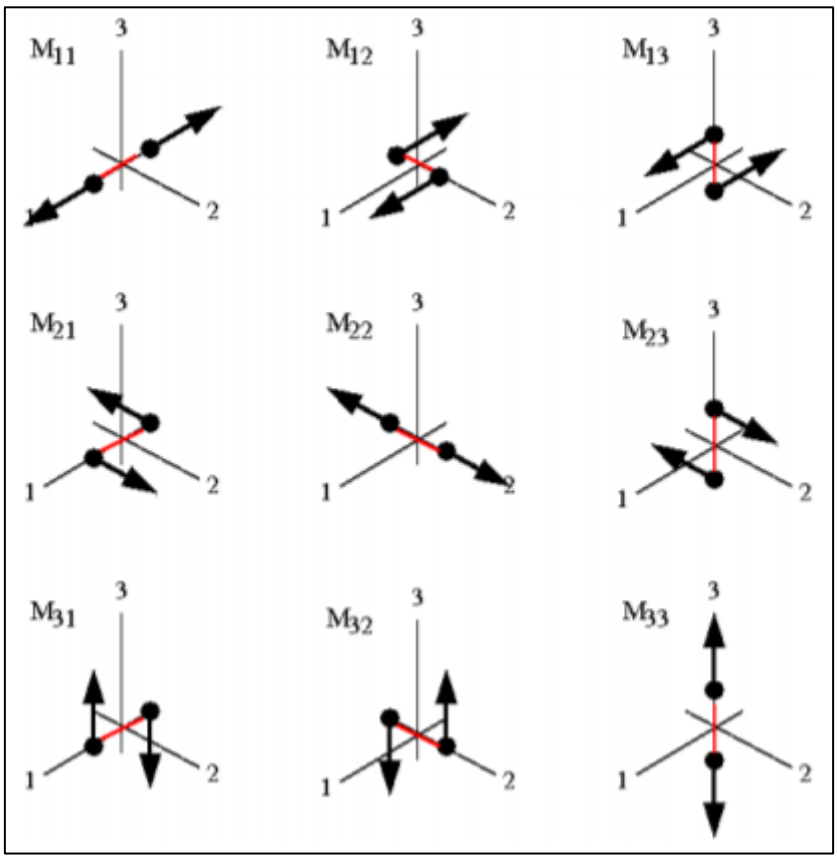

Figure 6. Representation of the nine possible couples M_{ij}. The directions of the force and arm of the couple are denoted by the indices I and j respectively.

The moment tensor can be linearly related to ground displacements recorded by a seismometer. If general equivalent force systems representing a seismic source is expressed as a linear combination of couples with moments M_{ij}, then the displacement u_k (displacement in the k^{th} direction) is the sum of the displacements caused by the individual couples. This linearity allows the seismic data to be inverted to obtain the source parameters.

For a source located at (ζ_1 ζ_2 ζ_3) and receiver at (x_1 x_2 x_3), the complete expression for u_k is given as follows (Ryder and Jager, 2002):

$$u_k = \left(\frac{15\gamma_k\gamma_i\gamma_j - 3\gamma_k\delta_{ij} - 3\gamma_i\delta_{kj} - 3\gamma_j\delta_{ki}}{4\pi\rho}\right)\frac{1}{r^4}\int_{r/\alpha}^{r/\beta}\tau M_{ij}(t-\tau)\,d\tau$$
$$+\left(\frac{6\gamma_k\gamma_i\gamma_j - \gamma_k\delta_{ij} - \gamma_i\delta_{jk} - \gamma_j\delta_{ki}}{4\pi\rho\alpha^2}\right)\frac{1}{r^2}M_{ij}(t-r/\alpha)$$
$$-\left(\frac{6\gamma_k\gamma_i\gamma_j - \gamma_k\delta_{ij} - \gamma_i\delta_{jk} - 2\gamma_j\delta_{ki}}{4\pi\rho\beta^2}\right)\frac{1}{r^2}M_{ij}(t-r/\beta)$$
$$+\frac{1}{4\pi\rho\alpha^3}\gamma_k\gamma_i\gamma_j\frac{1}{r}\cdot M_{ij}(t-r/\alpha) - \frac{1}{4\pi\rho\beta^3}(\gamma_k\gamma_i - \delta_{ki})\gamma_j\frac{1}{r}\cdot M_{ij}(t-r/\beta) \qquad (2.3)$$

Where ρ indicates density, α and β are the P and S-wave velocities respectively, r is the distance between the source and receiver, $\gamma_i = (x_i - \zeta_i)/r$ are the direction cosines between source and receiver and form the components of a unit vector $\Gamma = (\gamma_1\ \gamma_2\ \gamma_3)$ directed along the source-receiver direction. δ_{ij} is the Kronecker delta ($\delta_{ij} = 1$ for i = j, and $\delta_{ij} = 0$ for i ≠ j). A dot over M_{ij} indicates the derivative with respect to time.

The first term decays as $1/r^4$ with distance from the source and is called the near-field radiation since it generates strong displacements near the source but negligible displacements at greater distances. The next two (intermediate-field) terms decays with $1/r^2$ and the last term decays with 1/r and is called the far-field radiation. The far-field radiation generates the dominant seismological effects at greater distances from the source where most seismological observations are made. Only the far-field components are normally used in moment tensor analyses (Ryder and Jager, 2002).

The interpretation of a full moment tensor traditionally proceeds as follows. The preliminary operation involved is exactly analogous to analysis of a general stress tensor into its principal stress components and directions. The resulting set ($M_1\ M_2\ M_3$) of principal moments ranked in order of moment M_0 is given by

$$M_0 = [(M_{1+}^2 + M_{2+}^2 + M_3^2)/2]^{½} \qquad (2.4)$$

If the source were a pure shear event (pure double-couple), M_1 and M_3 would be equal and

opposite, and the intermediate principle moment M_2 would be zero. This corresponds to a stress state of pure shear and the plane of maximum shear stress; i.e. the fault solution, lies midway between the major and minor principle axes. In mine seismology this is generally not the case and many events contain significant elements other than pure shear on a single plane and a more complete solution is desirable. This is accomplished by first subtraction out an isotropic part given by

$$\frac{1}{3}tr(M_0) = \frac{1}{3}(M_1 + M_2 + M_3) = \frac{1}{3}(M_{11} + M_{22} + M_{33}) \quad (2.5)$$

The resulting deviatoric principle moments are then further decomposed into a pure shear part and a compensated linear vector dipole (CLVD) which expresses a triaxial compression with radial dilations at constant volume (Ryder and Jager, 2002).

A practical example is given here to explain the typical interpretations made by a rock engineer when confronted with a moment tensor solution:

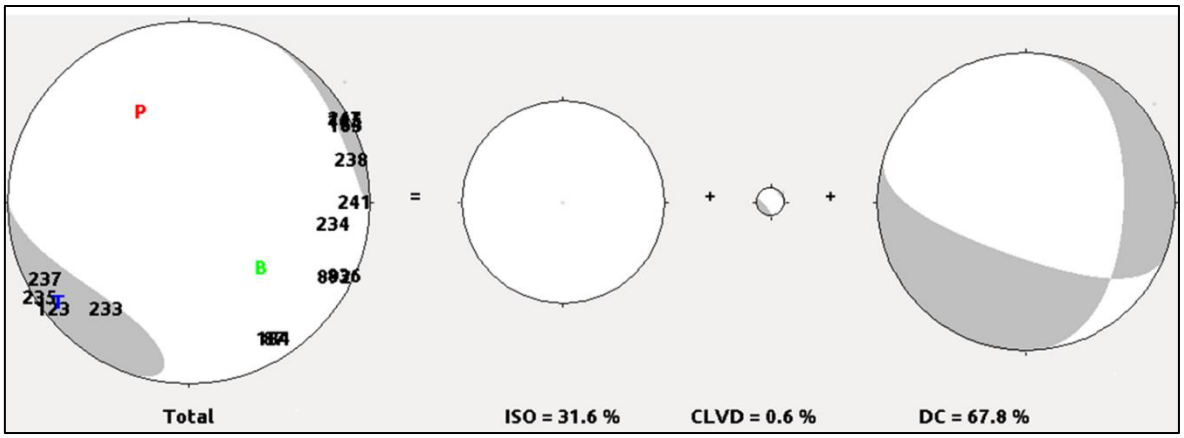

Figure 7. Moment tensor solution as provided by IMS of a magnitude M_L = 2.0 event on Mponeng Mine.

The first sphere represents the combined or total event mechanism. The next three spheres represent the moment tensor decomposed components. The ISO component of the event can be explained as 3D volume change towards the source; i.e. implosion. In this example the isotropic component of 31.6% indicates that a large component of this event can be

interpreted as bursting or deformation of the rock immediately surrounding a mining excavation that is likely to cause damage to the excavation in the form of face bursting and other forms of hangingwall, footwall or face ejection or deformation. The CLVD component of the event mechanism can be explained by triaxial compression and radial dilation. This is analogous to a pillar failure where the radial dilation is in the direction orthogonal to the pillar failure. In this example the CLVD component of 0.6% is very small or even negligible, indicating that it is unlikely that pillar failure played an important role in this event. The double couple (DC) component refers to the portion of the event that can be associated with pure slip on a simple source plane. This can be associated with slip on a fault plane or shear through intact rock (Ortlepp shear). The orientation of the source slip plane and direction of slip can be read from the sphere as well; the dark shading indicates compression and white areas indicate dilation, indicating slip orientation of the two orthogonal source plane solutions. In this example the DC component of 67.8% dominates the event mechanism, indicating slip on a structure or shear through intact rock to be the most dominant mechanism of this event. The orientation of the most likely slip plane is northwest-southeast with steep normal slip in the west-southwest direction.

2.5 MECHANICAL PROPERTIES OF ROCK

Mechanical properties of rock; Both brittle rock and ductile rock typically behaves elastically up to the point of failure. Post this point of failure, brittle rock behaviour can be described as the formation of fractures, sometimes dynamic fractures, and a sudden reduction in unconfined strength. Ductile rock will start to flow post the point of failure. Most of the rock types associated with deep level mining in the gold industry of South Africa exhibit elastic behaviour up to stress levels higher than the virgin stress field. Consequently, in calculating the stresses at points removed from the excavation, the theory of elasticity can probably be considered adequate for most practical purposes. In fact, considering the triaxial compressive strength of the rock mass, which is considerably higher than the UCS due to the confinement, even at great depth, the rock mass strength will be significantly higher than the virgin stress field, supporting the use of elastic theory and elastic numerical modelling

programs to calculate stresses at points remote from excavations.

The literature study further reveals that rock properties play a direct role in the rock mass response to mining. Jager and Ryder (1999) describes the factors governing rock behaviour in Chapter 1.3 of their book as rock stresses, rock strength (and friction properties), rock types and geological weaknesses. The host rocks in which mining takes place is inhomogeneous and layers of quartzites of varying compositions are interbedded with weak shale bands and are interrupted by occasional strong dyke and sill intrusive. Fracturing can be affected due to induced tensile stresses in the stiffer rock layers adjacent to softer ones. The presence of weak shale layers in the immediate footwall can cause special mining and strata control difficulties, particularly at abutments where high stress and stress changes occur.

The basic criterion for rock failure used in rock mechanics is based on the stress/strength ratio; i.e. failure will occur when the stress in the rock/rock mass is greater than the strength. The strength of the rock or rock mass is very much a property of the rock type and presence of discontinuities or weak partings in the rock mass.
There are three methods in which the properties of rock and rock behaviour under loading can be assessed (Ryder and Jager 2002). These are summarised in Table 1.

Table 1. Methods of assessing rock properties and behaviour in sequence of (a) relative accessibility, (b) relevance, (c) generality

	(a) Laboratory testing	(b) Field observations and Measurements	(c) Mathematical and numerical modelling
Specimen size	Often < 0.01 m	Unlimited	Unlimited
Setup difficulty	Low	Very high	Moderate
Degree of control	High	Low	High
Measurement accuracy	High	Low	High
Relative cost	Moderate	High	Low
Relevance	Moderate	High	Moderate to uncertain
Interpretability	Easy	Difficult	Often difficult

Laboratory testing provides the starting point for inferring the physical behaviour of rocks and rock masses, and for estimating the numerical parameters involved. Mathematical and numerical models, underpinned by sound back-analyses of actual field observations and measurements can then in principle be used to describe and predict the behaviour of excavations in a given rock mass, and to permit rational designs to be carried out.

It is fair to deduce that for similar mining geometries at similar depth, a difference in rock mass response may be possible and would most likely be explained by the difference in rock mass properties as described by the lithology at each site. The lithology at the reef horizon refers to the rock type where mining takes place, and therefore indirectly refers also to the rock properties at the mining front. This clearly establishes the link between lithology and rock mass response in general, including the seismic response to mining.

In deep level and other high stress mining areas, the mining faces will fracture due to the high stress and stress concentrations on the edges of excavations. In these situations, mere

knowledge of failure criteria (the ability to predict onset of fracturing) is inadequate (Ryder and Jager, 2002). At Mponeng Mine all tunnel sidewalls and mining stope faces fracture immediately on creation or advance of the excavation face (stope or tunnel). In these conditions it is important to describe and understand the post-failure behaviour of the rock or rock mass.

Laboratory strength tests of rock samples are aimed at determining rock properties such as the Uniaxial Compressive Strength (UCS), Young's Modulus (E), Poisson's ratio and even triaxial compressive strength. These properties can all be used to describe the elastic behaviour of the rock and rock mass and are also used as input parameters into elastic stress modelling. Strength tests are typically done to specimen failure. "*A hard rock type loaded in an ordinary testing machine will usually fail in an uncontrolled and violent fashion: there is a loud report, potentially dangerous shards of rock may fly out of an unguarded uniaxial testing configuration…. The whole episode bears a striking resemblance to the phenomenon of strain-bursting in hard rock…"* (Ryder and Jager, 2002). Such behaviour was considered to be an intrinsic property of the rock, but it is now known to be associated with the stiffness of the testing machine (Cook, 1965). When testing a hard rock sample in a relatively soft testing machine, the machine frame or similar components will strain during the loading of the rock sample, thereby storing energy in the testing machine itself (Figure 8).

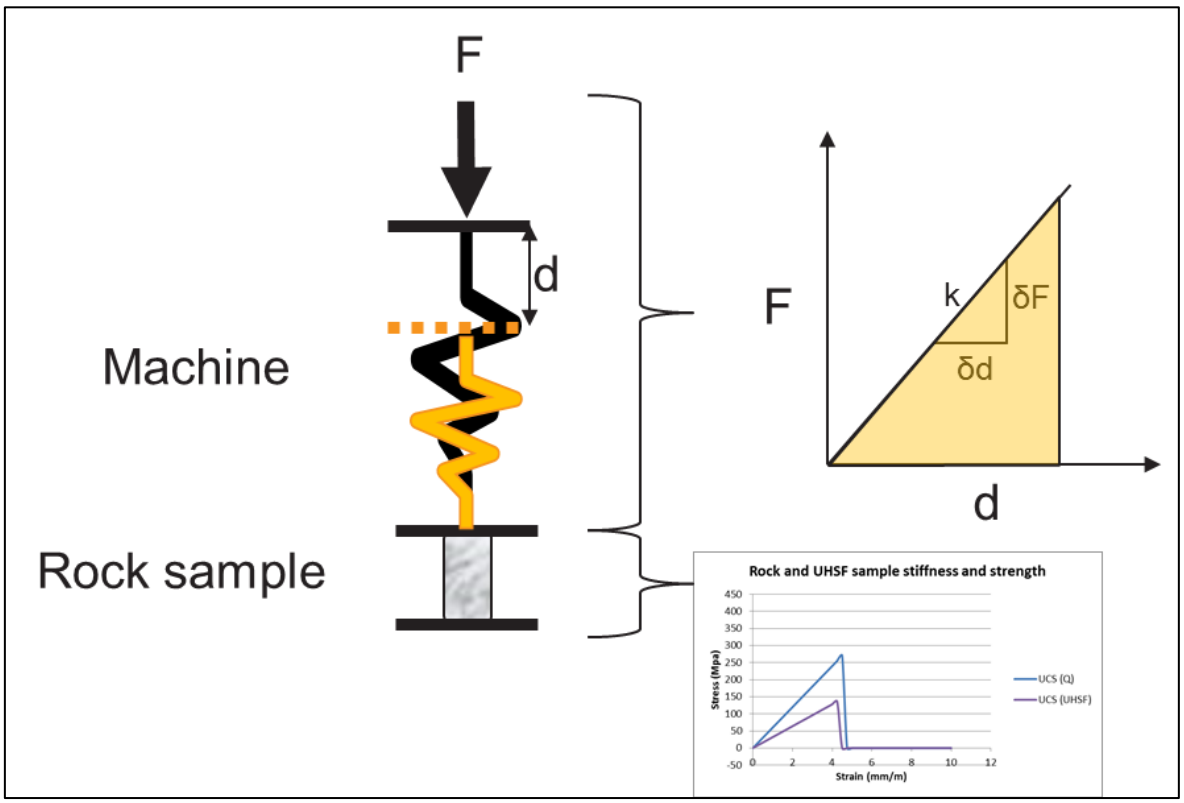

Figure 8. Schematic of a testing machine and rock sample where the testing machine is represented by a spring with stiffness k and where the machine components deform by distance d under loading of force F

The stiffness of the machine (k) is equal to the slope of the Force-deformation graph of the testing machine. The energy stored in the machine is calculated from the area under the Force-deformation graph of the testing machine (E = ½dF). When the rock sample reaches its peak strength and starts failing, the machine is allowed to deform back to its original position (at start of test). This continues to drive the rock sample during failure resulting in violent and uncontrolled failure of the rock sample and the stored energy (in the machine) is released during the failure process of the rock sample.

Important analogies from face or strain-bursting underground can be drawn from this: if the stiffness, i.e. loading line slope, of the strata bearing on an over-loaded face is lower than the post-failure load-shedding slope of the face, then a burst with violent energy release will result, the violence being derived not intrinsically from the bursting rock itself, but mainly

from elastic strain energy released from the enveloping “soft” strata (Cook, 1965).

Several factors may impact on loading system stiffness: lithology: where relatively stiff rock in close proximity of the mining horizon is surrounded by relatively soft rock layers (above or below), this can be interpreted as a soft loading system. Proximity and frequency of structures: where the frequency of structures (with relatively low cohesion contacts) is high, the loading system is relatively soft. Mine designs/layouts/geometry: mining areas with high extraction ratio and large mining spans represent a lower system stiffness compared to mining areas with low extraction ratio and small mining spans (regular large regional stability pillars).

Loading system stiffness can be used as a parameter to evaluate the potential for rockburst (Wiles, 2002). In Figure 9, loading system stiffness (LSS) is simply the slope of the load-deformation response curve (during pillar failure from stage 1 (pillar intact) to stage 2 (pillar completely failed/obliterated). The total amount of energy released from the surrounding rock mass during the pillar failure is the area of the triangle:

$$W_t = W_k + W_f \tag{2.6}$$

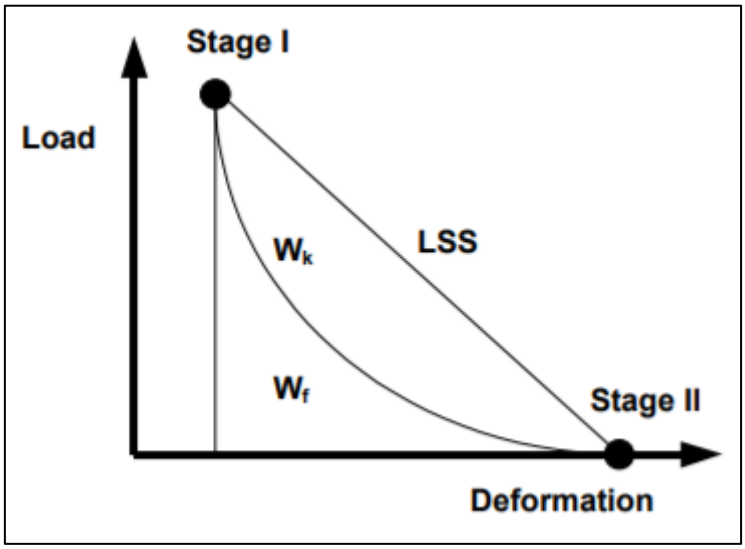

Figure 9. Load-deformation response of a pillar.

The amount of energy released as kinetic energy is the area of the upper portion of the triangle labelled as W_k.

One should expect this to correlate with the observed event magnitude. The amount of energy that would be used in crushing the pillar is the area of the lower portion of the triangle labelled as W_f. One should expect this to correlate with the amount of damage observed at the event source. The local energy release rate for this pillar is determined as:

$$LERR = W_t/Volume \quad (2.7)$$

The problem is that this parameter is a strong function of the local stress level. Anywhere the stresses are high, so is LERR. Conversely, anywhere the stresses are low, so is LERR. Although it is straightforward to determine the likelihood of failure from the stress state, if we now ask whether failure would be violent or not, the LERR concept does not distinguish between controlled failure and violent failure. Some sort of normalisation is required to eliminate the dependence of LERR on stress level.

A measure of the rate of energy release as the non-linear strains accumulate is well encapsulated by considering loading system stiffness (LSS) rather than LERR. For a large value of LSS, energy is released relatively slowly with progressive damage, whereas with small values, energy is released at a much higher rate. The question of burst proneness now becomes a question of whether the failure occurs in a controlled manner, where all of the energy released can be used in accumulating damage (i.e. crushing of the pillar). Alternatively, the failure could occur in an uncontrolled manner, where there is more energy released than can be used in crushing of the pillar.

From Figure 9 the total energy released from the surrounding rock mass during pillar failure is the area of the triangle: $W_t = W_k + W_f$. This is now readily calculated in a numerical model by integrating the forces through the displacements that occur from Stage I to Stage II, over

all surfaces in the numerical model, thus:

$$W_t = \iint (\sigma_n du_n + \sigma_s du_s + \sigma_t du_t) dS \quad (2.8)$$

Here, u represents the displacement, σ represents the surface stress, the subscripts n, s and t refer to the normal and two shear components on each surface S.

A representative LSS can be expressed in terms of the mean stress σ_m, and volumetric strain ϵ_v:

$$\sigma_m = \text{LSS}\ \epsilon_v \text{ Where: } \sigma_m = \tfrac{1}{3}(\sigma_1 + \sigma_2 + \sigma_3) \text{ and } \varepsilon_v = \varepsilon_1 + \varepsilon_2 + \varepsilon_3 \quad (2.9)$$

We can calculate the strain energy of volume change as:

$$W_v = \iint \sigma_m d\varepsilon_v dV \quad (2.10)$$

Where the volume integral is taken over the surfaces of the pillar that fails. Now substituting for the volumetric strain:

$$W_v = \iint \sigma_m d\sigma_m dV / LSS \quad (2.11)$$

By equating this to the actual energy released from the loading system (W_t from Equation 3), we can determine the LSS:

$$W_t \equiv W_v = \iint \sigma_m d\sigma_m dV / LSS \quad (2.12)$$

$$LSS = \iint \sigma_m d\sigma_m dV / W_t \approx \tfrac{1}{2}\overline{\sigma_m}^2 V \quad (2.13)$$

where $\overline{\sigma_m}^2$ represents the square of the average value of σ_m in the pillar with volume V. Now

$$1/LSS = W_t / \iint \sigma_m d\sigma_m dV \approx W_t / (\tfrac{1}{2}\overline{\sigma_m}^2 V) = 2LERR/\overline{\sigma_m}^2 \quad (2.14)$$

which shows that calculation of LSS in this way is actually equivalent to normalising LERR by the square of the mean stress in the pillar.

A representative measure of loading system stiffness can be obtained by normalising the local energy release rate by the square of the mean stress. This eliminates dependence on the local stress level and provides an indicator that can be used to predict the expected nature of failure regardless of whether the stress state is exactly at the point of failure.

Loading system stiffness can therefore be used to determine the likelihood that a failure will be violent. This provides a technique to identify locations that are rockburst prone (Wiles, 2002).

In this project the area of interest is specifically high stress (deep mining) in strong brittle rock and the difference in seismic response in areas with similar mining geometry but different rock mass properties based in the lithology; i.e. strong lava hangingwall, conglomerate reef and quartzite footwall in the west of the mine and shale footwall in the east of the mine. It can be argued that the loading system is softer on the east side of the mine on the shale footwall and with more frequent faults and dykes compared to the western side of the mine on the quartzite footwall and slightly fewer structures.

2.6 MODELLING INPUT PARAMETERS

Numerical modelling was used to quantify the stress conditions prevailing in the areas of interest, specifically to confirm if these areas are subject to similar stress levels.

Map3D, is a fully integrated three-dimensional layout, visualisation and boundary element modelling stress analysis software package, (MineModelling, 2013). Map3D is limited to elastic behaviour (an elasto-plastic yield setting is available to model non-linear deformation on a plane, i.e. ride). As with most modelling techniques, the simulated values are not used as a reflection of the actual values, but to compare areas or scenarios. Care was taken to use appropriate input parameters for stress and rock mass strength based on in-situ stress measurements and other field observations as well as laboratory results of UCM (Uniaxial

Compressive Strength and Young's modulus) tests of the different rock types found on the mine (Table 3).

The UCS (Uniaxial Compressive Strength) of the shale is fairly consistent with a small range between 156.6 MPa and 194.3 MPa and average of 172.5 MPa.
The UCS of the Lava hangingwall shows a large variance and ranges between 201.8 MPa and 336.2 MPa (ignoring the low value of specimen number 5 that failed on a pre-existing discontinuity) with average of 270.3 MPa.
The UCS of the Quartzite footwall shows a large variance and ranges between 159.5 MPa and 332 MPa with an average of 252.2 MPa.

Even though it is important to understand the strength of the different rock types near the reef horizon in terms of UCS, it is not used as input into elastic numerical modelling (Young's modulus is used).

Table 2. Laboratory strength test results for the relevant rock types found on Mponeng Mine (Mponeng internal report)

Specimen Ref No	Diameter (mm)	Length (mm)	L/D	Mass (g)	Density (kg/m3)	Failure Load (kN)	UCS MPa	E (GPa)	ν	Test Type
Mponeng East Booysens Shale										
1	41.95	104.70	2.5	397.3	2745	216.7	**156.8**	65.05	0.27	UCM
2	41.70	104.60	2.5	395.3	2767	213.9	**156.6**	61.78	0.33	UCM
3	41.90	106.20	2.5	401.3	2740	267.6	**194.0**	69.35	0.26	UCM
4	41.80	104.50	2.5	394.3	2750	266.7	**194.3**	60.46	0.23	UCM
5	42.00	104.65	2.5	398.6	2749	222.9	**160.9**	64.65	0.27	UCM
Mponeng East Lava										
1	41.90	106.10	2.5	412.6	2820	279.4	**202.6**	83.38	0.27	UCM
2	42.00	106.20	2.5	422.5	2872	465.8	**336.2**	92.50	0.22	UCM

3	42.00	106.10	2.5	416.5	2833	363.1	**262.1**	86.09	0.23	UCM
4	41.90	106.40	2.5	413.1	2816	399.9	**290.0**	81.86	0.26	UCM
5*	41.90	106.30	2.5	426.4	2909	170.9	**123.9**	97.10	0.25	UCM
Mponeng West Lava										
1	42.00	104.20	2.5	412.3	2856	418.1	**301.8**	85.12	0.27	UCM
2	41.90	104.80	2.5	415.1	2873	460.3	**333.8**	87.28	0.21	UCM
3	41.80	104.70	2.5	401.2	2792	292.0	**212.8**	72.41	0.27	UCM
4	41.90	104.00	2.5	401.0	2796	278.2	**201.8**	77.96	0.24	UCM
5	42.00	104.00	2.5	404.7	2809	389.5	**281.2**	83.59	0.27	UCM
Mponeng West Kimberley Quartzite FW										
1	42.00	105.40	2.5	388.1	2658	360.0	**259.9**	79.05	0.19	UCM
2	42.00	105.00	2.5	386.3	2656	447.0	**322.7**	81.31	0.11	UCM
3	42.00	104.90	2.5	386.9	2662	460.2	**332.2**	82.02	0.13	UCM
4	42.00	104.20	2.5	383.7	2658	447.8	**323.2**	80.97	0.09	UCM
5	42.00	104.80	2.5	388.0	2672	375.3	**270.9**	76.02	0.16	UCM
Mponeng Far West Amygdale Lava										
1	32.00	88.50	2.8	203.00	2852	187.87	**233.6**	77.43	0.24	UCM
2	32.00	88.40	2.8	200.90	2826	217.70	**270.7**	78.48	0.22	UCM
3	32.00	88.50	2.8	201.60	2832	177.04	**220.1**	77.08	0.22	UCM
Mponeng Far West Fine-grained Lava										
4	31.90	88.50	2.8	204.8	2895	215.0	**269.0**	88.42	0.22	UCM
5	32.00	88.40	2.8	206.1	2899	296.1	**368.2**	89.53	0.25	UCM
Mponeng Far West Elsberg Quartzite										
1	31.60	87.90	2.8	184.2	2672	134.6	**171.6**	74.52	0.18	UCM
2	31.60	88.00	2.8	184.4	2672	151.3	**192.9**	75.39	0.16	UCM
3	31.60	88.00	2.8	184.7	2676	176.2	**224.6**	74.43	0.20	UCM
4	32.00	88.00	2.8	188.2	2659	212.3	**264.0**	75.72	0.17	UCM

5	31.60	88.00	2.8	185.2	2683	125.1	**159.5**	72.16	0.16	UCM

Table 3. Averages for the relevant laboratory strength data

Averages	UCS (MPa)	E (GPa)	ν
Shale footwall	172.5	64.3	0.272
Lava hangingwall	270.3	82.9	0.242
Quartzite footwall	252.2	77.2	0.155

The Young's modulus (modulus of elasticity) of the shale varies between 60.46 GPa and 69.35 GPa with average of 64.3 GPa. The Young's modulus of the lava hangingwall ranges between 72.41 GPa and 89.53 GPa with average of 82.9 GPa. This is 29% higher than the Young's Modulus for shale and indicates that the shale is significantly softer than the lava hangingwall in the elastic range of these rock types. The Young's modulus of the Quartzite ranges between 74.43 GPa and 82.2 GPa with average of 77.2 GPa. This is 7% lower than the Young's modulus for the lava hangingwall, but 20% higher than the Young's modulus for the shale footwall.

An average Young's modulus of 70 GPa is used as input into the elastic numerical model to represent the average modulus of elasticity of the rock mass if there is no attempt to distinguish between the different rock types.

The Poisson's ratio describes the ratio between radial strain and axial strain in the elastic range during the UCM laboratory tests. The Poisson's ratio for the shale ranges between 0.23 and 0.33 with an average of 0.272, and for the lava hangingwall it ranges between 0.21 and 0.27 with an average of 0.242. The Poisson's ratio for the quartzite footwall is surprisingly low and ranges between 0.09 and 0.2 with an average of 0.155. An average value for Poisson's ratio for the combined rock mass of 0.2 is used as input into the numerical models.

As a starting point, the virgin vertical stress is assumed to be determined by gravitational loading based on a rock mass density for the host rock. The rock mass density for the shale ranges between 2745 kg/m³ and 2767 kg/m³, for the lava hangingwall between 2792 kg/m³ and 2899 kg/m³ and for the quartzite footwall ranges between 2656 kg/m³ and 2683 kg/m³. An average density for the overall rock mass of 2689 kg/m³ is used as initial input into the numerical models (Hofmann, 2013).

In 2000, a stress measurement, using the hollow inclusion over coring method (CSIRO cell) was done in the shaft pillar of TauTona mine (sister mine of Mponeng Mine) on 2000 m below surface. Owing to the fact that the shaft pillar was (and is) stressed above virgin stress levels due to extensive mining outside the shaft pillar, numerical modelling was used to interpret the measured field stress in the shaft pillar and relate it back to virgin stress. This was achieved by adjusting the input stress for the model until the modelling result are the same as the measured stress levels. The result indicated a vertical virgin stress gradient of 25 MPa/km (similar to a rock mass density of 2500 kg/m³) with a trend of 247° and plunge of 75° (Hofmann, 2013). The k-ratio for the intermediate principle stress component was determined to be 0.8 with trend of 143° and plunge of 14°. The k-ratio for the minor principle stress component was determined to be 0.5 with trend of 234° and plunge of 6°.

In 2005, observations of borehole breakout of several holes drilled on TauTona Mine was used to derive a stress state, again using numerical modelling, where the input stress state for the model is adjusted until the model simulated the observed borehole breakout. The stress gradient of the major stress component was determined to be 27 MPa/km; i.e. similar to a rock mass density of 2700 kg/m³, with trend of 345° and plunge of 80°. The k-ratio for the intermediate principle stress field was determined to be 0.88 with trend of 157° and plunge of 10°. The k-ratio for the minor principal stress field was determined to be 0.51 with trend of 247° and plunge of 1°. These results are similar to the results obtained through the stress measurements in the shaft pillar and other areas in TauTona Mine (Hofmann, 2013).

In 2007, a seismic event with magnitude M_L = 2.4 at TauTona mine triggered a seismic event with magnitude M_L = 2.7 at a location 300 m away from the first event. The sources of the two events were modelled in terms of surface shear stress exceeding shear strength and the stress state modified slightly to explain coulomb stress triggering (Hofmann et al, 2013).

In 2012 a new stress measurement technique was introduced to AngloGold Ashanti South Africa Region by Professor Hiroshi Ogasawara; the CCBO method (Compact Conical-ended Borehole Over coring). In this method the procedure of stress measurement through over coring was optimised and found more suitable to the South African deep level gold mines in that the required drill hole size is reduced from NQ size to BQ size, and the same hole for instrumentation is used for over coring (Ogasawara et al, 2012). This technique was implemented in 2013 at Mponeng Mine for direct stress measurements, but practical problems were experienced, causing a level of uncertainty in the results. The major principal stress was lower than for TauTona Mine, but stress orientations of the three stress components were similar to the previous interpretations. The fact that the stress measurements had to be completed in 5 to 7 m deep holes rather than the recommended 10 m depth due to borehole breakout and instabilities, may explain the lower stress measured as the measurement position may still experience some of the de-stressing effect of the tunnel from where drilling was done. Even through the stress measurement result was compromised, it could still be used to support the estimation of the stress input tensor into models for TauTona and Mponeng Mines. The information from the four projects to understand the virgin stress magnitude and orientation applicable to TauTona and Mponeng Mines were combined to determine the best possible stress input tensor into numerical modelling. This is summarised in Table 1 and the final derived stress input information is given under the column “Final stress state (2013)”.

Table 4. Summary of the stress input tensor information for TauTona and Mponeng Mines.

	TT SCIRO (2000)			Borehole breakout (2005)			Coulomb stress (2007)			CCBO (2013)			Final stress state (2013)		
	Δσ	Trend	Plunge	Δσ	Trend	Plunge	Δσ	Trend	Plunge	Δσ	Trend	Plunge	Δσ	Trend	plunge
σ_1	25	347	75	27.2	345	80	27.2	344	68	27.4	283	69	27.2	330	78
σ_2	0.8	143	14	0.88	157	10	0.93	168	22	0.71	147	15	0.74	150	12
σ_3	0.5	234	6	0.51	247	1	0.48	257	1	0.3	53	14	0.44	60	0

Subsequently, the CCBO technique was employed at a number of sites at TauTona to better estimate the pre-mining stress state in this environment. The sites for the four projects discussed above, as well as the CCBO stress measurement sites, are shown in Figure 10.

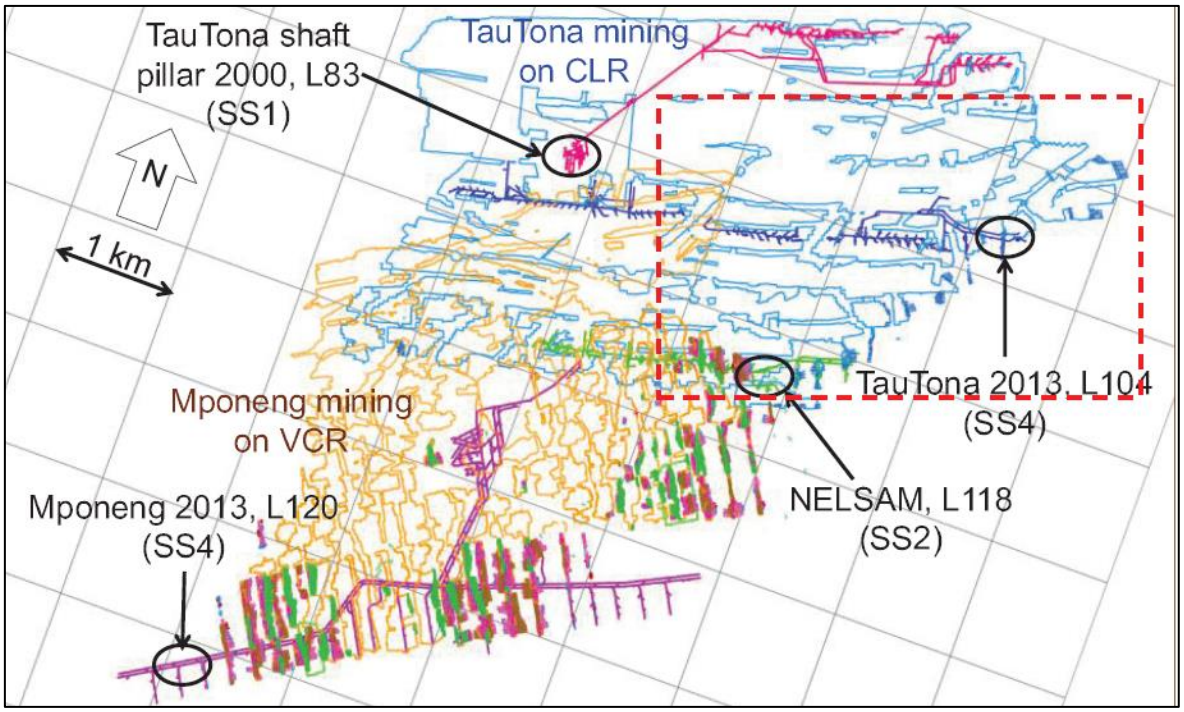

Figure 10. Plan view of TauTona and Mponeng mining outlines (2013). The positions where stress data were gathered are indicated by black ellipses.

In Figure 11, the stress project data are plotted in a lower hemispherical stereonet plot, with the outlined area indicating the spread in the data. It is clear that the stress tensor orientations from the different sources are tightly grouped together in the stereonet plot.

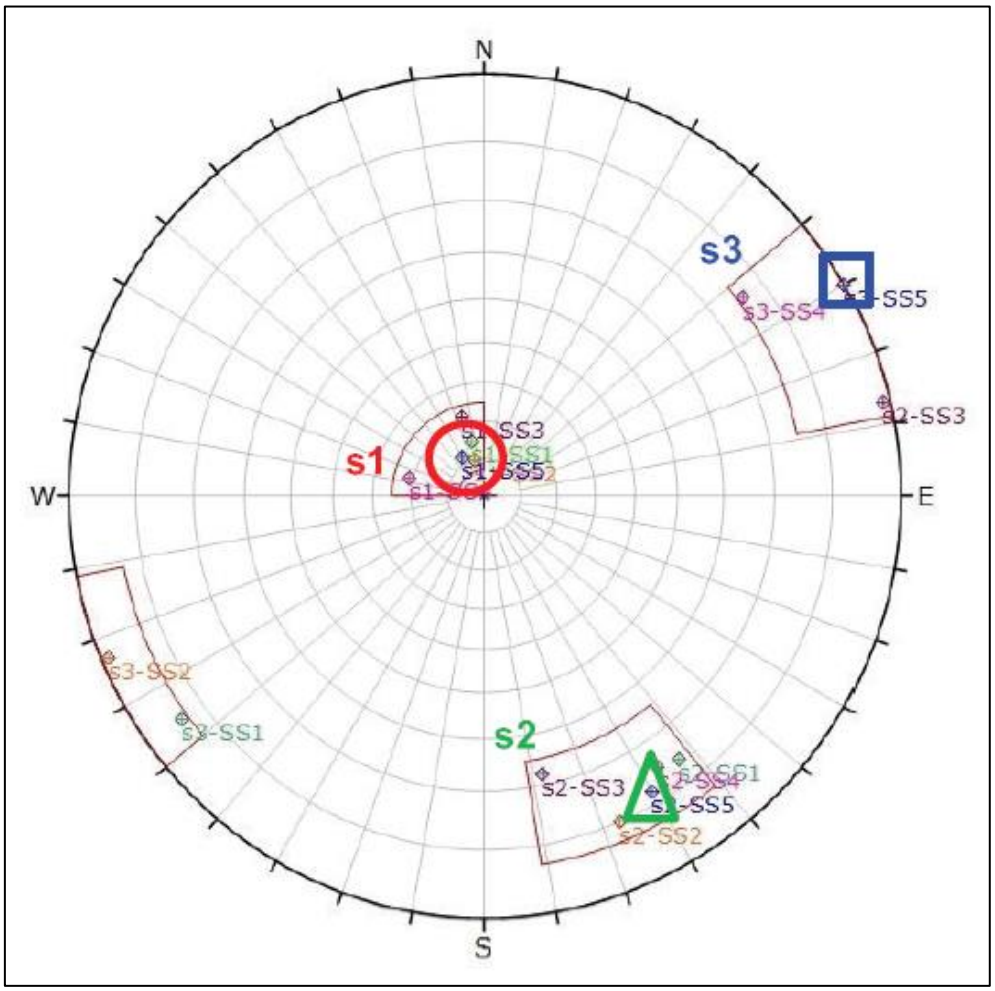

Figure 11. Lower hemispherical stereonet plot of the stress input information (Hoffman, Internal rock engineering document).

The stress tensor data from the different methods for determining the stress input is consistent, providing confidence in the stress input parameters into the model. It is important to note that the major principal stress is similar to overburden loading with orientation orthogonal to the reef plane, the intermediate principle stress k-ratio is high (0.74) with orientation parallel to the dip of the reef and the minor principle stress k-ratio is low (0.44) with orientation along the strike direction.

2.7 CLOSURE AS A DESIGN CRITERION AT MPONENG MINE

For Mponeng Mine, the modelled volumetric closure correlates well with the recorded potency, but maximum closure follows a similar trend under controlled conditions and therefore that maximum closure can be used as a modelling criterion in mine design (Scheepers et al, 2012).

For this project, seismic hazard is defined as the likelihood of having damaging seismic events in a mining area. Even though magnitude is not a complete description of the potential for damage associated with a seismic event, it is fair to say that on average the potential for damage increases with increased magnitude. The other important consideration for damage potential is distance from a working place. An event that occurs close to an excavation is much more likely to cause damage to that excavation than a distant event. Owing to the unpredictability of exact location of potential events, it is assumed that for a large number of events, it is likely that some of the events will occur near the mining faces. Therefore the larger the number of events, the higher the probability that some events will be positioned near enough a mining excavation to cause damage (Scheepers et al, 2012).

Potency was described by Mendecki (2005) as a robust parameter to describe the size of a seismic event. It is derived from the primary parameters recorded by the seismic system and can be calculated as seismic moment divided by rigidity. Potency refers to the strain change at the source and the source volume. The unit for potency is m^3.

In terms of potency, the seismic hazard is defined as the cumulative potency of all the events recorded by the seismic system per unit of time or volume of production.

A back analysis was conducted to establish the relationship between mining volume and seismic hazard at Mponeng Mine. The back analysis focussed on a number of typical raise lines where sufficient detail in terms of geology, mining span, sequence and layout in monthly mining steps as well as seismic response in the form of an event catalogue was

available. The cumulative recorded seismic potency is plotted against the cumulative production. This is called a PvP (Potency versus Production) graph (Figure 12).

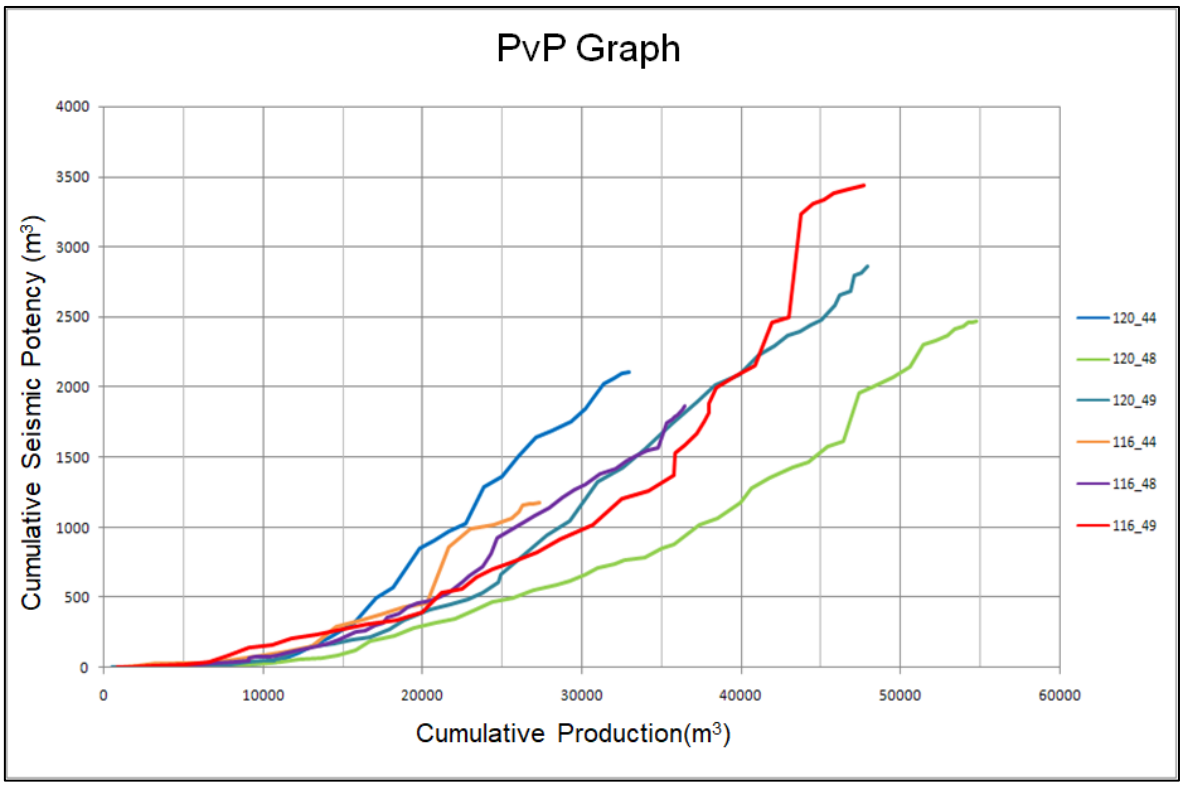

Figure 12. Cumulative Potency versus Cumulative Production for six raise lines in the back analysis (Scheepers et al, 2012).

The slope of the PvP graph represents the seismic hazard normalised to production instead of time; i.e. a steeper slope indicates a relatively higher seismic response to production as compared to a flatter slope that would indicate a lower seismic response to production. Large events tend to result in large increases in potency and towards the end of each graph the slope of the graphs become more erratic due to the large increases in potency associated with large magnitude seismic events. The trends are not identical. This shows that the unique distribution of geological discontinuities as well as unique micro sequencing and mining shapes of the different raise lines have a secondary influence on the seismic response to mining. However, from the graphs the rate of seismic response (cumulative potency) increasing with mining volume (cumulative production). At low cumulative production (when the mining spans are still small) the slope of the PvP graph is flat, indicating low

seismic response to mining. At high cumulative production (when the mining spans are nearing maximum), the slope of the PvP graph is steep, indicating high seismic response to mining.

The cumulative modelled volumetric closure is plotted against cumulative production in Figure 13.

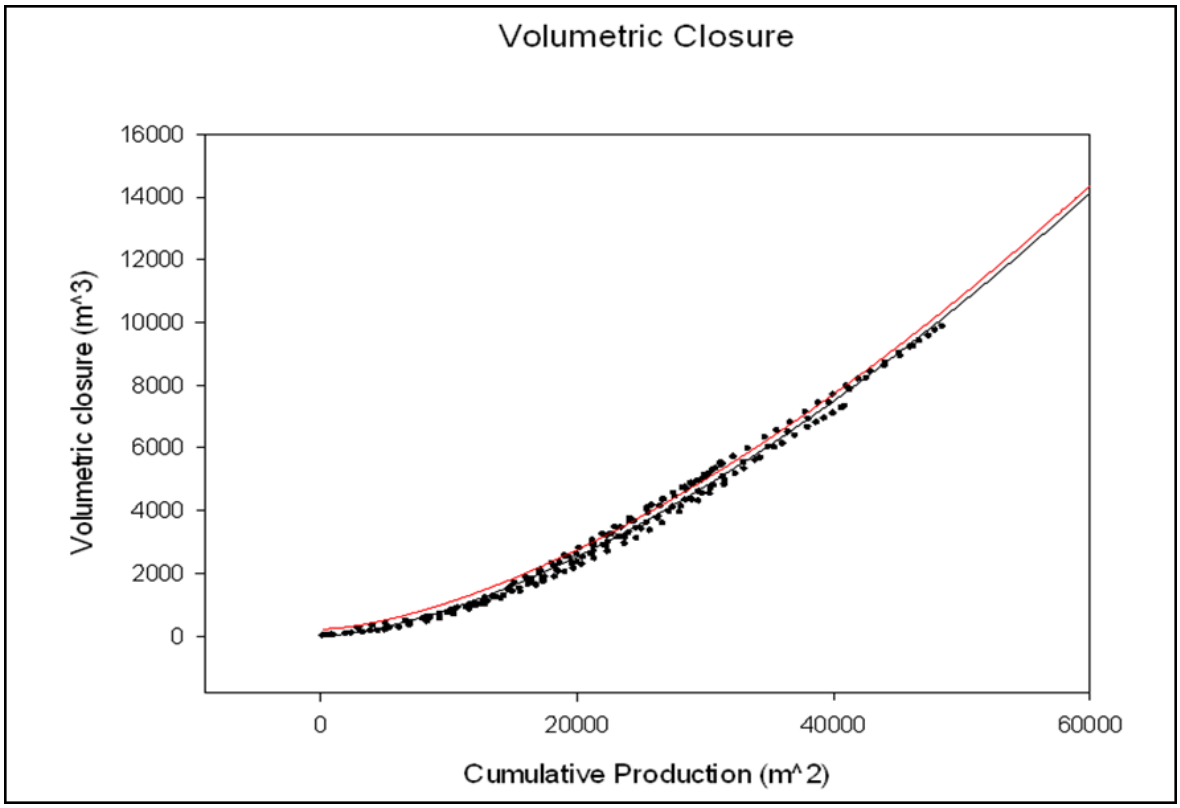

Figure 13. Modelled Cumulative Closure volume versus Cumulative Production for seven raise lines in the back analysis. The solid black line is the exponential fit though the data and the red line one standard deviation (Scheepers et al, 2012).

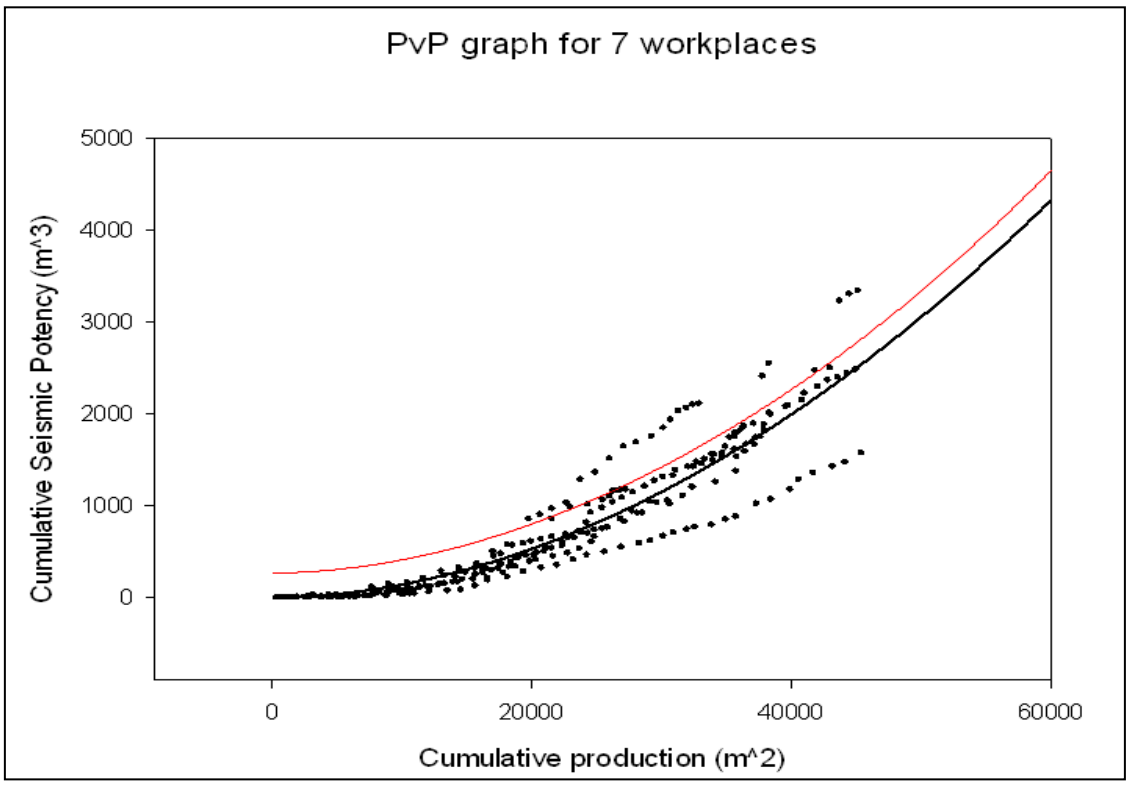

Figure 14. Cumulative seismic potency versus cumulative production for seven raise lines in the study. The solid black line is an exponential fit through the data with the red line one standard deviation (Scheepers et al, 2012).

The trends of the data indicate that the volumetric closure is low at low cumulative production (and small mining spans) and high at high cumulative production (large mining spans). This indicates that modelled closure volume appear to be a useful tool to indicate the seismic hazard.

The slope of the closure volume graph is defined as a measure of seismic hazard in terms of seismic potency per square metre mined. In Figure 15, the slope of the closure volume graph is plotted against the cumulative production. On the secondary axis, the modelled maximum closure is also plotted.

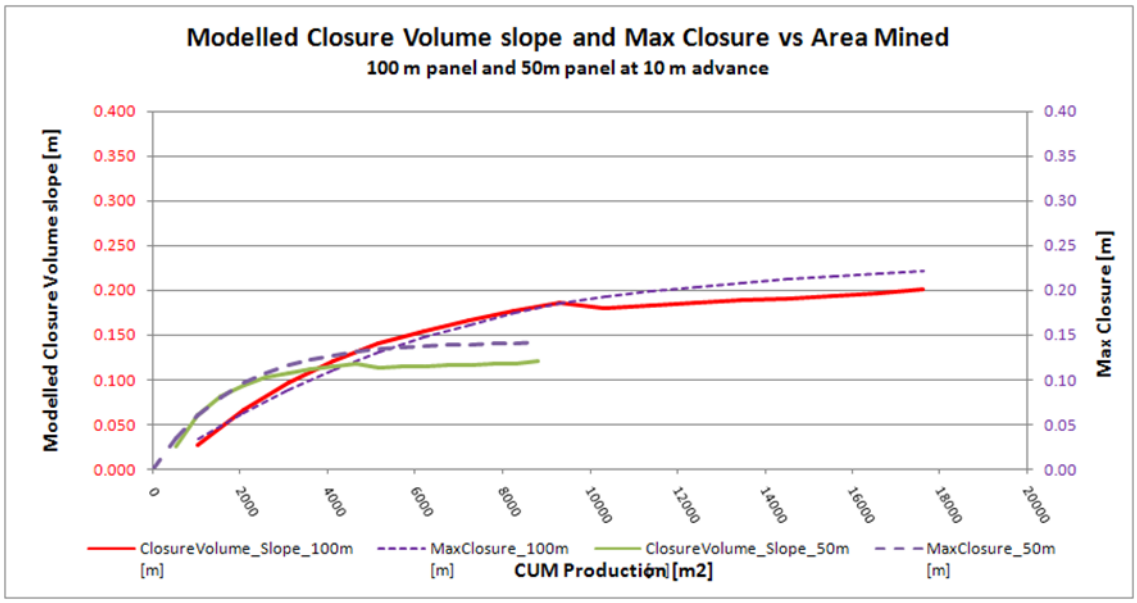

Figure 15. Modelled closure volume slope and maximum closure versus cumulative production for an idealised raise line layout (Scheepers et al, 2012).

CHAPTER 3 DATA SELECTION FOR DIFFERENT FOOTWALL LITHOLOGIES

Several parameters influence the seismic response to mining (combined effect of depth below surface, mining spans, mining geometry, rock mass properties and geological structures). For the aim of this study, it is important to isolate the rock properties' influence on the seismic response by identifying areas and time windows where the parameters that impact on the stress level (depth below surface, mining spans and mining geometry) were similar or comparable for the identified shale polygon and quartzite polygon and discarding areas and time windows where these parameters differ.

The seismic response to mining is recorded with a mine-wide seismic system consisting of 42 seismic stations, mostly 4.5 Hz geophones, and supporting hardware (seismometers, cables and modems) that communicate the recorded seismograms to a seismic server on surface in real time. The Institute of Mine Seismology (IMS) is the seismic service company that provide a contracted seismic service to Mponeng Mine, including the processing of seismograms and management of the seismic data.

The seismic system at Mponeng Mine was installed in 1996 and all recorded seismic events are kept in the Mponeng database. Between 1996 and 2001, the mining method was longwall mining. With the change from longwall mining to sequential grid mining in 2001, the normalised seismic response to mining reduced significantly due to the reduction in mining spans (from 300 m during the longwall period to 180 m for the sequential grid strategy).

In 2011 another change was made to the mine design at Mponeng in that strike pillars were introduced in addition to the dip pillars to further reduce the mining spans and associated seismic response. Owing to the impact of these changes on the seismic response to mining, only data from 2011 to 2018 are considered for this study (no further changes to the regional pillar design was made between 2011 and 2018).

3.1 SEISIMC DATA SELECTION BASED ON THE MAGNITUDE DISTRIBUTION ASSOCIATED WITH DIFFERENT FOOTWALL LITHOLOGIES (SHALE FOOTWALL AND QUARTZITE FOOTWALL)

3.1.1 Seismic data selection based on appropriate magnitude range

The annual recorded seismicity in Mponeng Mine for the period 2011 to 2018 in the different magnitude ranges are shown in Table 5 and in Figure 16. From Table 5 it is clear that the number of events recorded annually in the smaller magnitude ranges by far outnumber the number of events recorded in the larger magnitude ranges. The number of events recorded annually generally reduce with increase in magnitude range. The number of events in the small magnitude range ($-3 \leq ML < -1$) dominate the graph in Figure 16, masking any possible trends in the larger magnitude ranges. From Table 5 it seems that the number of events in the small magnitude range ($-3 \leq M < -1$) is erratic as it decreases from 158083 events recorded in 2011, to 99003 events recorded in 2012, just to pick up to 112591 in 2013 and even up to 176726 in 2014. The fluctuations in the number of events recorded annually in the small magnitude event range continued in the years 2015 to 2018 and no clear trend can be identified. The erratic nature of the recorded data in the small magnitude range is likely associated with minor changes in settings and fluctuations in the sensitivity of the seismic system. The fluctuating data in the small magnitude range cannot be used for interpretation as the likely source of the fluctuations is associated with the seismic network settings, processing protocols and sensitivity of the seismic network rather than real fluctuations in the occurrence of events.

Table 5. Annual recorded number of seismic events in Mponeng Mine in different magnitude ranges from 2011 to 2018

	Mponeng (east and west combined)					
	-3≤M<-1	-1≤M<0	0≤M<1	1≤M<2	2≤M<3	M≥3
2011	158083	17277	3499	586	57	2
2012	99003	10038	1876	321	33	2
2013	112591	11783	1696	278	50	0
2014	176726	13191	1688	263	33	0
2015	106672	11182	1311	182	12	1
2016	85381	10984	1028	116	9	1
2017	120579	15887	1377	170	12	2
2018	147222	9742	1337	220	15	2

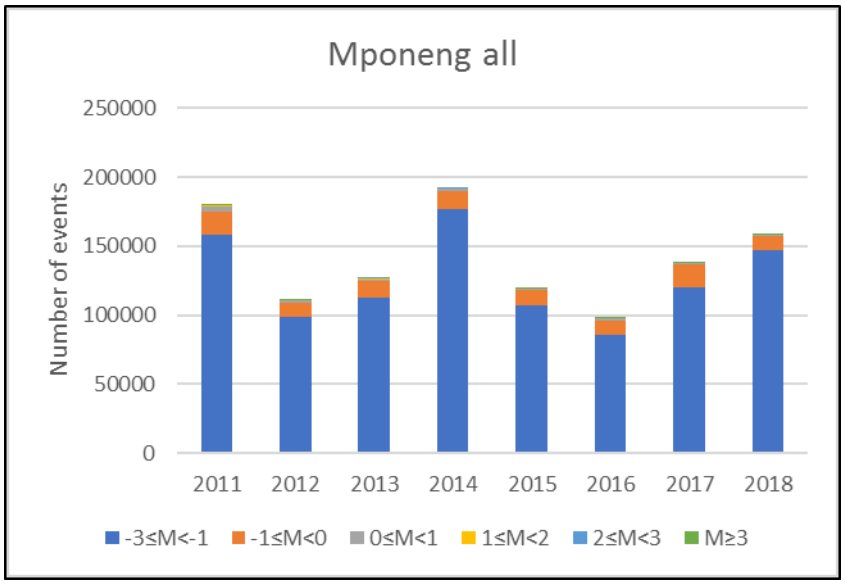

Figure 16. Graph of the recorded number of seismic events at Mponeng Mine from 2011 to 2018 for different magnitude ranges.

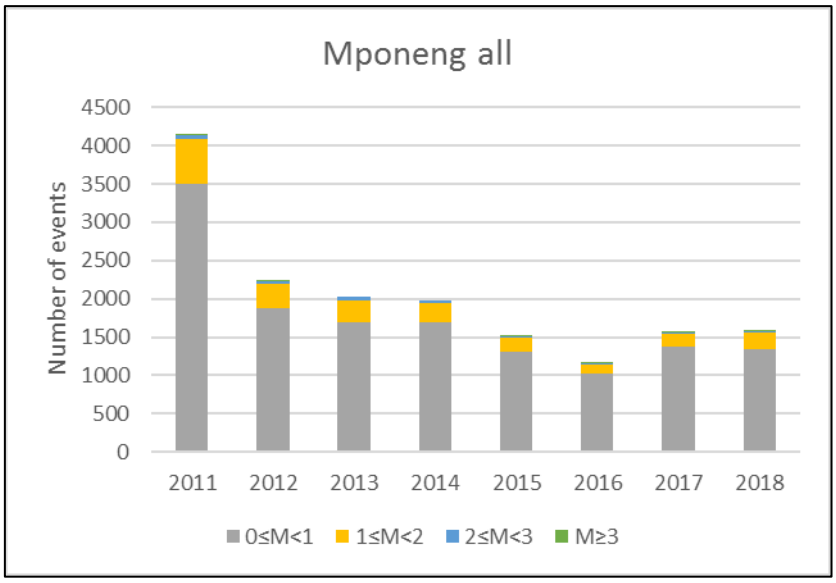

Figure 17. Graph of the recorded number of seismic events in Mponeng Mine from 2011 to 2018 for the selected magnitude range M_L = 0.0 to $M_L \geq 3.0$

Looking at the number of events in the magnitude range $M_L \geq 0$ in Table 5 and the graph in Figure 17, a trend of reducing numbers of events year-on-year from 2011 to 2016 can be identified. In 2017 the number of events increased with similar numbers also in 2018. These numbers are stable (not fluctuating due to human factors or network settings) and can be interpreted as real changes in the recorded seismicity, and therefore can be used in the seismic review in this study.

3.2 SEISMIC DATA SELECTION FOR THE DIFFERENT FOOTWALL LITHOLOGIES (SHALE FOOTWALL AND QUARTZITE FOOTWALL) BASED ON SIMILARITY OF MINING DEPTH

The seismic response to mining on Mponeng Mine is plotted on the simplified footwall geology plan to identify appropriate seismic analysis polygons to gather the appropriate data for the comparison. The intention is to separate data associated with the shale footwall from data associated with the quartzite footwall and identify time periods where the mining on the shale footwall is comparable in terms of mining depth and mining spans for proper comparison of the seismic response associated with these different footwall lithologies.

In Figure 18, the seismic events (coloured spheres) recorded in 2011 are plotted on the footwall lithology plan. The locations of seismic events are closely associated in space with the active mining faces and three distinct active mining areas can be identified where seismic analysis polygons can be drawn around data that is clustered in space. The first cluster is on the quartzite footwall on the western side of the mine. The second cluster is in the centre of the mine on the zone where the quartzite footwall transition from thin to thick. In order to support clear interpretations, this data from the transition area (from thin quartzite to thick quartzite) is excluded from the comparison, as the data from this zone may portrait a mixture of influences from the shale area as well as the quartzite area. The third cluster is on the shale footwall in the eastern side of the mine. It is possible to analyse the data from each of the polygons separately as no duplication of data exist (the polygons are sufficiently separated in space) and it is therefore possible to compare the seismicity in areas mining on the shale footwall with the seismicity in areas mining on the quartzite footwall.

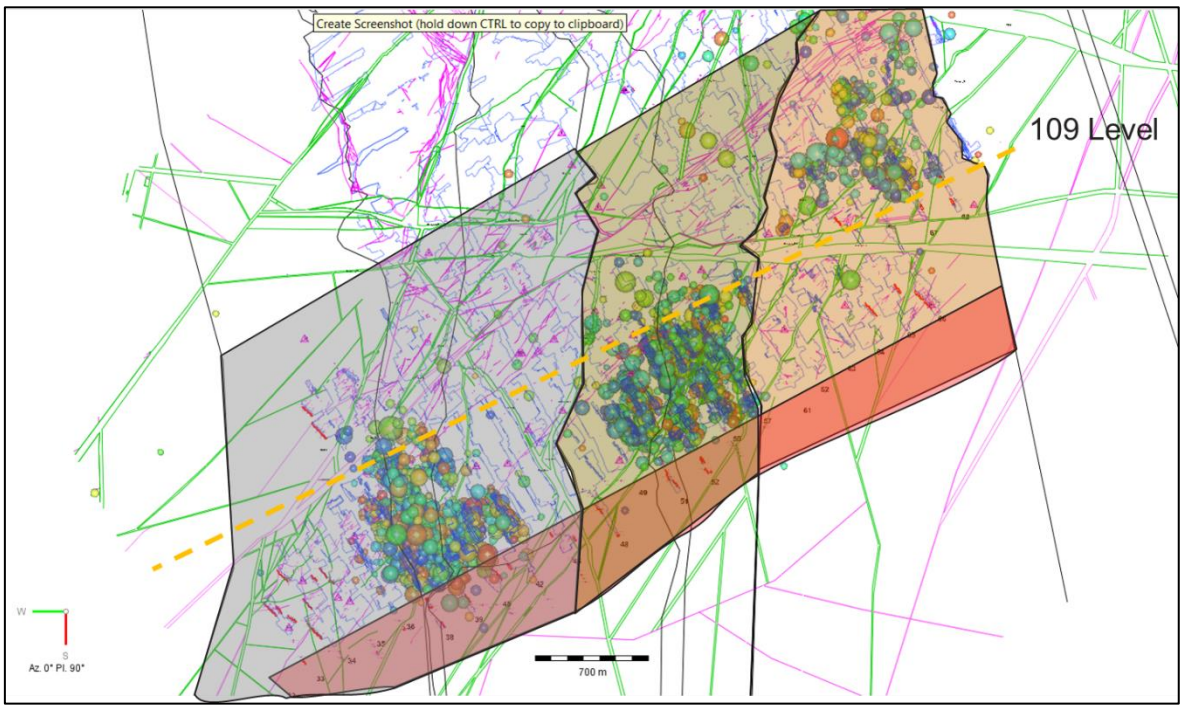

Figure 18. Recorded seismic events in 2011.

From Figure 18 it is clear that the mining in 2011 on the shale footwall (eastern side) is mostly on or above 109 level. The bulk of the mining for the same year on the quartzite footwall (western side) is on 116 and 120 levels, significantly deeper in comparison. It can therefore be expected that the difference in mining depth will be the primary reason for a difference in the seismic response (if identified). For this reason, it was decided to exclude data from 2011 in this project comparison.

The same discussion is valid for the years 2012 to 2014 (Figures 21 to 23) where the mining on the east side on the shale footwall was on average shallower than the mining on the western side on the quartzite footwall. In these years the mining on the eastern side slowly progressed further south (deeper) year-on-year to 116 and 120 levels, whilst the mining on the quartzite footwall on the western side of the mine progressed further west and remained on 116 and 120 levels for the same time period. Due to the difference in mining depth, the data from these years were also excluded from the project comparison.

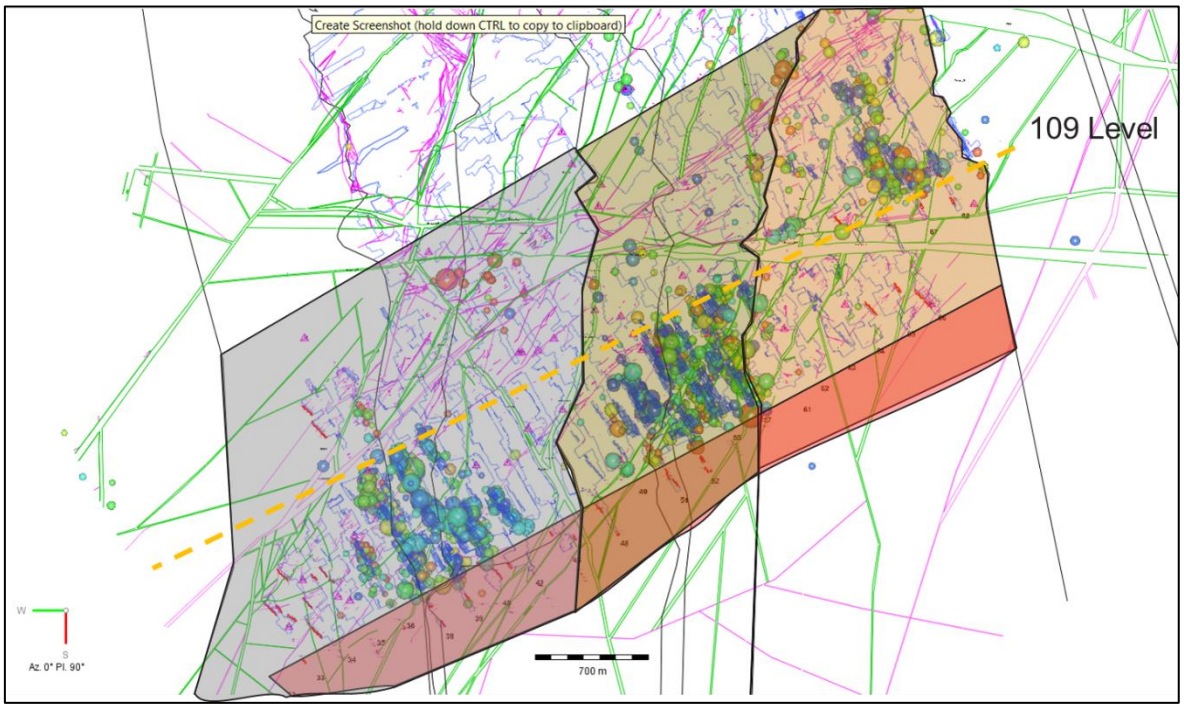

Figure 19. Recorded seismic events in 2012.

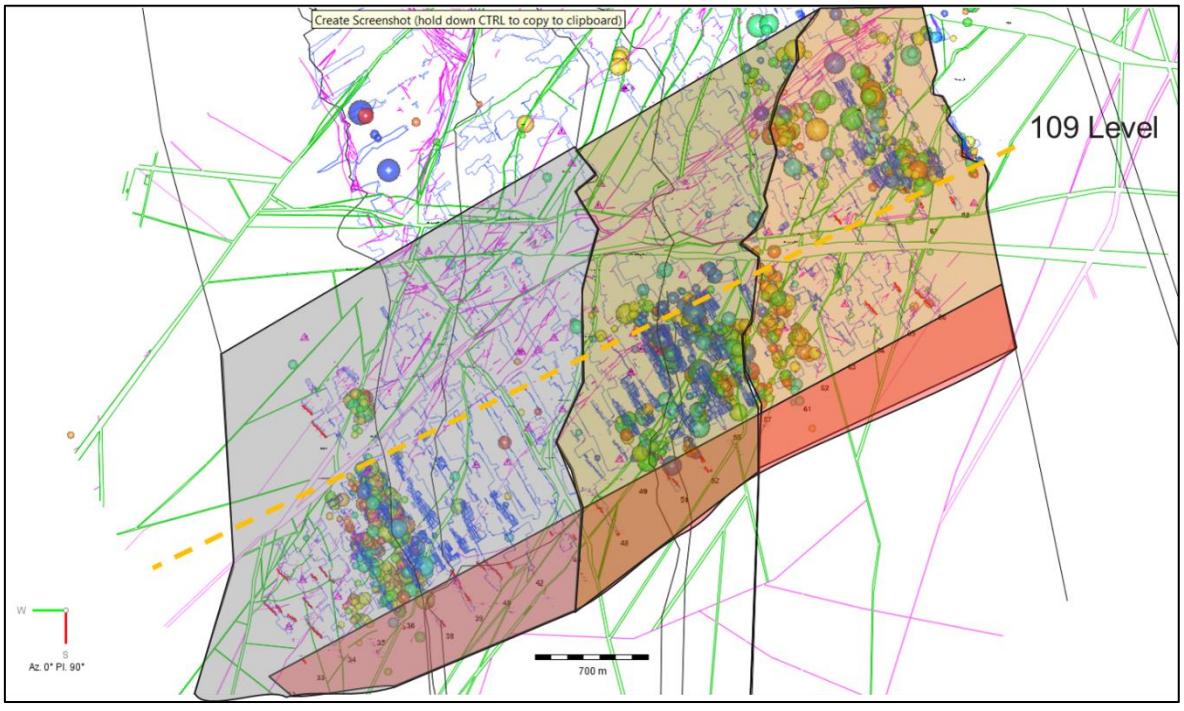

Figure 20. Recorded seismic events in 2013.

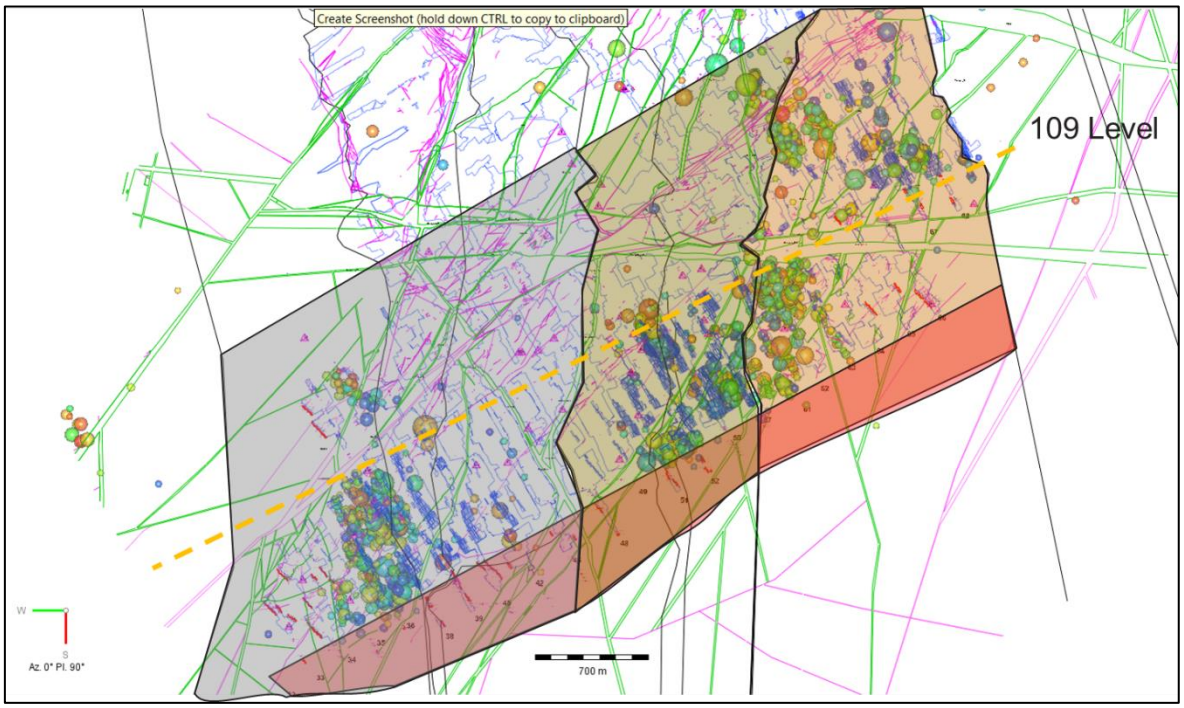

Figure 21. Recorded seismic events in 2014.

By 2015, most of the mining on the shale footwall was on the same level as the mining on the western side of the mine (116 and 120 level - Figure 22), but the volume of mining in 2015 on the eastern side of the mine on the shale footwall was low compared to the mining on the quartzite footwall (western side). More importantly the mining spans were small on the eastern side of then mine compared to the western side (new raiselines), therefore it was decided to also exclude 2015 from the data comparison in this project.

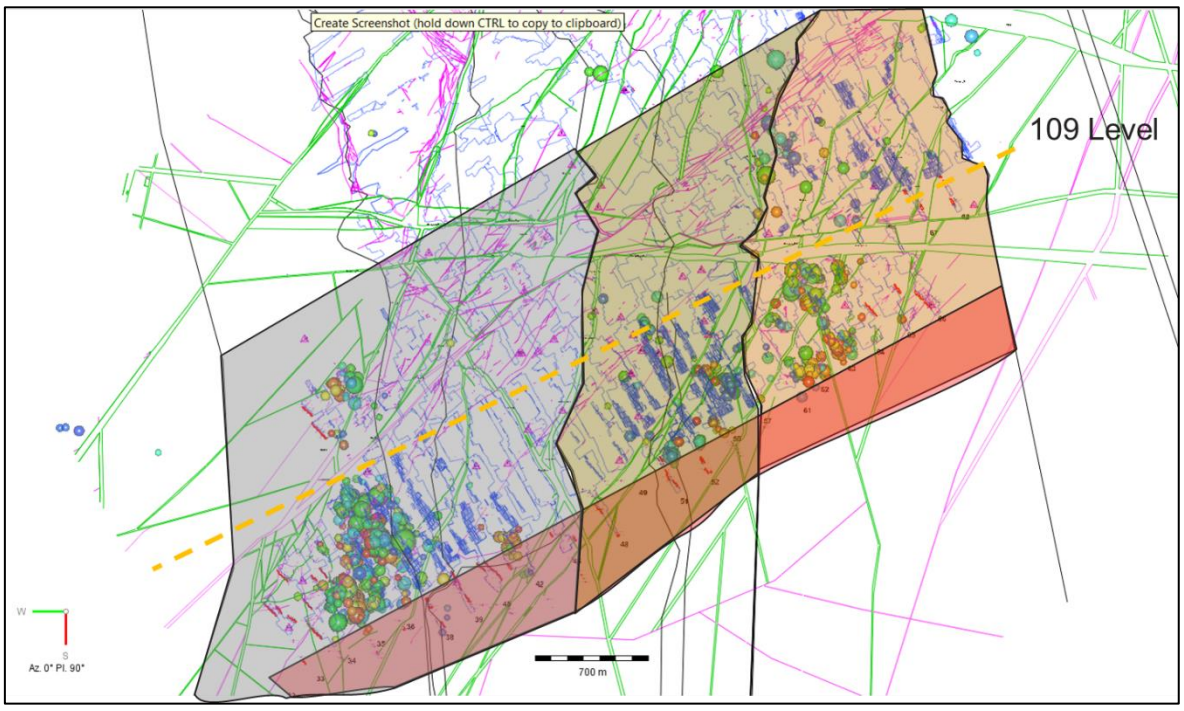

Figure 22. Recorded seismic events in 2015.

In the years 2016 to 2018 (Figures 25 to 27), the mining levels and yearly volumes were comparable between the shale area and the quartzite area, but the mining volumes below 120 Level on the quartzite footwall increased year-on-year. This is, however, easy to exclude from the comparison polygons based on clustering. It was therefore decided that the focus of this study will be on the three years (2016 to 2018) on the above 120 Level data. This strict data selection is deemed prudent to ensure a fair comparison that only accounts for the influence of the footwall lithology without the influence of additional factors on the seismic response to mining.

Based on the discussion above, the polygons for data comparison were adapted to suit the appropriate data to be used in each year.

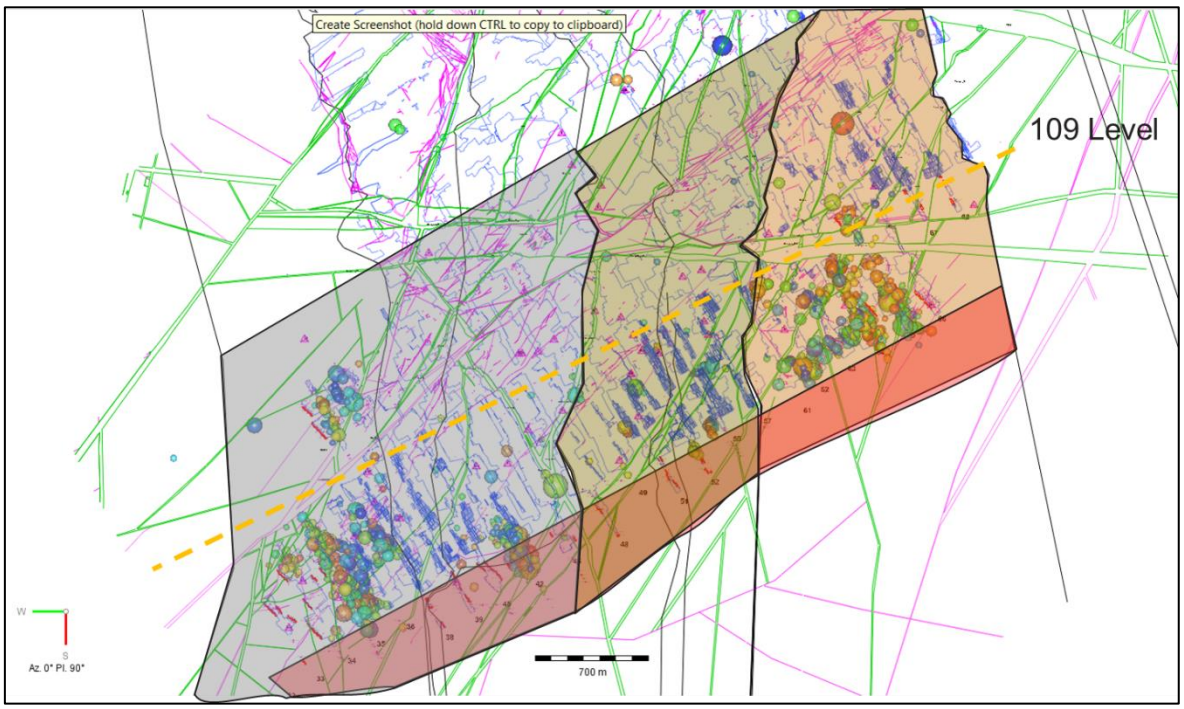

Figure 23. Recorded seismic events in 2016.

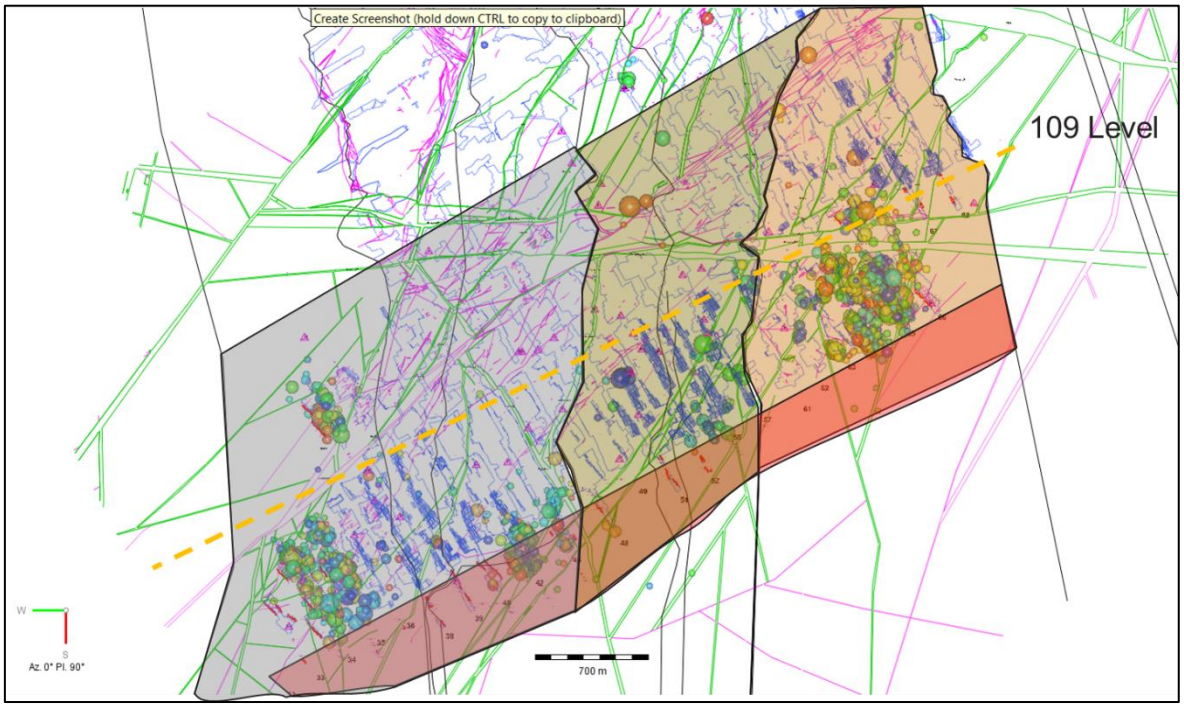

Figure 24. Recorded seismic events in 2017.

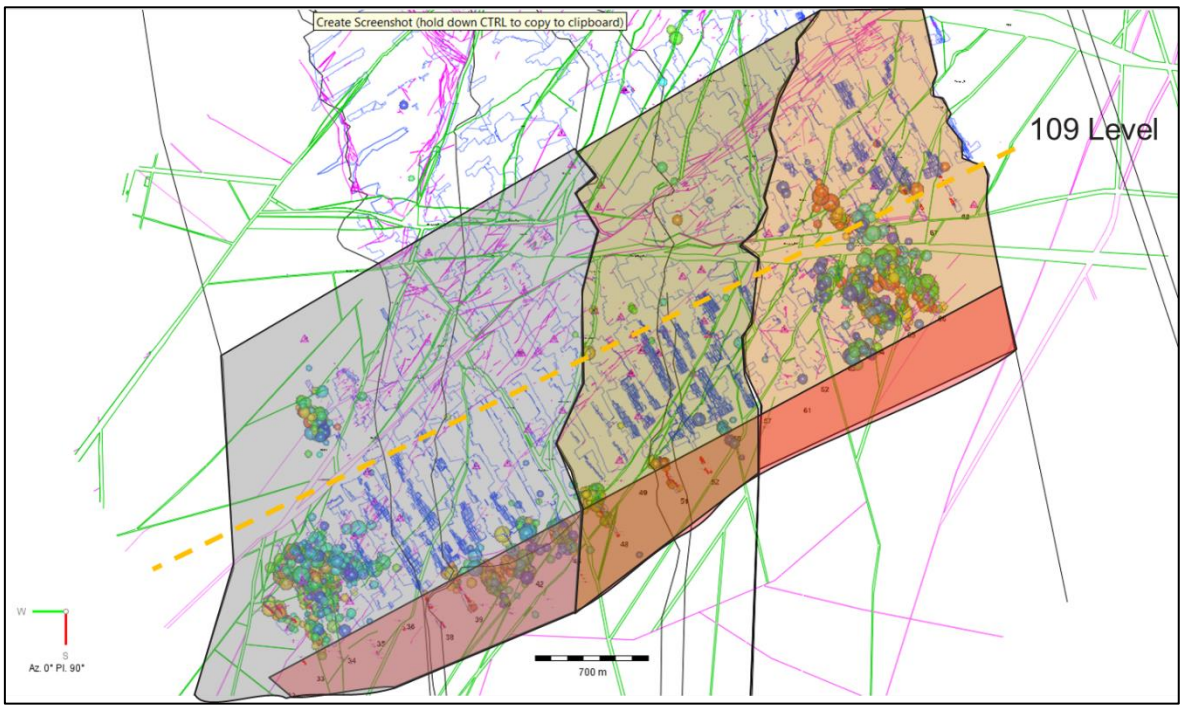

Figure 25. Recorded seismic events in 2018.

3.3 SEISMIC DATA SELECTION BASED ON MODELLED ERR TO TEST FOR SIMILAR STRESS CONDITIONS

3.3.1 ERR modelling rationale

The act of straining an elastic body requires input of work, and this is stored in the form of elastic strain energy (Ryder and Jager, 2002). The strain energy density, W, at a given point in the body is given by:

$$W = \int \sigma \, d\varepsilon \text{ [J/m}^3\text{] (Ryder and Jager, 2002)} \quad (3.3.1)$$

For a linear elastic material:

$$W = \tfrac{1}{2}(\sigma_1\varepsilon_1 + \sigma_2\varepsilon_2 + \sigma_3\varepsilon_3) \text{ (Ryder and Jager, 2002)} \quad (3.3.2)$$

A reasonable assumption for the rock found at Mponeng Mine, is that they exbibit linear elastic behaviour up to the point of the onset of internal damage, followed by ultimate failure. The rock mass remote from mine openings is confined and therefore strong. It is reasonable to assume linear elastic behaviour even under high stress conditions. Due to high stress and low confinement , it is mostly the rock mass in close proximity to mining excavations that are strained beyond the elastic limit and therefore behave inelastically in the form of fracturing and other inelastic behaviour.

If a horizontal stope is enlarged by mining an area ΔA, and the resulting change in volumetric convergence in the stope is ΔV, then the change in potential energy of the overlying strata is $q_v \Delta V$, where q_v is the virgin vertical stress. If no significant support is present, then one half of the energy change is stored as extra strain energy in the rock mass. The remaining one half is immediately released (in the form of shearing/crushing/heating of the fracture zone in front of the face). This released energy, in MJ per unit face advance area ΔA, is called the (spatial) Energy Release Rate (ERR) (Jager and Ryder, 1999):

$$\text{ERR} = \tfrac{1}{2} q_v \, \Delta V / \Delta A \quad (3.3.3)$$

In other words, ERR is calculated from the stress and change in closure associated with a mining step.

Energy Release Rate (ERR) is a convenient, and relatively easily calculated, measure of the severity of mining conditions at depth (Ryder and Jager, 2002). ERR is a measure of the stress concentration associated with tabular mining faces and is expressed in MJ/m².

3.3.2 ERR modelling results

AGA SAR contracts IMS to do routine modelling analysis, including monthly ERR (Energy Release Rate). IMS uses an in-house developed elastic modelling program for the routine modelling.

In Figure 28, the modelled ERR for the areas compared in the study are shown; i.e. shale footwall area (east) as well as the quartzite footwall area (west). The ERR values used for the graph are the calculated average ERR of all the active mining panels for each month in a polygon. Of importance is that the modelled ERR associated with inactive panels (not mined in that month) are not included in the calculated average. This is important when the seismic response is compared to the modelled ERR (later) as the seismic response will be associated primarily with the active mining panels (as this is where the highest localised stress changes occur). When the two graphs are compared, it is noted that the modelled ERR levels are comparable for the two areas in the years 2016 to 2018. Furthermore, the average ERR values trend upwards with time from 2016 to 2018, and this is associated with increased mining spans in the raise lines in those years.

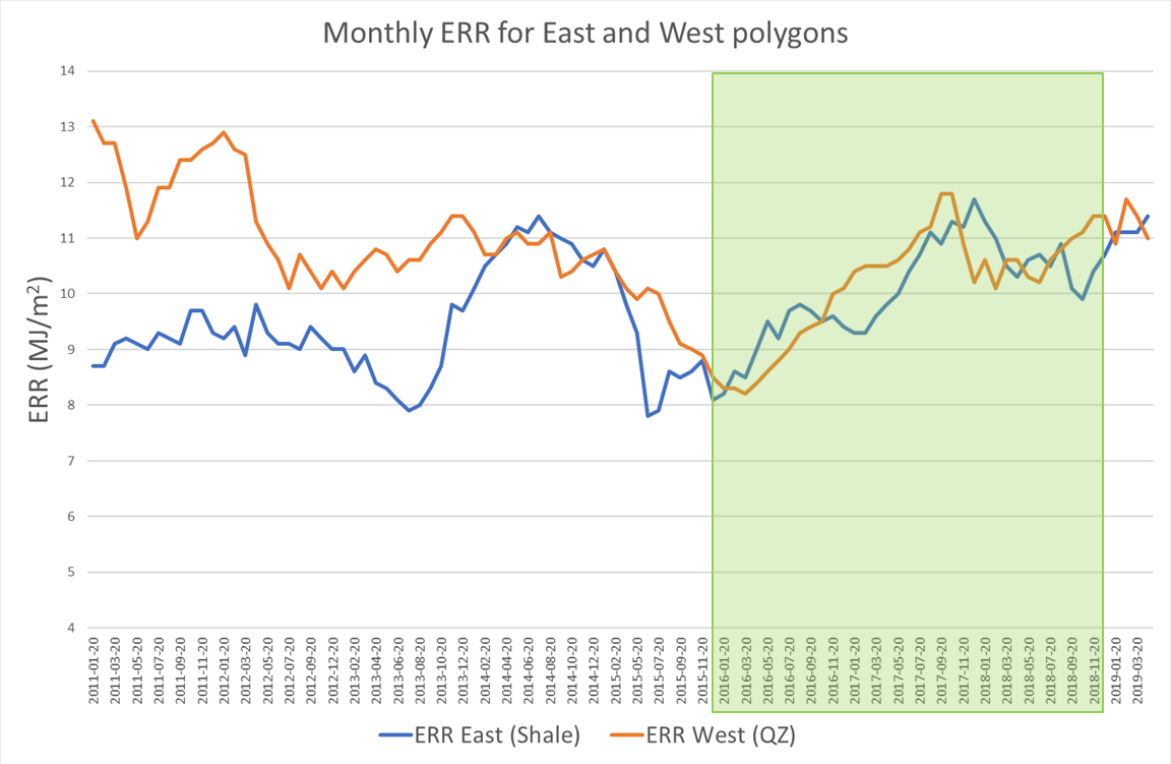

Figure 26. Monthly modelled Energy Release Rate (ERR) for the shale footwall (East) and quartzite footwall (West) polygons with the years 2016 to 2018 highlighted in green.

3.4 SEISMIC DATA SELECTION BASED ON CLOSURE MODELLING FOR SIMILARITY OF STRESS AND MINING SPANS

3.4.1 Closure modelling rationale

McGarr, A. Wiebols GA.1977, proposed that the overall seismic deformation or integrated seismicity is measured by ΣM_0, the summation of all seismic moments of tremors in a given region and time period. ΣM_0 is related to the mining by

$$\Sigma M_0 = G\Delta V_c \tag{3.4.1}$$

Where G is the modulus of rigidity and ΔV_c is the volume of stope closure due to mining (McGarr, A. Wiebols, G.A., 1977). It can be interpreted that mining areas where the closure volume is high will experience more and larger events compared to mining areas where the closure volume is low (for similar rockmass properties). As simple volumetric closure calculation was conducted. Of particular interest was the relationship between the maximum closure recorded in the stope and the volumetric closure.

Closure for a two-dimensional plain strain parallel sided stope (simple geometry) is given by the formula (Budavari, 1983):

$$S_z = \frac{2(1-\nu)q}{G}\sqrt{l^2 - x^2} \tag{3.4.2}$$

Where S_z is the vertical convergence (elastic component of closure), *v* is the Poisson's ratio of the rock mass, *q* is the vertical virgin stress, *G* is the modulus of rigidity of the rock mass (and can be calculated from $G = E/(2(1+\nu))$, *l* is the excavation half-span and *x* is the distance from the excavation centre line.

This formula can be used to calculate the closure at any distance from the excavation face. Closure is a maximum at the maximum distance from the excavation face, i.e. where x = l, and the maximum closure is then calculated from the formula:

$$S_{zmax} = \frac{2(1-\nu)ql}{G} \tag{3.4.2}$$

The volume of closure (m^3)for the same simple 2D plain strain geometry can be calculated by integrating equation 3.4.1 along the length of the stope from *–l* to *l* where the out of plane dimension is assumed to be given by b :

$$V_c = b\int_{-l}^{l}\frac{2(1-\nu)q}{G}\sqrt{l^2-x^2}\,dx$$
$$=\frac{2(1-\nu)qb}{G}\int_{-l}^{l}\sqrt{l^2-x^2}\,dx$$
$$=\frac{2(1-\nu)qb}{G}\int_{-l}^{l}(l^2-x^2)^{½}\,dx$$
$$=\frac{2(1-\nu)qb}{G}.\frac{\pi l^2}{2} \qquad (3.4.4)$$

This equation can be rewritten as:

$$V_c=\frac{2(1-\nu)ql}{G}.\frac{\pi bl}{2} \qquad (3.4.5)$$

Substituting equation (3.4.2) in equation (3.4.4) we get:

$$V_c = S_{zmax}.\frac{\pi bl}{2} \qquad (3.4.6)$$

This is considered an important result as it illustrates that the volumetric closure is proportional to the maximum closure. That is, for this simple stope geometry (two-dimensional horizontal slot in a perfectly elastic medium), the closure volume scales with maximum closure in that, for the simple geometry two-dimensional stope, the closure volume is calculated from the maximum closure, multiplied by the product of the excavation span and the out of plane dimension *b* (and a constant $^{\pi}/_{2}$).

Numerical modelling takes care of the geometry complexity and modelled maximum closure can be used to compare mining areas with different mining geometries. For this modelling, the input parameters are kept similar for the entire mine as the influence of mining depth and mining geometry (impacting on stress redistribution) is the focus of this exercise.

3.4.2 Closure modelling results

Historcally the influence of the footwall rock type was not considered in modelling-based mine design and modelling input parameters were not changed for modelling to compare maximum closure for mining on the shale footwall with maximum closure for mining on the quartzite footwall (using similar rock mass input parameters). In Figure 27 the closure for the western side of the mine (quartzite footwall) is shown. The red colours represent higher closure values and the green colours lower closure values. The scale setting for the legend is set to show values between 0 and 0.27 m maximum so that all closure values in excess of 0.27 m are shown in grey. This is the calibrated design criterion for determining strike pillar positions for the new mine design at Mponeng Mine (Scheepers et al, 2012). This design criterion is based on a study of the seismic response to mining for increased mining spans at Mponeng Mine where it is shown that the seismic response to mining can be managed by breaking up the mining span through the implementation of strike pillars in addition to the dip pillars implemented at the mine. The spacing or positioning of the strike pillars are determined through modelling, using the maximum closure design criterion of 0.27 m.

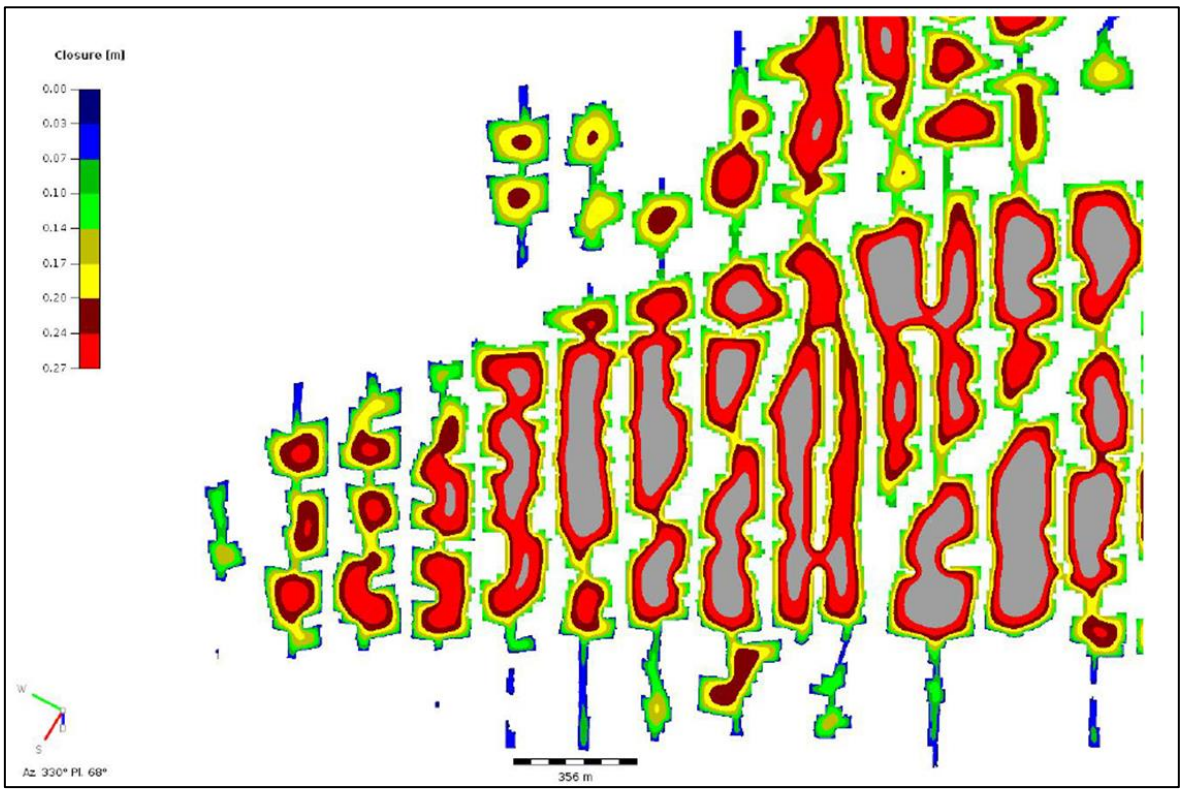

Figure 27 Modelled maximum closure for the west side of the mine (on quartzite footwall) for the layout in December 2018.

From this view of modelled closure, it is clear that the recent mining to the west, where the strike pillar strategy is fully implemented (last 4 raise lines to the west), do not exceed the design criterion of 0.27 m maximum modelled closure, and that prior to implementation of this design criterion (older mining) the modelled maximum closure exceeded 0.27 m in nearly all the raise lines. In Figure 28, the modelled closure is shown for the eastern side of the mine (shale footwall) and it is clear that the recent mining (last six raise lines to the east) also complies with the maximum closure criterion. Owing to low grade patches in this area, some ground has not been mined and the extraction ratio is even lower than designed and the associated modelled maximum closure is also even lower than the modelled maximum closure on the western side of the mine. This indicates that the seismic response on the eastern side of the mine is expected to be slightly lower than the seismic response on the western side of the mine based on the hypothesis that the seismic response is proportional to closure volume (McGarr and Wiebols, 1977) or maximum closure.

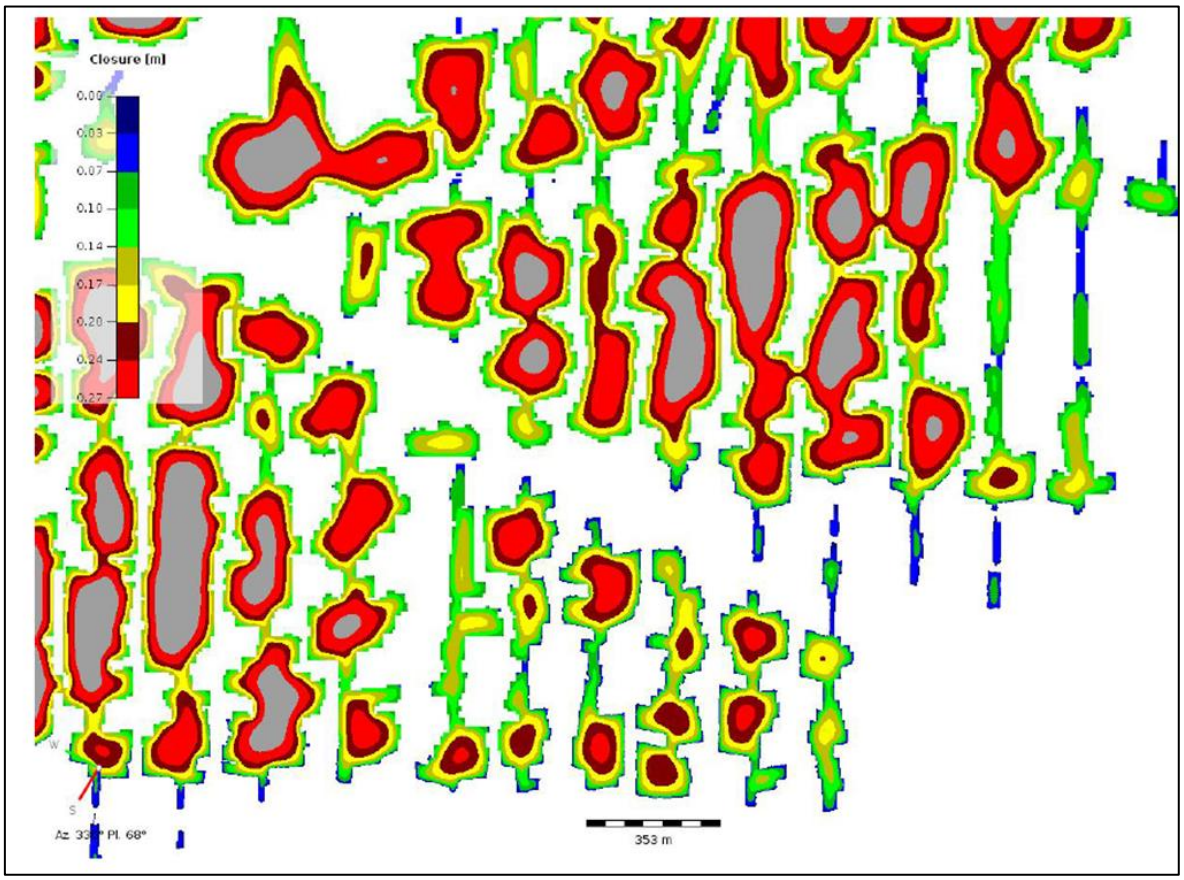

Figure 28. Modelled maximum closure for the east side of the mine (shale footwall).

3.5 SEISIMIC DATA SELECTION: EVENT SOURCE MECHANISMS

In this study, the influence of the footwall rock type needs to be isolated from other factors, including geological structures. Geological structures are generally weak along contact planes and allow for slip if excess shear stress, caused by the field stresses, exist on the structure. Seismicity caused by structures is therefore dominated by the shear strength of the contact planes and not the footwall lithology. Very little data in terms of the strength properties of geological contact planes are available, therefore, if most events in the study are structure related, it will be near impossible to isolate the impact of footwall lithology on the seismic response to mining.

In the literature study (Chapter 2), different event source mechanisms were discussed, and it was indicated that the magnitude of events on geological features can be very large (up to magnitude M_L = 5.0) and events associated with mining abutments, including face related Ortlepp shears (that may cause face parallel bursts) can be in the magnitude range up to magnitude M_L = 3.0. The magnitude range of events associated with geological structures overlap with the magnitude range of events associated with face related Ortlepp shears, and event magnitude is therefore not a reliable parameter for identifying the source mechanism of a seismic event.

Event location can be used as a tool to identify the most likely source of a seismic event and when the source is known, the source mechanism can be assumed. For example, if an event is located on a geological structure, it can be assumed that the structure is the source of the seismic event and hence that the source mechanism is slip on the geological structure plane. Or if an event is located on a mining abutment, it can be assumed that the mining abutment is the most likely source of the seismic event and that the source mechanism is face parallel shear through intact rock (Ortlepp shear). Location accuracy directly impacts on event location as a tool to identify the source mechanism. In narrow tabular mining operations, like Mponeng Mine, where the seismometers are installed in a narrow envelope around the reef horizon and spread over a large area to cover the horizontal extent of mining, location

accuracy is insufficient to be used as a tool to identify the likely source. Often several potential seismic sources can be identified within the excepted location accuracy limits of the seismic network for a single event. Additional tools are required to identify the most likely source and source mechanism of individual seismic events.

Observed damage to mining excavations is a useful tool to confirm event location and source mechanism, but is also insufficient on its own as a tool to identify the source and source mechanism of seismic events in general as most events do not cause observable damage and where damage is observed, the damage mechanism is controlled more by the rock mass properties and stress field surrounding the mining excavation than the event mechanism (refer to the example discussed below).

A tool that is often used by seismologists to describe the source mechanism of a seismic event is called Moment Tensor Inversion (as described in the literature study in Chapter 2). This is a numerical technique aimed at giving a more general and more accurate description of the seismic source by decomposing the event source into different components that are more easily described or understood. Typically, an event source can be described as a combination of three potential components; that is: Isotropic component, that describes the three dimensional volume change associated with an event and interpreted as bursting mechanism, Compensated Linear Vector Dipole component, that describes uniaxial compression and radial dilation at the source without volume change and interpreted as pillar failure mechanism, and Double Couple (DC) component, that describes pure slip on a simple plane and is interpreted as either slip on a geological structure or shear through intact rock (Ortlepp shear). Importantly, the likely orientation of the source plane and direction of slip is given by the orientation of the nodal planes of the DC component.

It is important to have confidence in the moment tensor solutions if it is to be used in event source interpretation. The only check available in terms of the correct identification of source mechanism and orientation is a comparison between the reported moment tensor solution event mechanism and observations from an underground investigation where the failure

mechanism (in reaction to the source mechanism) can be observed. A case study of such a comparison is detailed below.

A magnitude 3.1 event occurred on the eastern side of the mine in the shale footwall area with reported damage to the travelling way and the gully (Figure 29). The reported damage location gave confidence in the event location.

The damaged area was visited. The area in the gully, where specific damage mechanisms were observed, is shown in detail in Figure 30. Five different damage mechanisms were observed in the gully.

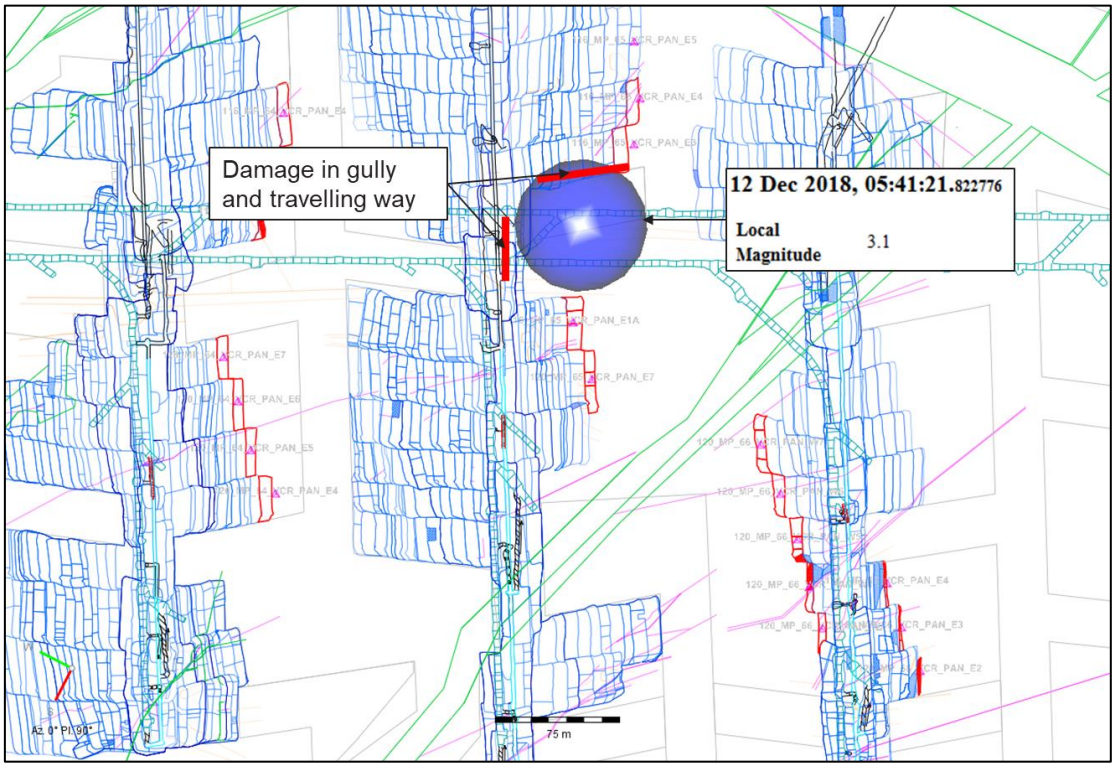

Figure 29. Location of the M3.1 event and reported damage areas.

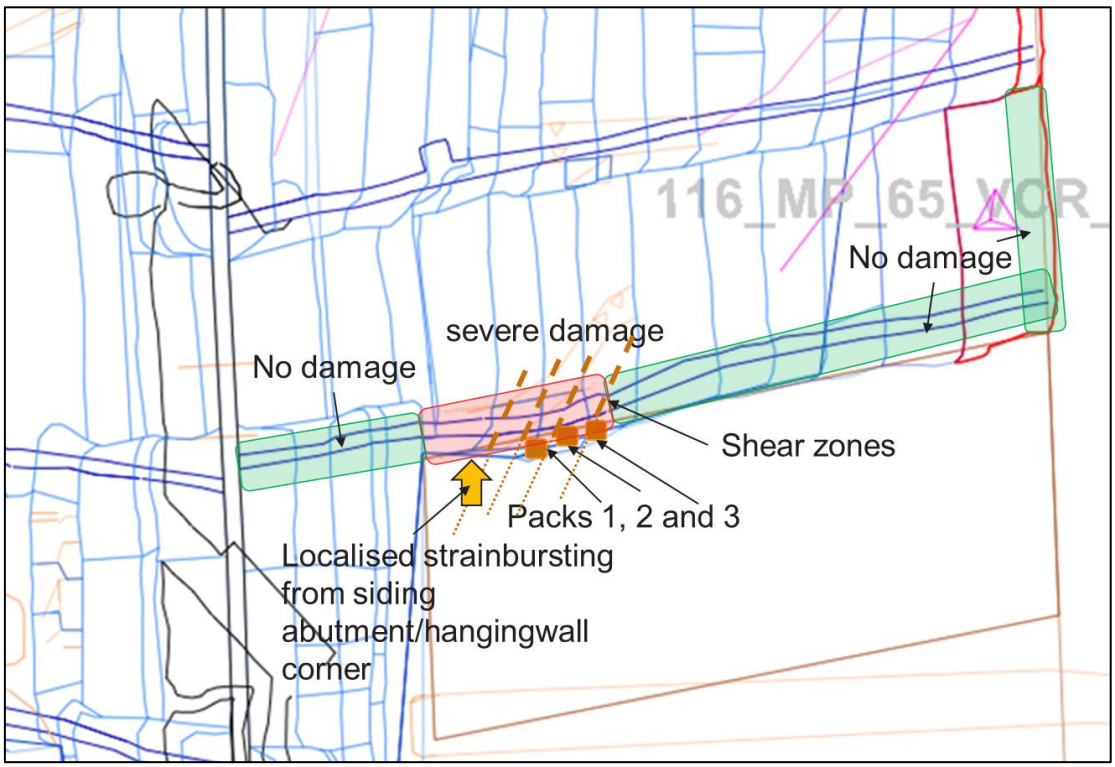

Figure 30. Detailed location of observed damage.

Figure 31. Shear zone observed in gully northern sidewall and stope footwall.

The first damage mechanism observed was the formation of shear fractures; four shear fractures or shear zones were observed in the gully northern siding and stope footwall. One such shear zone is shown in Figure 31. This is not a common occurrence as new fractures or fracture zones do not normally propagate through the already fractured footwall rock. It can be assumed that the shear fractures or shear zones are part of the source mechanism and that the intensity of the shear fractures was such that it did not terminate on the fractured footwall but managed to propagate through the fractured zone and only terminated on the footwall free surface. The orientations of the shear fracture planes were north-northeast to south-southwest.

Figure 32. Observed strain burst from south siding corner with hanging wall.

The second damage mechanism was a secondary strain burst, triggered by the main shock; ejected rock from a localised strain burst was observed in the gully. The ejection velocity was sufficient to throw the rock fragments approximately three metres (up dip at 22°) from the gully siding corner with the hanging wall to the gully. The rock fragments showed clear mirror zones (fracture patterns often associated with the type of fractures associated with strain bursts). Similarly, mirror zones were observed in the hanging wall from where the rock fragments were ejected.

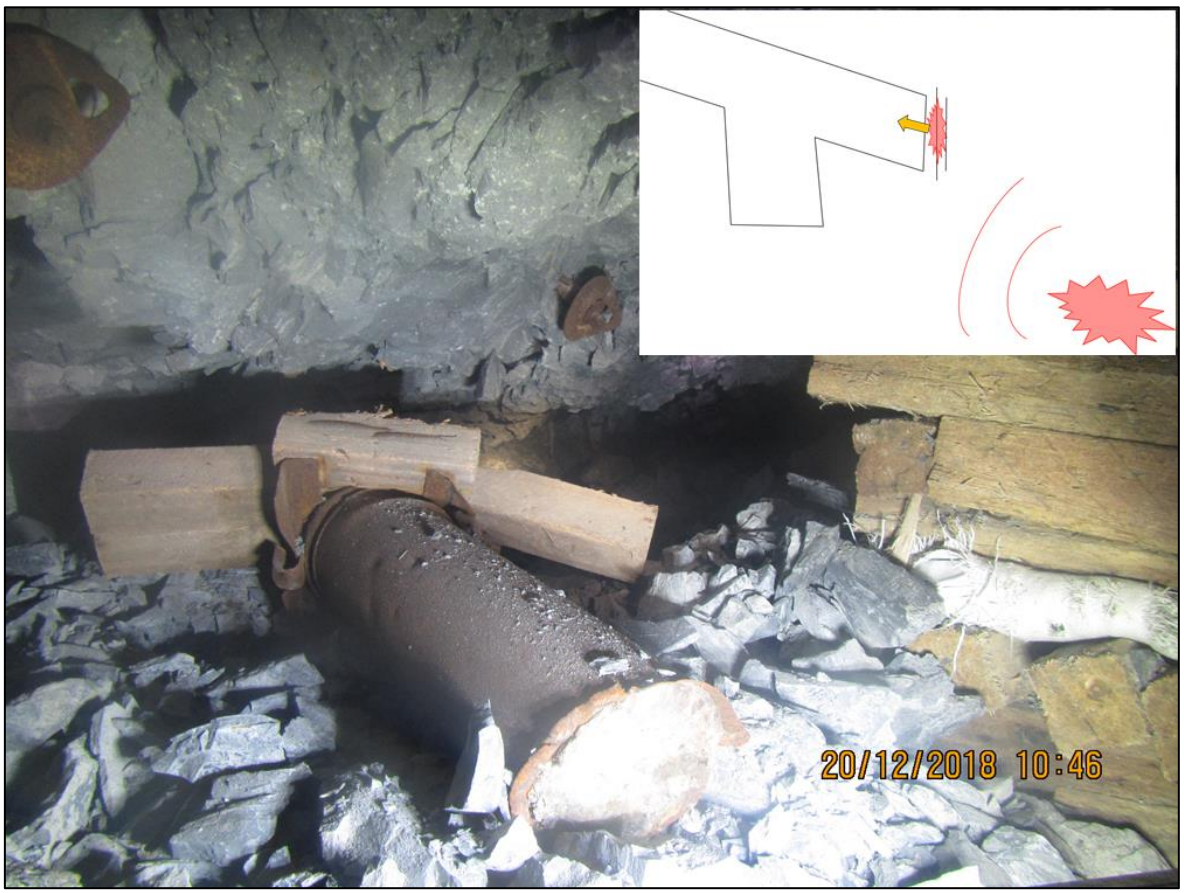

Figure 33. Observed ejection from south siding abutment.

The third damage mechanism was face bursting from the siding abutment, ejecting fist sized rock fragments into the siding and completely filling the siding. The ejected rock fragments impacted on some elongate support units that had been installed in the siding. In Figure 33, an example of a dislodged elongate is shown; the side impact on the elongate caused it to break and dislodge. Note that no falls occurred from the hangingwall.

Figure 34. Siding sidewall (southern) movement and pack shear.

The fourth damage mechanism is shown in Figure 34 where one of the packs that had been installed in the siding, sheared through due to excessive relative movement between the footwall and the hanging wall at the pack. The hanging wall is again intact (no falls from the hangingwall). The observed footwall movement is upwards and inwards into the gully (northwards). The footwall is still in relatively good condition and it is argued that the movement is associated with the bulking of the footwall deeper into the gully sidewall and siding footwall where new fractures caused the bulking due to a rapid increase in volume of the newly fractured rock. The new fractures are associated with the transient stress wave radiated from the seismic source at the time of the M 3.1 event.

Figure 35. Footwall heave in south siding.

The fifth damage mechanism is shown in Figure 34, where one of the packs that had been installed in the siding completely dislodged, and footwall heave was observed. The footwall is almost in contact with the hangingwall and it can be deduced that footwall heave in excess of 1.0 m occurred. The footwall heave is likely associated with the bulking of the footwall deeper into the gully sidewall and siding footwall where new fractures caused the bulking due to a rapid increase in volume of the newly fractured rock. The new fractures are associated with the transient stress wave radiated from the seismic source at the time of the M3.1 event.

From the discussion of the five observed damage mechanisms associated with the event, it is clear that the observed damage mechanism may not always explain the source mechanism

of the event. But in this case the presence of the shear fractures is likely directly associated with the shear mechanism of the M3.1 event.

IMS is the routine seismic data service provider to Mponeng Mine and also provides moment tensor solutions for events when requested by the mine. The moment tensor solution of the M3.1 event is shown in Figure 36:

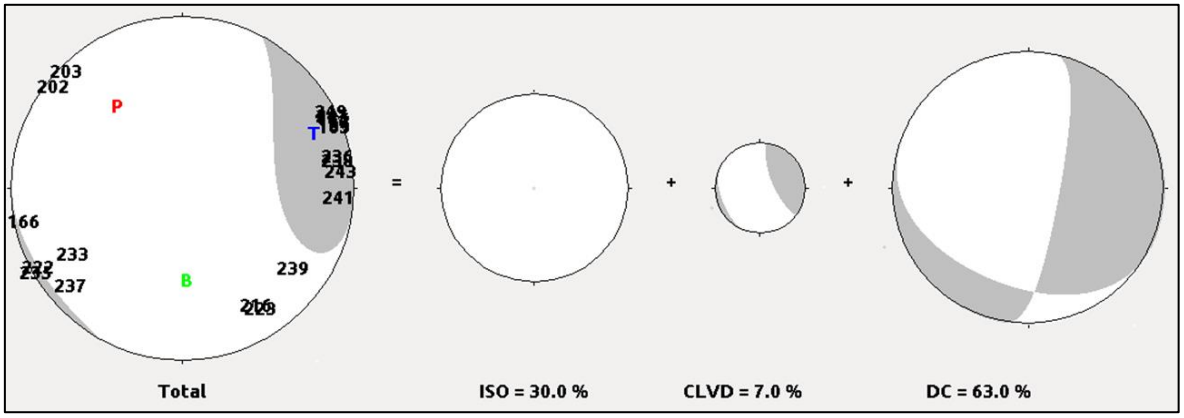

Figure 36. Moment tensor solution of the M3.1 event.

With reference to the moment tensor discussion in Chapter 2, the isotropic component (ISO = 30%) indicates that a large component of the event mechanism can be attributed to implosive volume change at the source. This typically indicates that stope closure and bursting occurred during the event and that the event was therefore relatively close to a mining excavation. This is supported by the observed damage; that is, the siding face burst and footwall heave, already discussed.

The CLVD component (CLVD = 7%) is small, indicating that only a small portion of the event mechanism is associated with pillar failure mechanism. This can likely be ignored in terms of the event mechanism.

The double couple component (DC = 63%) indicates that shear slip is the dominant event mechanism. This can be associated either with slip on the contact plane of a geological

structure or shear through intact rock (Ortlepp shear). With the event location not near a geological structure, it is deduced that the dominant event mechanism is shear through intact rock (face related event). The orientation of the double couple component is also indicated by the beachball presentation in the moment tensor and that is north-northeast to south-southwest. In Figure 37, the observed shear fractures are plotted with the moment tensor slip planes on the mining plan. It is clear that the orientations are similar and that there is good correlation between the moment tensor solution event mechanism and the observations underground at the damage site.

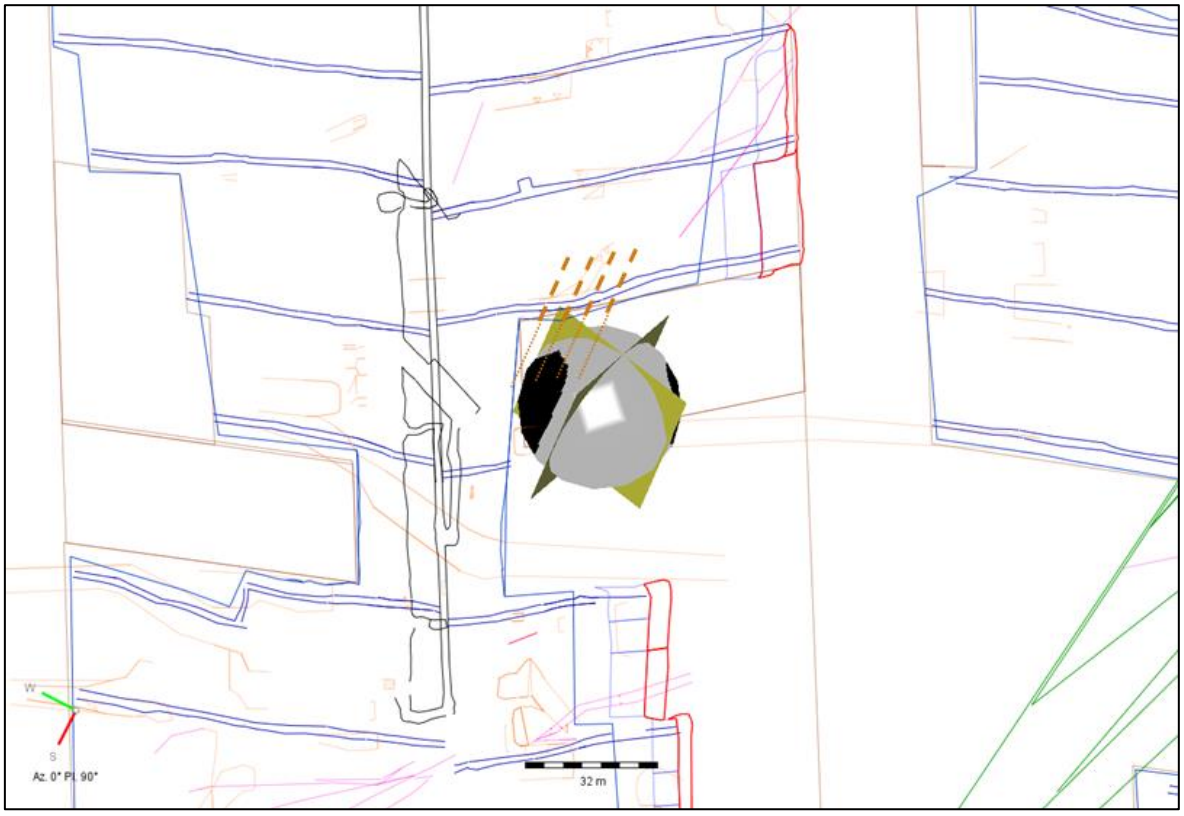

Figure 37. Moment-tensor slip plane orientations of the M3.1 event and the approximate orientations of the observed shear fractures underground.

With reference to the case study described above, moment tensor analysis can be used to assist in the interpretation of the seismic source mechanism and orientation of the likely slip plane associated with the slip component of the source mechanism.

Historically moment tensor solutions were only requested for large events or damaging events, but since the beginning of 2018, moment tensor solutions are provided for all events with magnitude greater or equal to $M_L = 1.0$. This is used to identify the most likely sources and source mechanisms of potentially damaging seismic events.

For this study, moment tensor solutions were requested for a large number of historic events where moment tensor solutions have not been done before. This provided a large database for analysis and identification of event mechanism orientations. In Figure 38, the locations of 47 events on the eastern side of the mine on the shale footwall is plotted on the mining and geology information plan. The event locations are shown as “beachballs” that represent the full moment tensor solutions. Moment-tensor solutions provide two conjugate planes, or nodal planes, for the DC solutions, with either of these planes a possible source plane. The dark lines through each beachball are the orientations of the intersection of the nodal planes, and therefore indicate the strike orientation of typical double couple source planes in this underground stress environment. Inspecting the lines representing the event double couple mechanism orientations, it can be seen that a large number of orientations are similar.

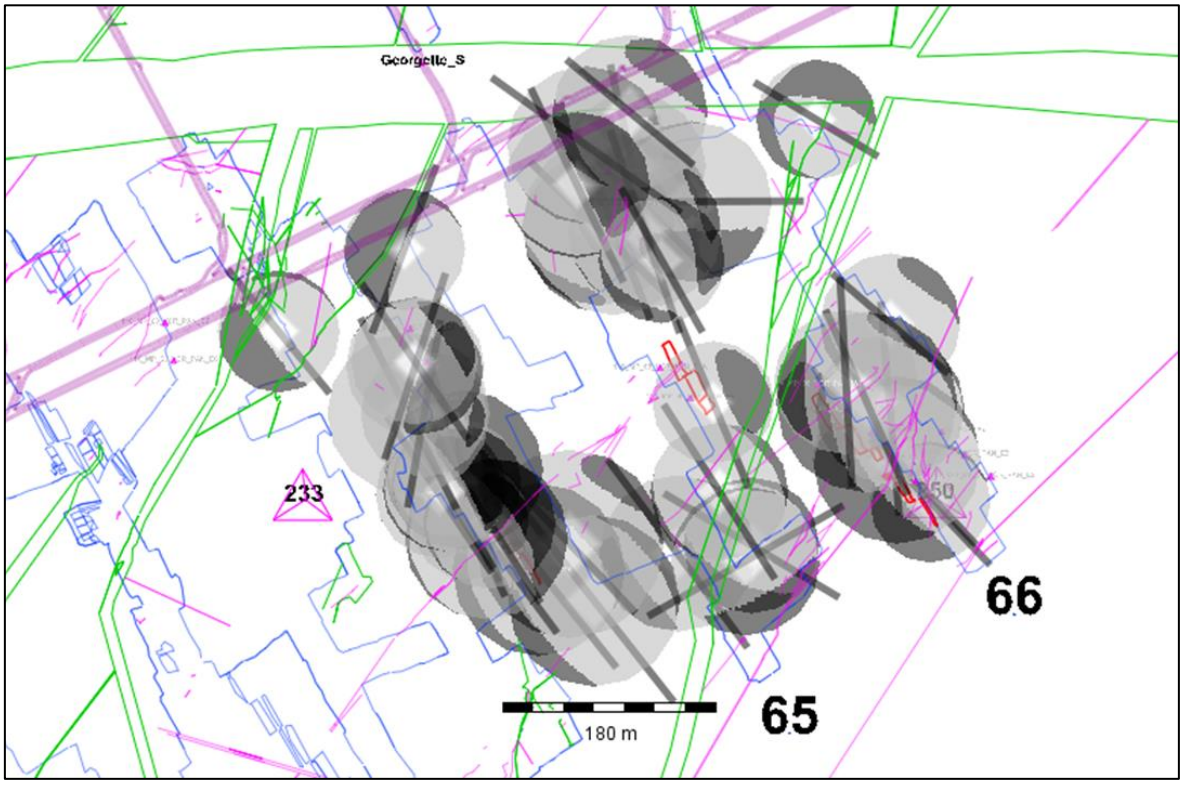

Figure 38. Events on the shale footwall (east) for which moment tensor solutions were provided by IMS. The dark lines through each beachball (event) is the orientation axis for each nodal plane of the DC component of the moment tensor.

In Figure 39, only the event source plane orientations are shown and compared to the orientation of a line representing the direction of dip of the strata as well as red lines representing the overhand and underhand face configuration lines or average face configuration for east and west mining fronts. The overhand and underhand face configuration lines form an envelope of approximately 25° both sides of the strata dip direction line. From inspection of the orientations it can be identified that 41 of the 47 event orientations are within the 25° face configuration envelop. The six events identified in Figure 39 whose orientations are not within the 25° envelope around the strata dip direction line can be associated with geological structures; i.e. dykes or minor faulting sympathetic to dykes nearby.

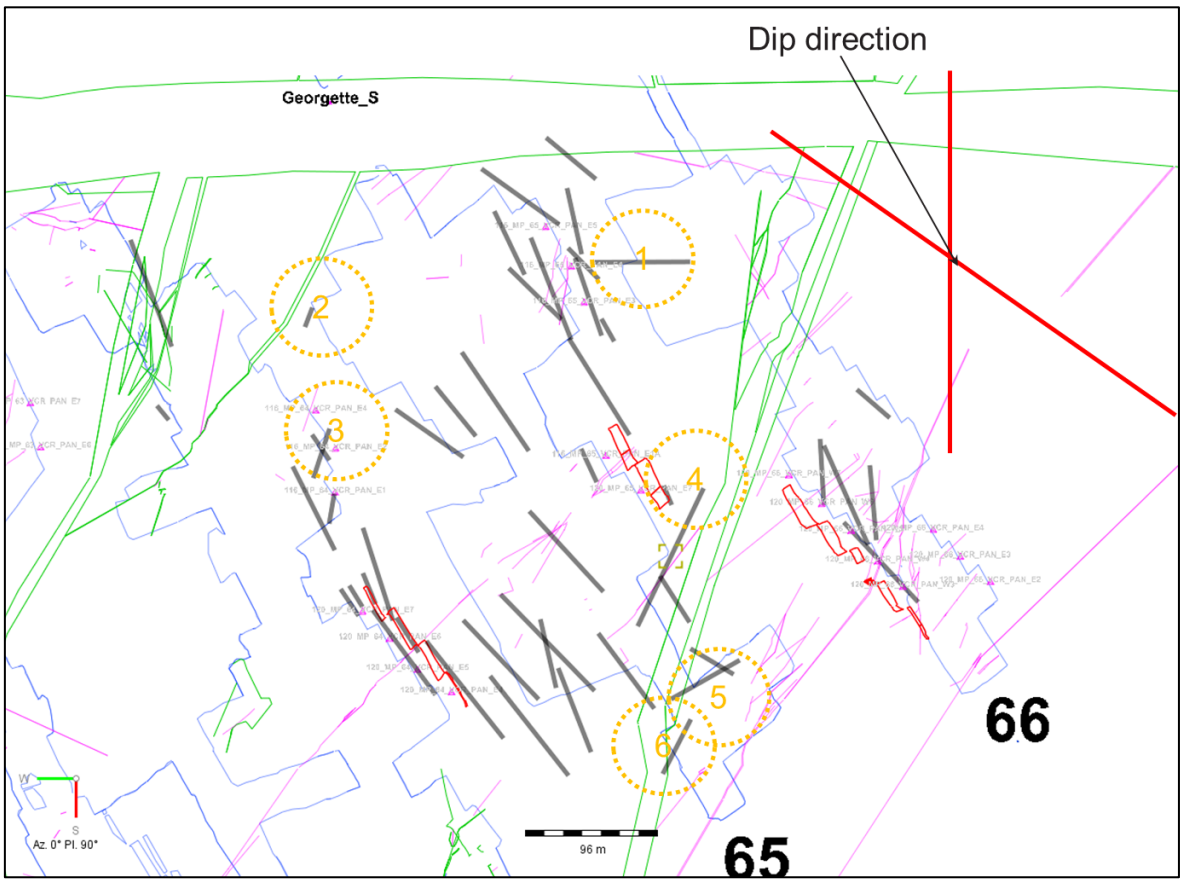

Figure 39. Plan view of event orientations of 47 events on the shale footwall (east). The red lines represent the overall underhand and overhand face configurations associated with the east and west mining fronts and form an approximately 25° envelope both sides of the line representing the dip direction of the strata. Six events that do not have event orientations inside the 25° envelope around the dip direction of the strata are circled with dotted yellow circles and numbered.

This crude review of event orientations indicated that a large percentage of events in the large magnitude range (events with magnitude greater than $M_L = 1.5$) are not associated with geological structures, but rather associated with the mining faces. Keeping in mind that this insight is contradictory to the author's previous understanding of sources of large events, i.e. that large events almost always were associated with geological structures, a more scientific assessment was needed. This is described in Chapter 4, section 4.3.

3.6 SEISMIC DATA SELECTION: NORMALISED SEISMIC RESPONSE TO MINING

The seismic response to production is induced and triggered by the mining activity. In general, more mining (production volume) will result in a higher seismic response. It is therefore improper to compare the seismicity in different mining areas or for different time periods if the volume of mining in such areas or time periods differ, unless the seismic response is normalised to the production volume.

In order to discuss the normalised seismic response, potency, as a seismic parameter for magnitude of a seismic event, needs to be discussed briefly and compared to other parameters for magnitude: Seismic potency of a single dislocation source is the product of the average slip and the source area (Menahem and Sing, 1981). Potency is a measure of the magnitude of a seismic event quantified in $[m^2]\times[m]=[m^3]$. It is calculated as a primary source parameter from the recorded seismograms (Mendecki, 2013).

$$P = 4\pi vr(\Omega_0/\Lambda) \quad (3.6.1)$$

Where v is the velocity of the P-wave or the S-wave, r is the distance from the geophone to the source of the event, Ω_0 is the fitted model plateau on the displacement graph in the frequency domain (at the corner frequency) and Λ is the cube root of the radiation pattern. Potency is the average for the calculated potency for P- and S-waves and potency magnitude is then simply the log of potency.

$$M_P = \log P \quad \text{(Mendecki, 2013)} \quad (3.6.2)$$

Moment is also calculated from the recorded seismograms;

$$M_0=(4\pi\mu vr\Omega_0)/R_c \quad \text{(Mendecki, 2013)} \quad (3.6.3)$$

Where μ is the rigidity (shear modulus) of the rock mass, a number that is assumed. R_c is the radiation pattern and the other parameters are the same as described for potency calculation.

Moment magnitude is calculated from moment using the formula;

$$M_w = \tfrac{2}{3} \log M_0 - 10.7 \quad \text{(Mendecki, 2013)} \quad (3.6.4)$$

Moment for a seismic event can be calculated by multiplying potency with rigidity.

The magnitude scale used at Mponeng Mine is called the local magnitude scale and is calculated from moment as well as energy. Energy is calculated from the area underneath the model fit on the stacked velocity spectra in the frequency domain. This is a volatile number as there is a large uncertainty in velocity and energy will vary to the square of the uncertainty in velocity;

$$M_L = 0.516 \log M + 0.344 \log E - 6.572 \quad (3.6.5)$$

The numbers in the formula are constants used to calibrate local magnitude to Richter magnitude.

The data source polygons were carefully chosen for each year to ensure that no contamination from other areas occurred in the data sets (Chapter 3). Only the polygons used for the 2018 period are shown in Figure 40 as an example. The normalised seismic response for Mponeng effectively reduced year-on-year from 2011 to 2016, then increased in 2017 compared to 2016 and in 2018 was still higher than 2016 despite a minor reduction from 2017 to 2018. The year-on-year reduction from 2011 to 2016 is associated with the implementation of strike stability pillars in addition to the dip stability pillars that had been part of the sequential grid mining strategy since 2011, as well as the early stopping (short of the designed mining limit) of panels where the seismic response was deemed unacceptably high. The addition of strike pillars effectively further reduced the extraction ratio, reducing the volumetric closure and therefore the normalised seismic response.

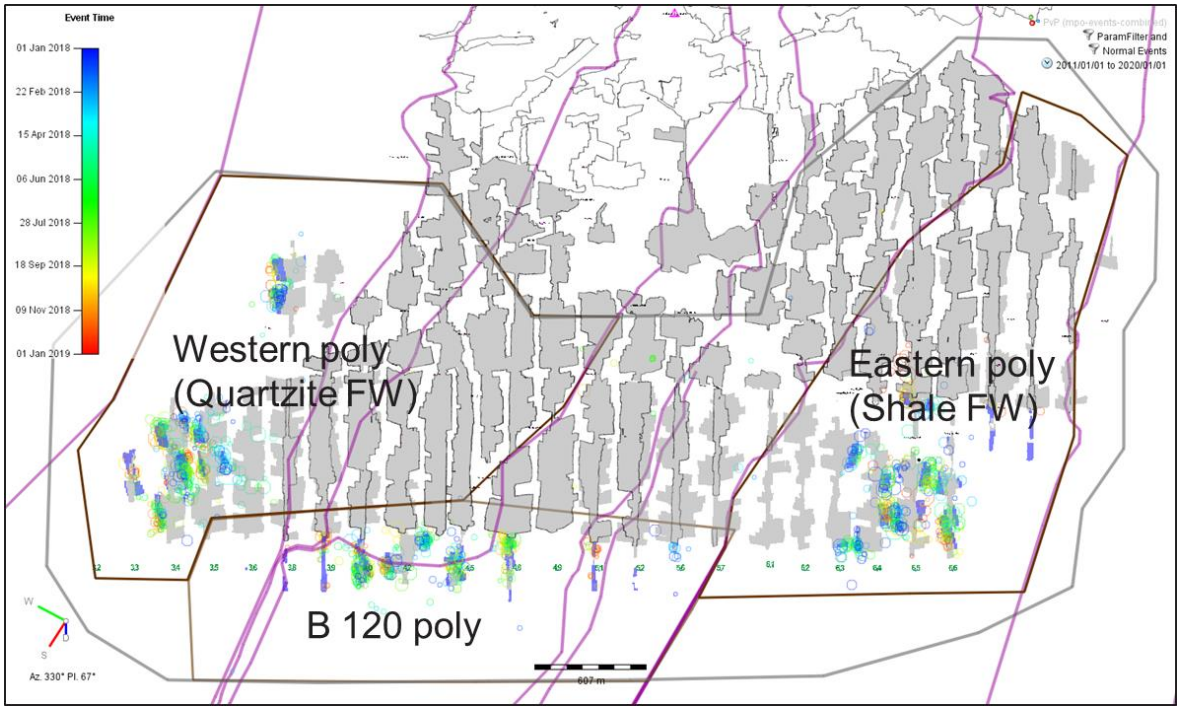

Figure 40. Polygon selection for the normalised seismic response review. The eastern polygon is in the area with shale footwall; the western polygon is in the area with quartzite footwall; the B120 polygon represents data from below 120 level and is filtered out for this study.

The Mponeng normalised seismic response, measured as annual cumulative recorded potency normalized to annual cumulative production at an average stoping width of 1.4 m, is graphed for the period 2007 to 2018 (Figure 41).

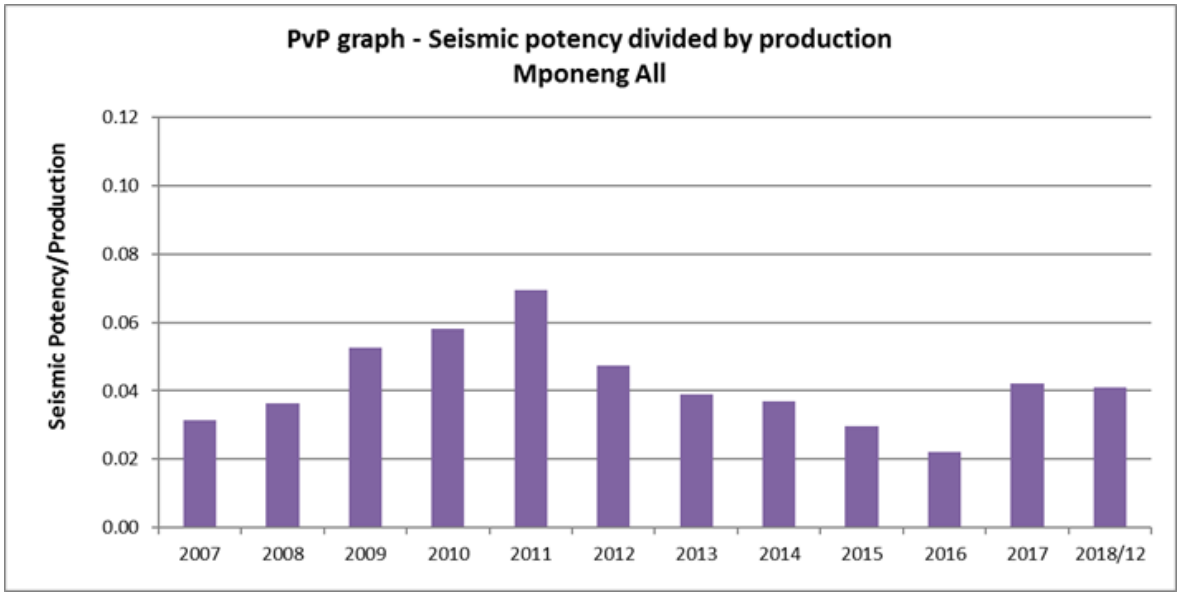

Figure 41. Annual normalised seismic response (potency/production for events with $M_L > 0$) at Mponeng Mine from 2007 to 2018.

CHAPTER 4 SEISMIC DATA ANALYSIS

4.1.1 Analysis of magnitude distribution for the different footwall lithologies (shale footwall and quartzite footwall)

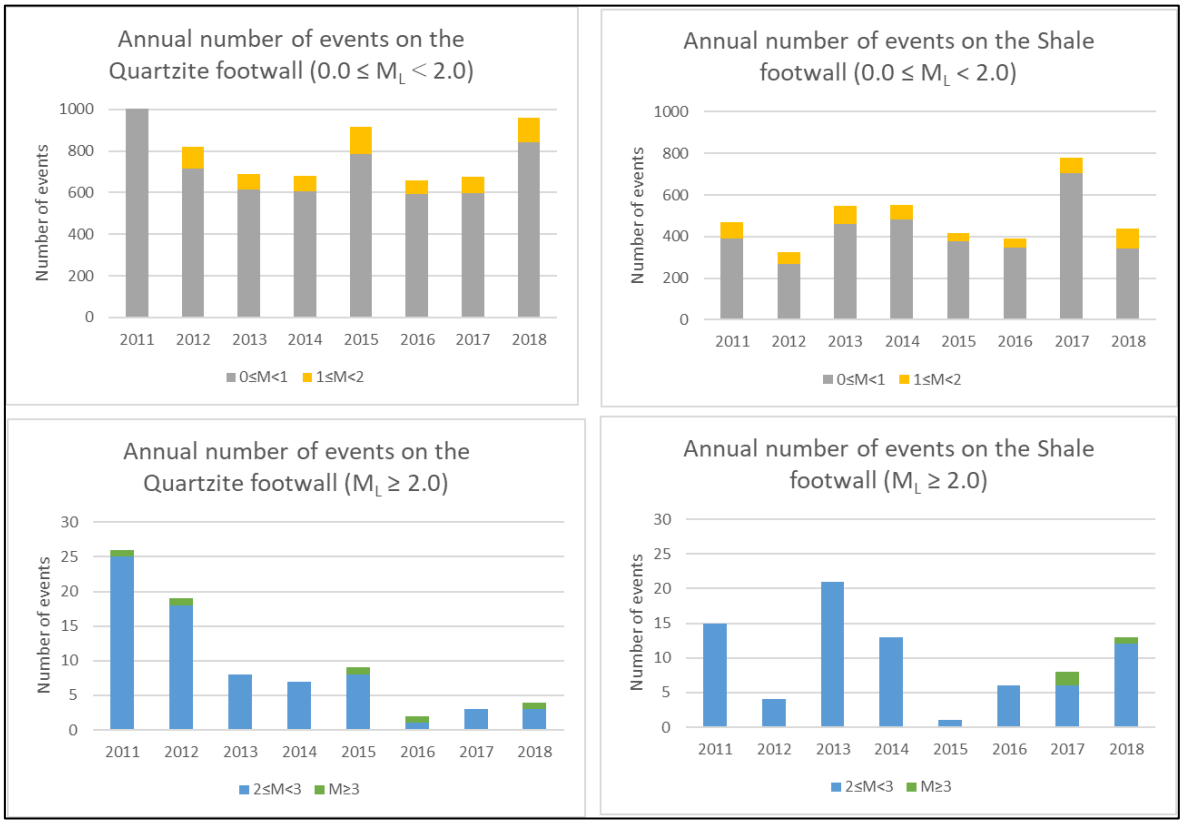

Figure 42. Summary of the recorded seismic events for the shale footwall area (east) and the quartzite footwall area (west) for the different data ranges for the years 2011 to 2018.

In Figure 42, four different graphs area shown: The top left graph plots the annual number of events in the magnitude bins $0.0 \leq M_L < 1.0$ and $1.0 \leq M_L < 2.0$ for the quartzite footwall polygon (west). The top right graph plots the annual number of evens in the magnitude bins $0.0 \leq M_L < 1.0$ and $1.0 \leq M_L < 2.0$ for the shale footwall polygon (east). Comparing these two graphs (and considering the careful data selection described in Chapter 3 to ensure that this data is not influenced by network sensitivity), it is clear that in the smaller magnitude range, more events were recorded in the west polygon (quartzite footwall) compared to the east polygon (shale footwall).

The bottom left graph plots the number of evens in the magnitude bins $2.0 \leq M_L < 3.0$ and $M_L \geq 3.0$ for the quartzite footwall polygon (west). The bottom right graph plots these events for the shale footwall polygon (east). In these larger magnitude ranges the number of events associated with mining on the shale footwall is lower than that for the quartzite footwall polygon in the years 2011 and 2012, but more than the number of events associated with mining on the quartzite footwall for the years 2013 and 2014. In 2015 the number of events associated with mining on the shale footwall is lower than that for the quartzite footwall and then in 2016 to 2018 the number of events associated with mining on the shale footwall is higher than that for the quartzite footwall.

Further data selection refinement is required to compare the occurrence of events in the large magnitude bins ($M_L \geq 2.0$).

4.1.2 Analysis of number of events in different magnitude bins for the different footwall lithologies (shale footwall and quartzite footwall) based on similarity of mining depth

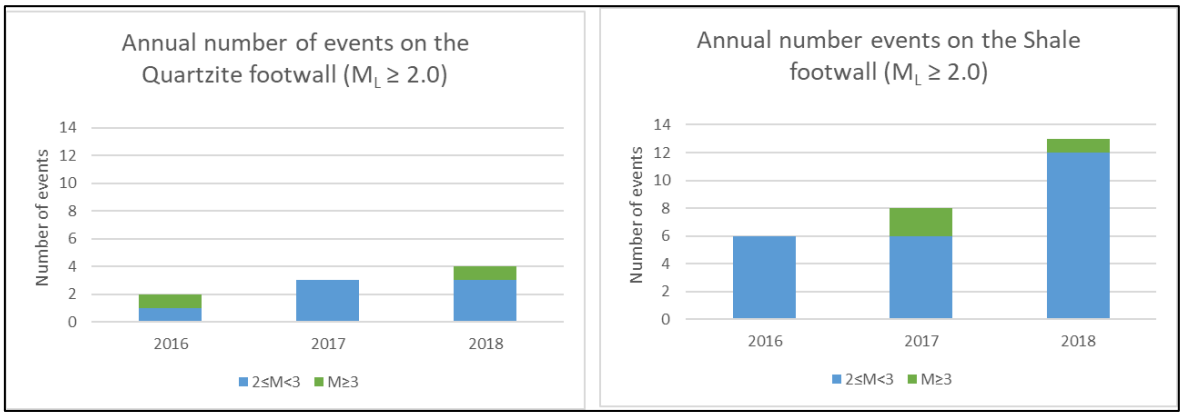

Figure 43. Graphs of the annual numbers of events for 2016 to 2018 for the magnitude bins $2.0 \leq M_L < 3.0$ and $M_L \geq 3.0$ for the quartzite footwall polygon (left) and the shale footwall polygon (right).

With the careful data selection to ensure that factors other than footwall lithology (that may impact on the seismic response to mining) are similar, it can be seen in Figure 43 that the number of large events (in the magnitude bins $2.0 \leq M_L < 3.0$ and $M_L \geq 3.0$) are significantly more on the shale footwall compared to the numbers on the quartzite footwall for every year from 2016 to 2018. The year-on-year increase in each polygon is attributed to the increase in mining spans in each mining area (polygon). The mining span increases are similar in the two areas.

It is interesting to note then that there is a tendency for more large events on the shale footwall compared to the quartzite footwall at similar mining depth and mining spans.

4.1.3 Seismic data analysis: normalised seismic response to mining

In order to quantify the difference in seismic response for the different footwall lithology (shale versus quartzite), the normalised seismic response review is repeated for the polygons representing mining on the shale footwall in the eastern side of the mine and mining on the quartzite footwall in the western side of the mine (Figure 44).

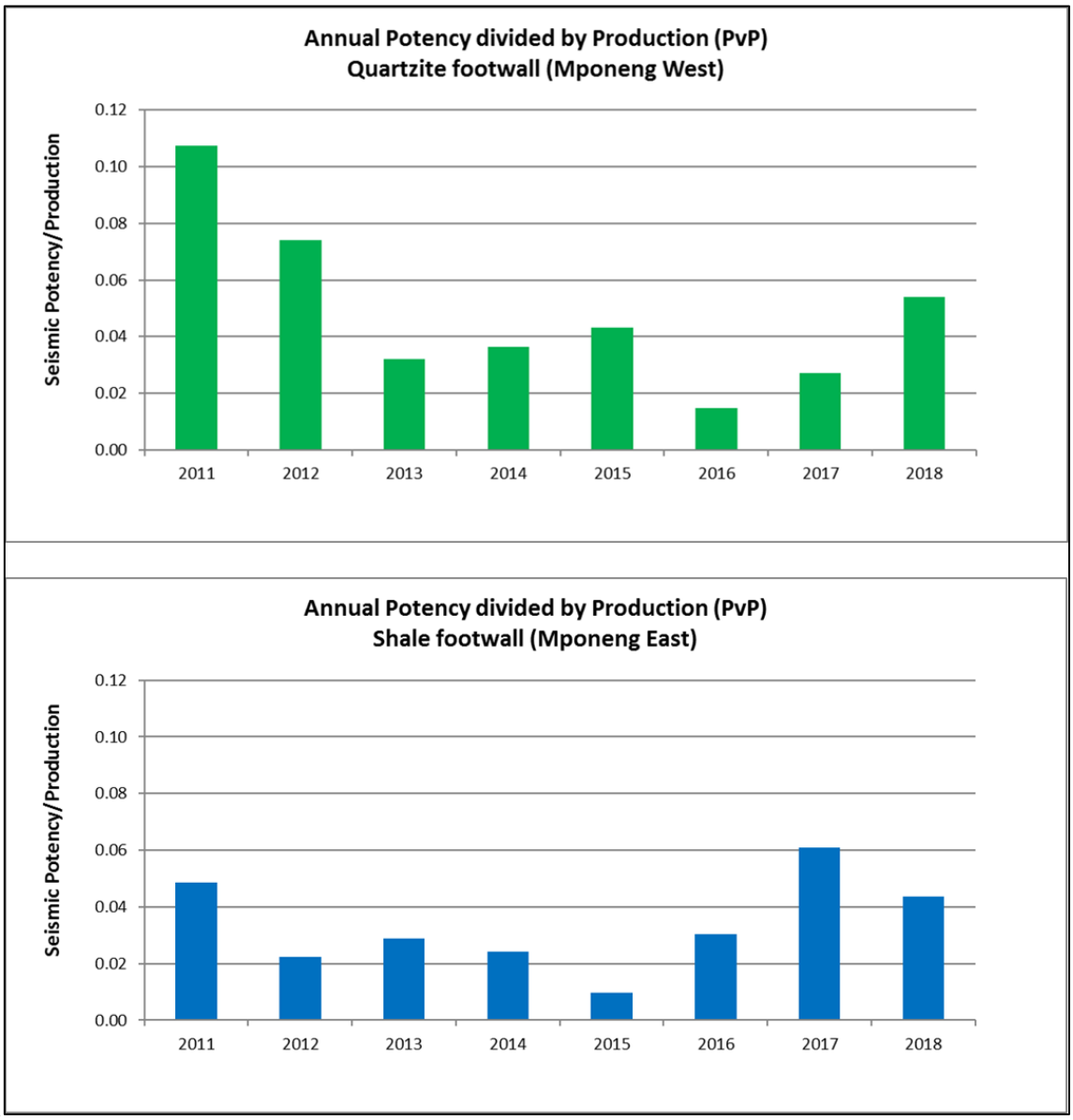

Figure 44. Annual normalised seismic response (PvP) for the quartzite footwall area (west) and the shale footwall area (east) on Mponeng Mine for the time period from 2011 to 2018.

In Chapter 3 it was established that only 2016 onwards should be used in the comparison and also that only events with $M_L > 0$ are used. From 2016 to 2018, the mining geometry and mining spans are comparable for the two areas of interest and a fair comparison in normalised seismic response can be made. It is clear that the normalised seismic response for the shale area was almost double the normalised seismic response for the quartzite area in 2016 and 2017. In 2018 the normalised seismic response in the shale area decreased and for the quartzite area continued to increase so that the normalised seismic response on the quartzite area was higher than for the shale area in 2018. This can be attributed to the fact that some mining on the shale was stopped before reaching the designed span (full maturity).

The observation that the normalised seismic response for mining on the shale footwall was measurably higher than the normalised seismic response for mining on the quartzite footwall (whilst other factors that may influence the seismic response are similar) supports the observation made in section 3.1 that the footwall lithology influences the seismic response to mining in that there is a tendency for more events with large potency (in the large magnitude range) on the shale footwall compared to the quartzite footwall.

The normalised seismic response to mining, as discussed above, is one measure of the seismic hazard associated with mining; i.e. where the normalised seismic response to mining, measured in cumulative potency divided by cumulative production volume, is higher, it can be re-worded to state that the seismic hazard is higher; i.e. the seismic response per unit area mined is higher.

4.2 SEISMIC HAZARD COMPARISON BASED ON FREQUENCY MAGNITUDE GRAPHS

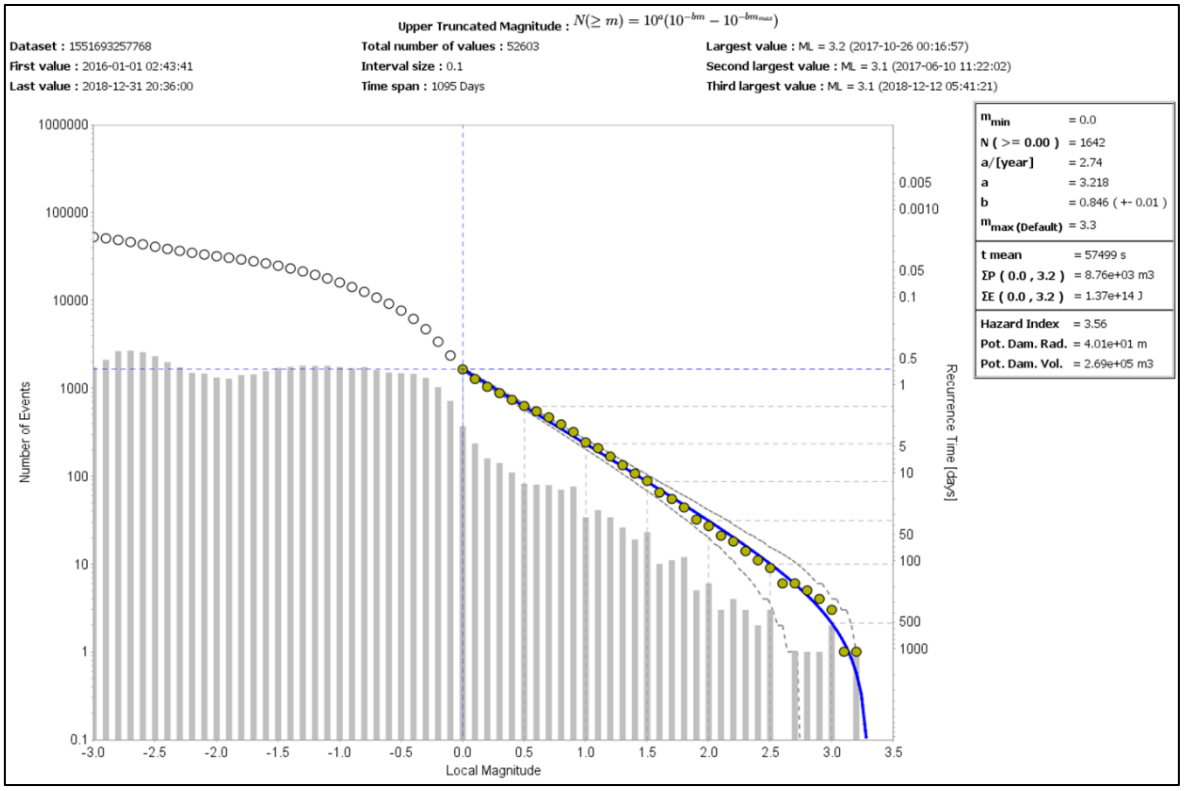

Figure 45. Gutenberg-Richter graph for the shale footwall for 2016 to 2018, with the fit point at M_L 0.0.

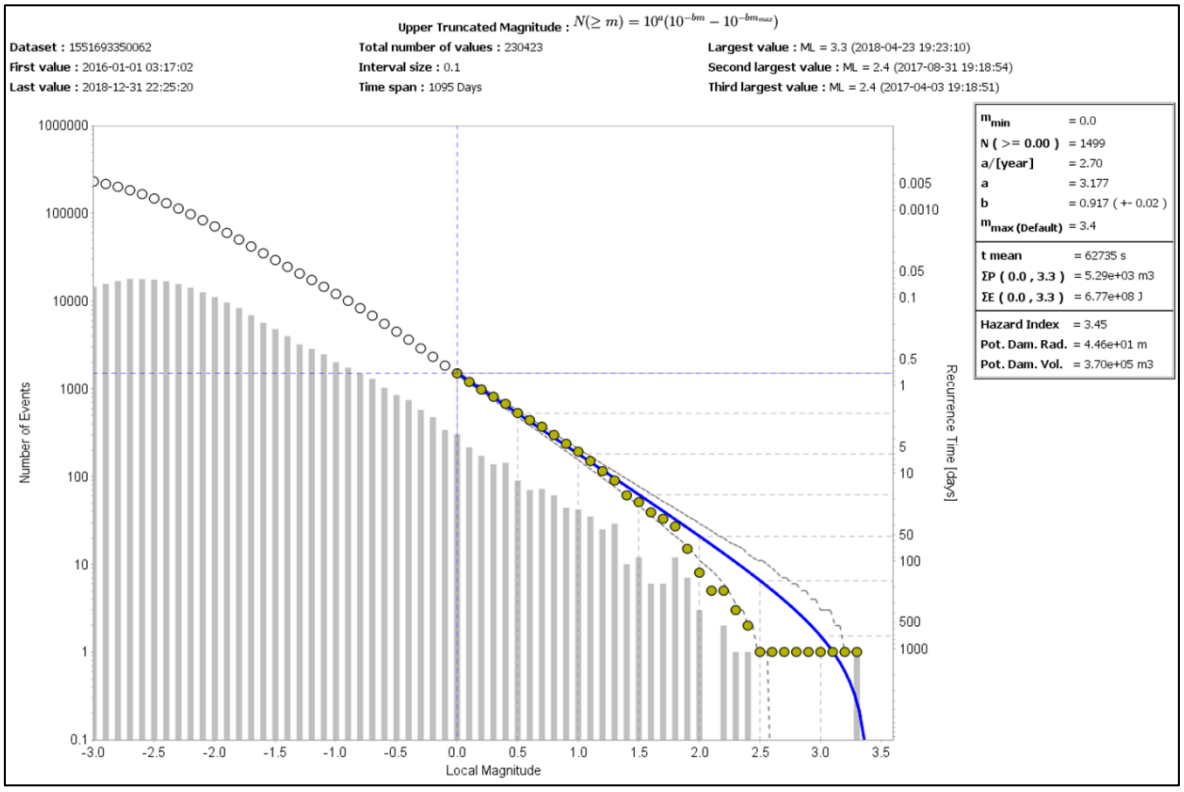

Figure 46. Gutenberg-Richter graph for the quartzite footwall for 2016 to 2018, with the fit point at M_L 0.0.

The b-value (slope of the fitted graph) can be viewed as a measure of the seismic hazard; i.e. a flatter slope indicates that the ratio of large events to small events is bigger (increased likelihood of large events for a certain number of smaller events). A steeper slope indicates that the ratio of large events to small events is lower. A b-value near unity is considered as normal.

For the two polygons, the b-slope for the shale footwall (after re-fitting the upper truncated magnitude graph for the shale footwall area) is flatter at 0.846 compared to 0.917 for the quartzite polygon, indicating that more large events can be expected on the shale footwall compared to the quartzite footwall for a similar number of smaller events. This confirms the observation made in sections 3.1 and 3.2 that there is a tendency for more events in the large magnitude range on the shale footwall as compared to the quartzite footwall for similar mining conditions.

Another measure of seismic hazard is the M_{max} value. In earthquake seismology M_{max} is the maximum magnitude earthquake that a given seismogenic region can deliver. (Mendecki, , 2016). The M_{max} for the western polygon (quartzite footwall area) of 3.4 is marginally larger than for the shale footwall area (3.3). The fit seems to be skewed by a M_L 3.3 event on a fault in the western polygon and is more likely associated with the specific structure than the footwall lithology. An attempt is made to improve the upper truncated data fit based on exclusion of the M_L 3.3 event. This is justified by inspection of the graph in Figure 47 where it seems that the M_L 3.3 event does not fit the signature response or shape of the graph on the rest of the data. It is argued that this event provide insight into the specific geological structure (event source) where this event occurred and not into the general face-related seismic sources in the event set. This "improvement" (Figure 47)shows that the M_{max} for the quartzite footwall should be somewhere between 2.5 and 3.0 if the M_L 3.3 event is excluded in the data set.

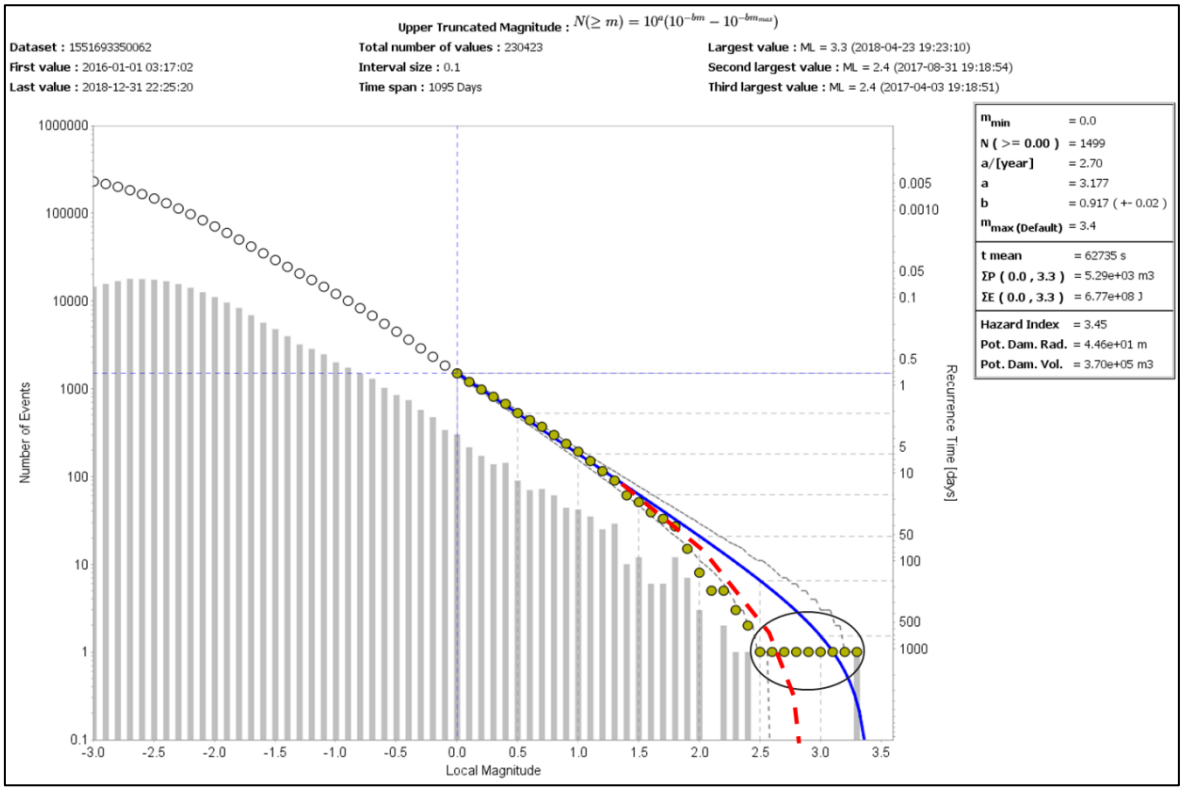

Figure 47. Hand-drawn "improvement" of the upper truncated data fit (red dashed line) to show what it may look like if the single structure-related event is removed from the data set.

In Figure 48, the GR is plotted again for the quartzite footwall for the time period 2016 to 2018, but the M_L 3.3 event is filtered out of the data set (excluded). This results in a significantly improved fit for the upper truncated fit on the data and the M_{max} is then 2.5; i.e. significantly lower than for the shale footwall area.

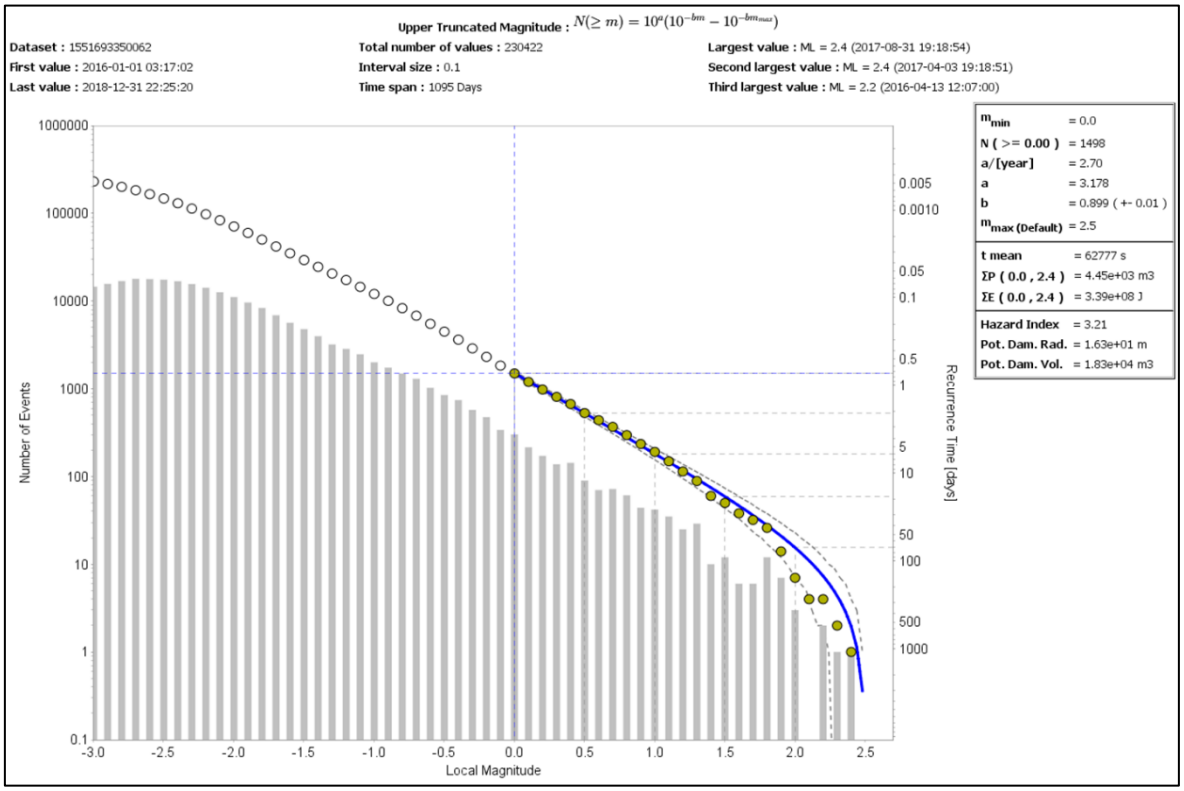

Figure 48. Gutenberg-Richter graph for the quartzite footwall for the time period 2016 to 2018, where the M_L 3.3 event is excluded.

The observation that the seismic hazard for mining on the shale footwall was measurably higher than the seismic hazard for mining on the quartzite footwall, based on the b-slope as well as the M_{max} from the GR graphs, supports the observation made that the footwall lithology influence the seismic response to mining and therefore the normalised seismic response, and that there is a tendency for more events in the large magnitude range in the shale footwall area compared to the quartzite footwall area for similar mining conditions.

4.3 SEISMIC DATA ANALYSIS RESULTS: EVENT SOURCE MECHANISMS

In this assessment, the moment tensor solutions of all events with magnitudes in excess of M_L = 1.5 that occurred in the time from the beginning of 2015 to the end of 2018, in the shale footwall polygon on the eastern side of the mine as well as the quartzite footwall polygon on the western side of the mine, were included. Each moment tensor solution has two possible slip plane orientations (nodal planes) for the DC component as the numerical technique cannot distinguish between two conjugate nodal planes. From a rock engineering perspective though it can be argued that the steeper plane is more likely; the stress orientation is such that the orientation of maximum shear stress is steep (AngloGold Ashanti internal modelling reports) and furthermore the damage observed underground is consistent with steep sources rather than shallow dipping event sources (AngloGold Ashanti internal rockburst investigation reports). Therefore, in this statistical assessment, only the steeper of each event's two nodal planes was used.

In Figure 49, the steepest nodal planes of each moment tensor solution of 56 events with magnitudes in excess of M_L = 1.5 that occurred in the time from the beginning of 2015 to the end of 2018 in the shale footwall polygon on the eastern side of the mine are shown, first in plan view (green lines on the mining plan) and then in a stereonet lower hemispherical density plot (white dots and density contours).

The black lines in the stereonet plot represent the pre-mining stress state, or more specifically the plane of maximum excess shear stress (ESS) associated with the pre-mining stress state, according to the Mohr-Coulomb failure criterion. The pre-mining stress state is discussed in detail in the modelling input parameter section (Chapter 2), but can be summarised as follows: the major principal stress is proportional to the weight of the overburden and orientated approximately orthogonal to the reef plane, the intermediate principal stress k-ratio is approximately 0.7 and is orientated in the strata dip direction and the minor principal

stress k-ratio is approximately 0.4 and is orientated in the strike direction. The plane of maximum ESS associated with this stress field will then be orientated in the intermediate stress field direction with dip determined by the k-ratio between the maximum and minimum principle stresses as well as the rock mass friction angle. This plane of maximum ESS is also the plane of most likely failure in an isotropic and homogenous rock mass; i.e. the most likely orientation of a shear fracture is represented by the black lines in the stereonet in Figure 49 (conjugate plane orientations).

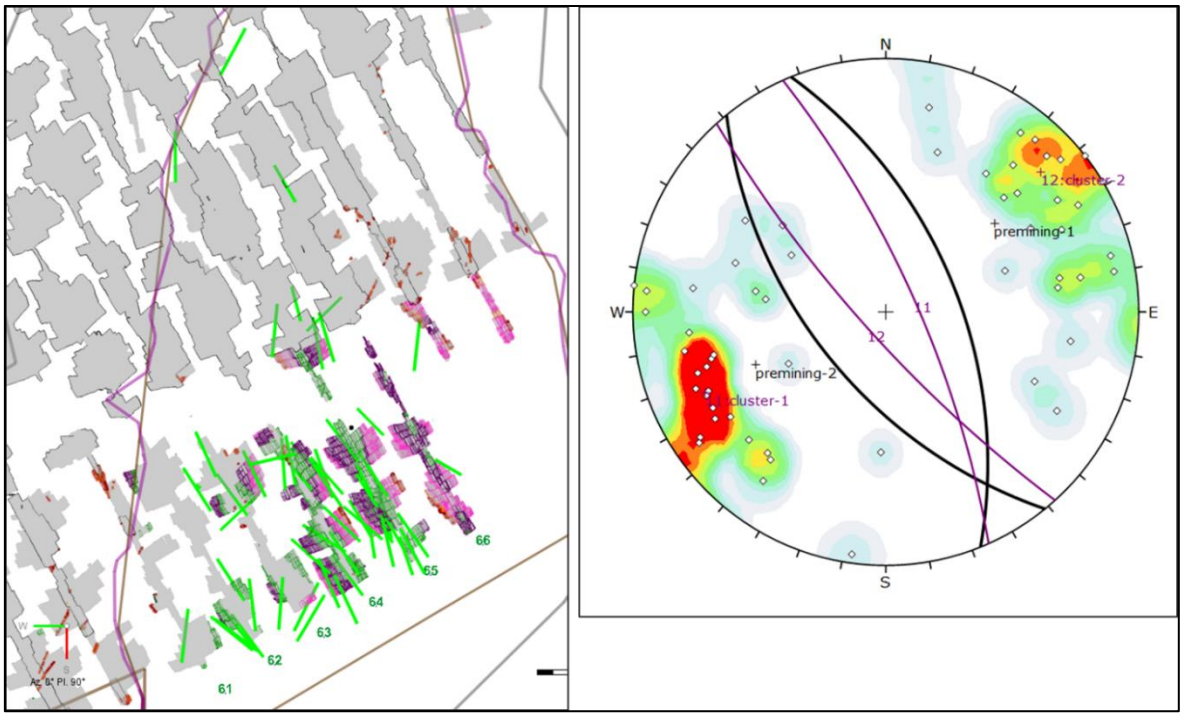

Figure 49. The nodal planes' orientations (steepest only) of the moment tensor solutions of 56 seismic events in the shale footwall polygon (east) in the magnitude range ($M_L \geq 1.5$, first in plan view (left side picture) and then in stereonet plot (right side picture). The purple lines represent the planes associated with the densest area and the black lines represent the ESS planes associated with the pre-mining stress state.

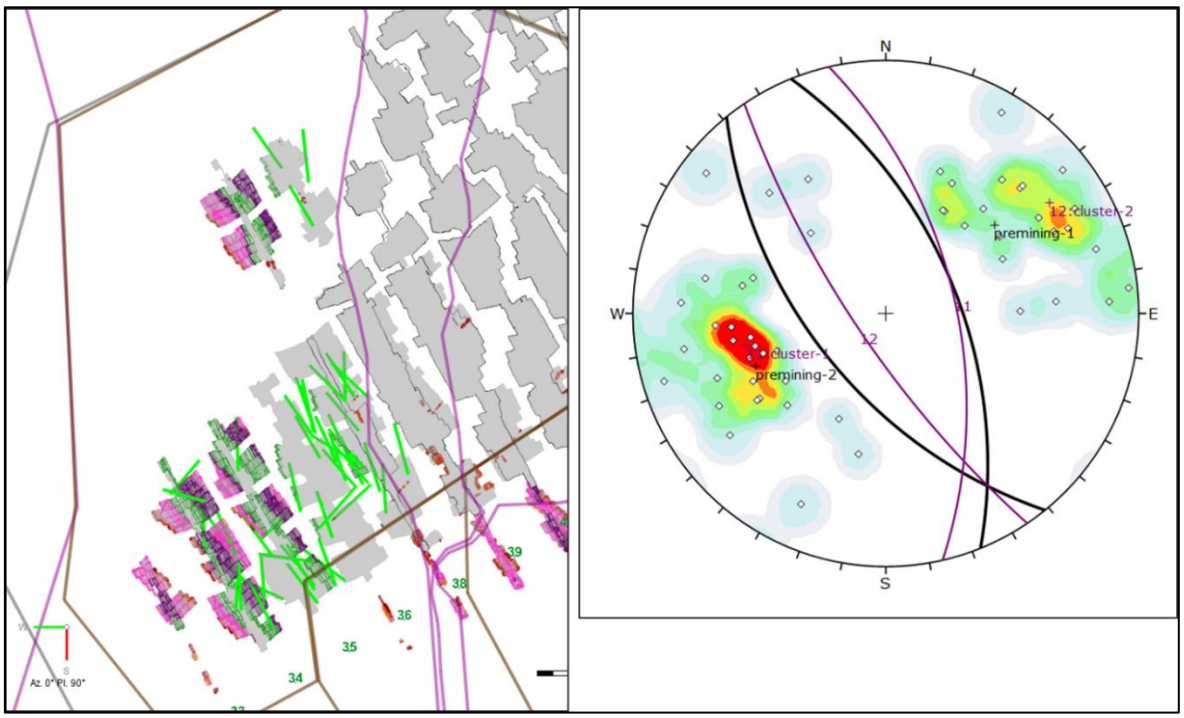

Figure 50. The nodal plane orientations (steepest only) of moment tensor solutions of 52 seismic events in the quartzite footwall polygon on the western side of the mine and in the magnitude range $M_L \geq 1.5$, first in plan view (left side picture) and then in stereonet plot (right side picture). The purple lines represent the planes associated with the densest areas and the black lines represent the ESS planes associated with the pre-mining stress state.

In Figure 50, the steepest nodal planes of the moment tensor solutions of 52 events with magnitudes in excess of $M_L = 1.5$ that occurred in the time from 2016 to the end of 2018 in the quartzite footwall polygon on the western side of the mine are shown, first in plan view (green lines on the mining plan) and then in a stereonet lower hemispherical density plot (white dots and density contours).

From the stereonet plots the high-density contours confirm the previous observation that a large number of event source planes have similar orientation. The purple lines in the stereonet in Figure 50 are the two most common nodal plane orientations of the moment tensor solutions of the 52 events in this data set. These lines have similar strike orientation but opposite dip directions; i.e. northeast and southwest. These planes (with similar orientation and opposite dip directions) are called conjugate planes. The southwest dipping source planes are likely associated with events on west mining faces and the northeast

dipping source planes are likely associated with events on east mining faces. The general northwest-southeast orientation of these planes confirms the observation made earlier that most of the event source planes are orientated in a relatively narrow envelope around the northwest-southeast direction. This adds an important new insight into the seismic sources on Mponeng Mine not observed before. Comparing the orientation of the purple lines with the orientation of the overall mining faces and final pillar abutments in the accompanying plan, it can be said that the majority of events in the data set were face related rather than geological structure related.

Observing the black lines (representing the ESS associated with the pre-mining stress state) in the stereonet it is clear that their orientations are similar to the purple lines and the overall mining face abutments. This confirms that the slip orientations of the majority of recorded seismic events with magnitudes in excess of M_L = 1.5 on both the shale footwall on the eastern side and the quartzite footwall on the western side of the mine tend to be similar to the orientation of the most likely fracture orientation associated with the stress field as well as the orientation of the mining abutments.

It is a profound observation not made before on Mponeng Mine. A way must be found to manage the seismic hazard associated with large mining spans orientated similar to the most likely failure orientation associated with the stress field.

CHAPTER 5 DISCUSSION

In Chapter 4 it is shown that the seismic hazard is higher when mining on the shale footwall as compared to the quartzite footwall. It is the responsibility of the rock engineer on the mine to recommend strategies to manage the seismic response to mining to acceptable levels. Based on the data analysis, additional mine design criteria need to o be developed to address the difference in seismic response in the shale footwall area compared to the quartzite footwall are.

The current modelled closure design criterion needs to be updated to accommodate the difference in seismic response in the shale area compared to the quartzite area.

Map3D numerical modelling was used to quantify the modelled closure volume for a conceptual raise line on Mponeng Mine on the same depth as 116 to 120 Level on Mponeng Mine (approximately 3500 m below surface). In the model the maximum mining span is limited to 180 m (separated by 30 m wide dip pillars) as per the historical sequential grid mining layout at Mponeng Mine (Figure 51). The dip span is limited to 300 m in the model.

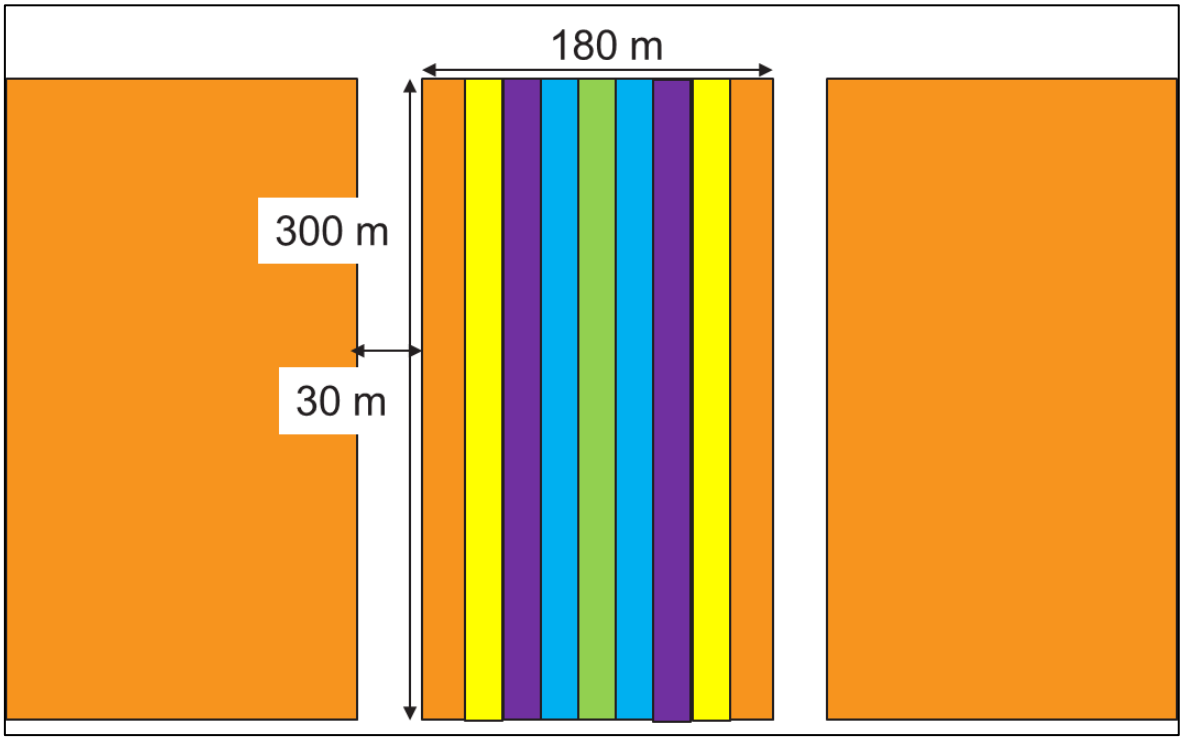

Figure 51. Conceptual model of a raiseline between 116 and 120 Level on Mponeng Mine. The strike span was increased in steps from ledging (green) to maximum (orange). The dip span remained constant.

The model input parameters applicable for Mponeng and described in Chapter 2 was used, but the Young's Modulus was changed from 77 GPa (average for the quartzite, Chapter 2) for the first run to 63 GPa (average for the shale) for the second run. This way all parameters that may impact on closure was kept constant except for the Youngs Modulus of the rockmass. The calculated closure volume versus the mining span for the two modelling scenarios is graphed in Figure 52. Although this approach can be criticised, as a single value of Young's modulus was used for the entire rock mass, whereas it is different for the hangingwall and footwall in reality, this modelling should be seen as a preliminary first attempt to illustrate the effect of changing the modulus if the rockmass on the volume of closure. Displacement discontinuity boundary element codes typically has the drawback that a single Young's modulus must be specified for the host rock mass (a single host rock type is allowed).

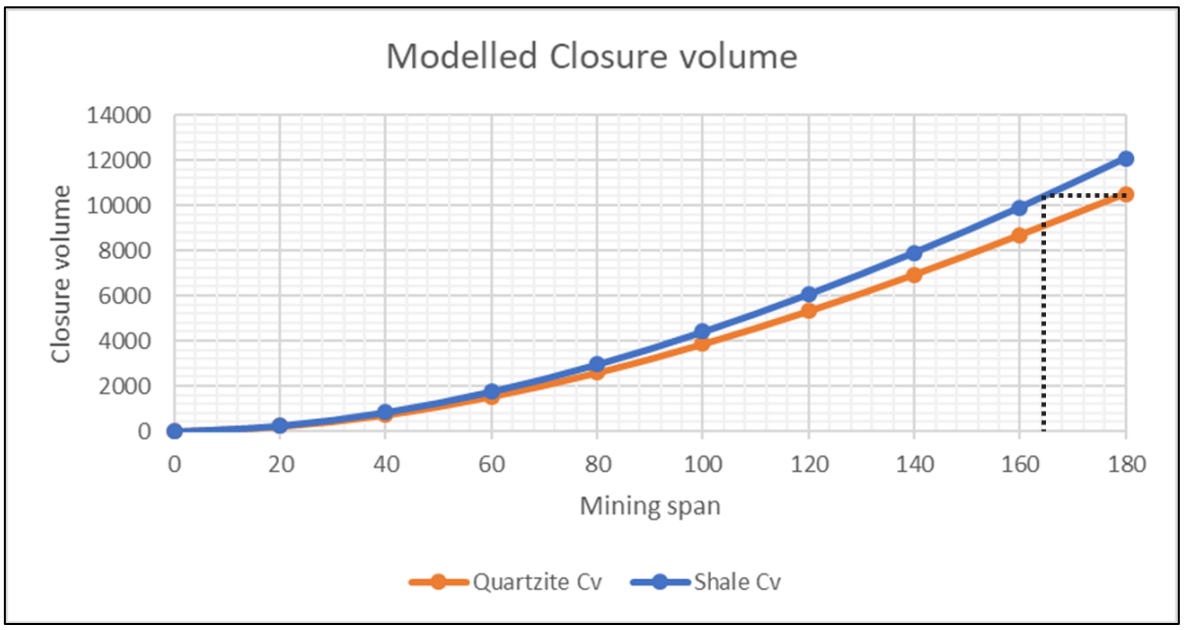

Figure 52. Modelled closure volume versus mining span on strike for the conceptual model for the quartzite footwall and shale footwall

Owing to the lower Young's modulus used for the shale footwall in the model, the closure volume is higher for the shale footwall compared to the quartzite footwall at similar mining spans. This is a partial explanation for the different seismic response on the shale footwall. No failure mechanisms were simulated in this preliminary modelling exercise and it is therefore not known why the b-values are different for the two footwall types. A detailed study of the mechanisms of failure is beyond the scope of this study and must be investigated in future. In the graph it is also shown that the equivalent closure volume associated with the quartzite footwall mining can be achieved on the shale footwall by limiting the mining span; that is, to achieve the same closure volume at maximum mining span of 180 m on the quartzite footwall, the mining on the shale footwall must be limited to 164 m.

For the same modelling scenario, maximum closure is graphed in Figure 53.

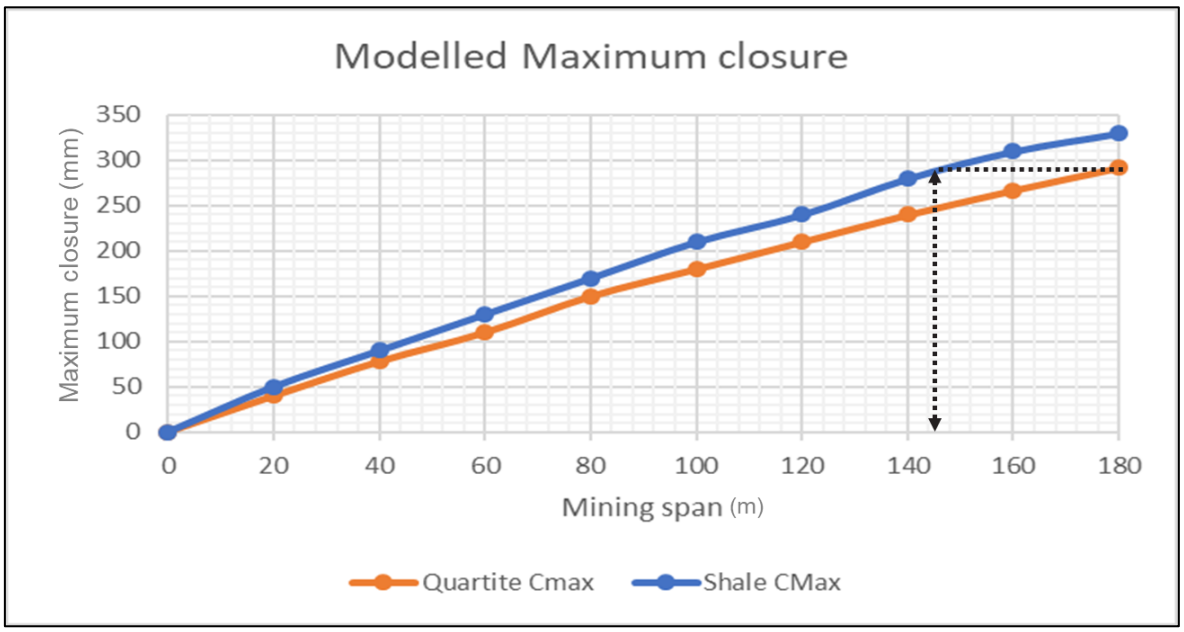

Figure 53. Modelled maximum closure versus mining span for the conceptual model for the quartzite footwall and the shale footwall

The shape of the graph of maximum closure is significantly different to that of closure volume, but again the equivalent maximum closure value on the shale footwall is reached at a smaller mining span (144 m) compared to the maximum closure value reached on the quartzite footwall at maximum span (180 m). This can be used to develop a new closure modelling criterion for mine design at Mponeng Mine that takes cognisance of the footwall type (lithology).

In this conceptual model, the maximum closure design criterion of 270 mm (for a 1 m stoping width in the model) is reached at a mining span of 164 m on the quartzite footwall. With the strike span fixed, this would require the introduction of a strike pillar in the conceptual model to reduce the maximum closure at maximum span to below 270 mm. A good starting point for the design process is to reduce the dip span to 164 m (Figure 55) and re-run the model.

To meet the maximum closure criterion on the shale footwall, the dip span must be further reduced to 136 m for a starting point (Figure 54). This would result in additional strike pillars in the conceptual model layout (Figure 56).

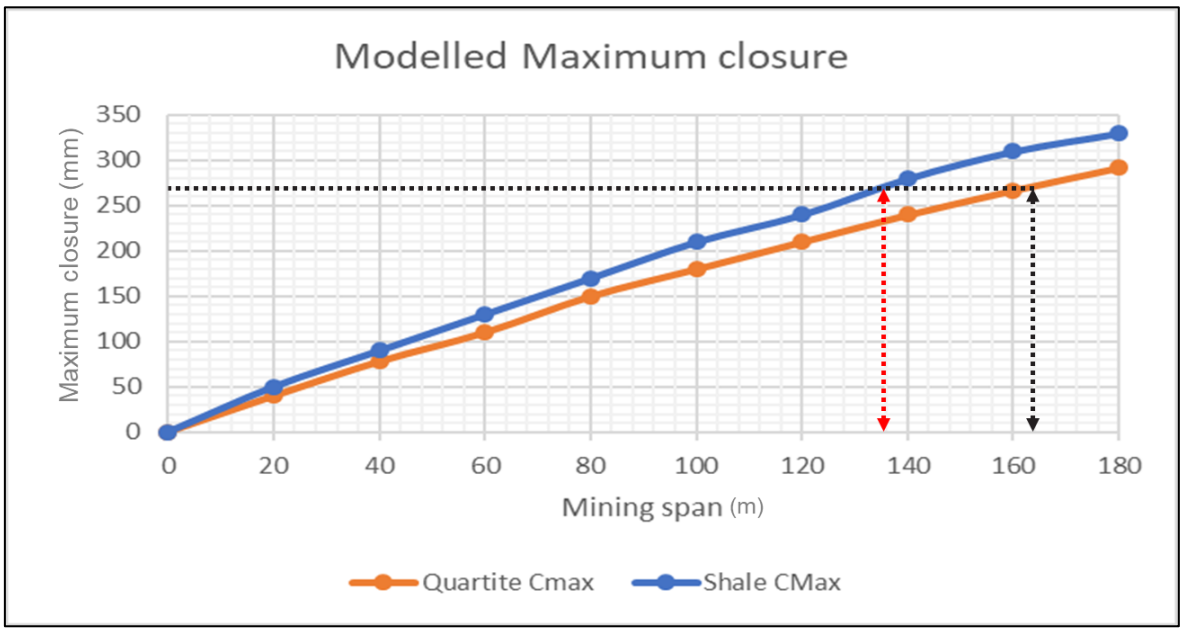

Figure 54 Modelled maximum closure versus mining span for shale footwall and quartzite footwall. The maximum mining span based on the maximum closure criterion is indicated for the quartzite footwall (black arrow) as well as for the shale footwall (red arrow)

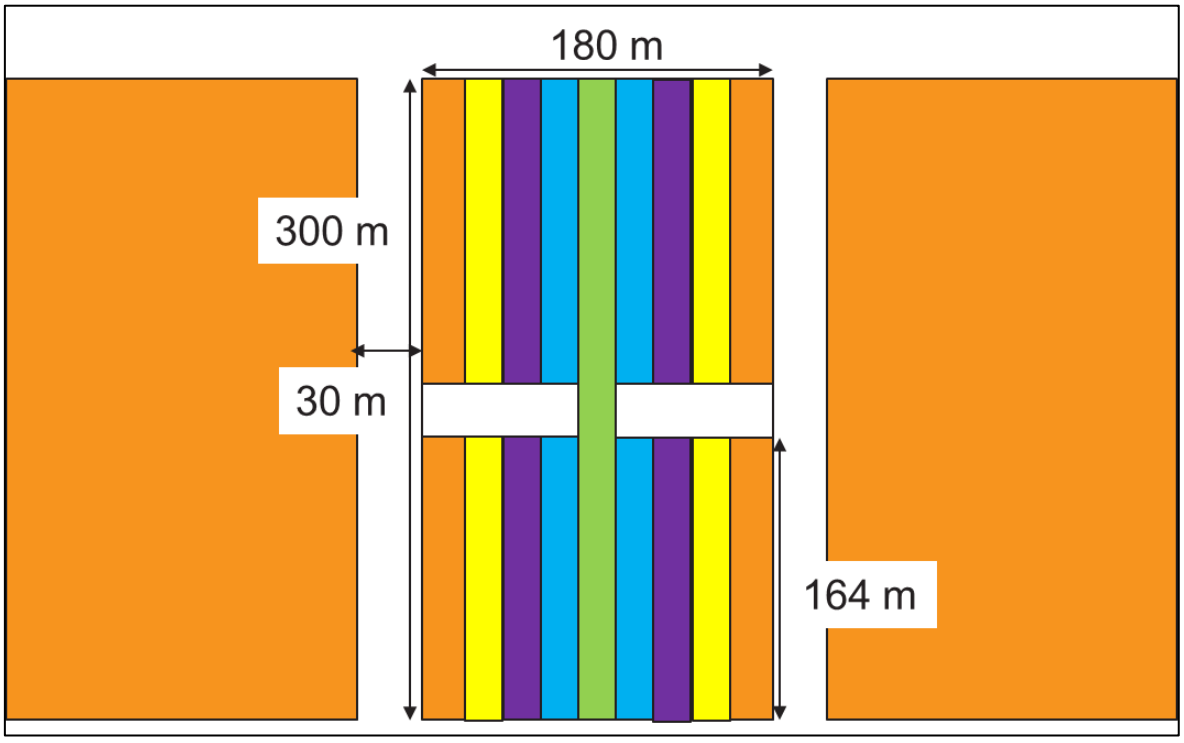

Figure 55. Conceptual model of a raise line on Mponeng Mine with strike pillars added based on the maximum closure criterion for quartzite mining.

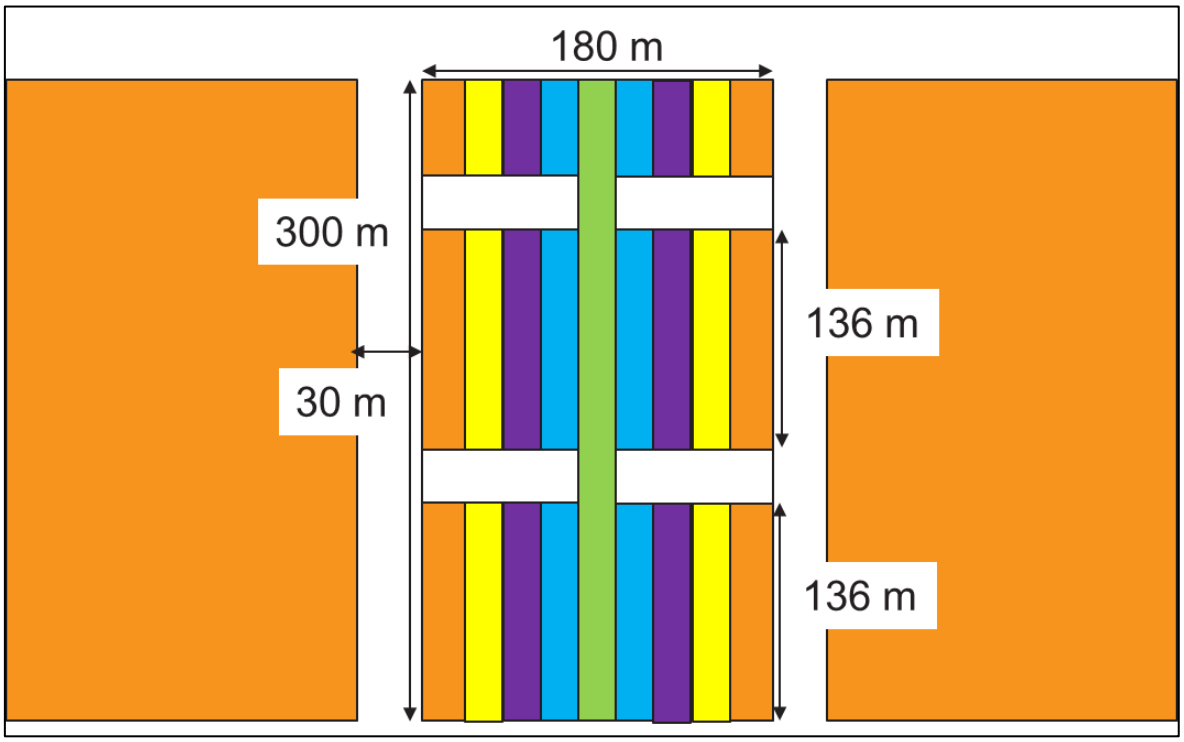

Figure 56. Conceptual model of a raiseline on Mponeng Mine with strike pillars added based on the maximum closure criterion for shale mining

Comparing the graph of modelled closure volume for the conceptual model (Figure 52) with modelled maximum closure (Figure 53), the required reduction in mining span to reach similar closure volume on the shale footwall compared to the quartzite footwall is significantly more when the maximum closure parameter is used compared to when the closure volume parameter is used. The shape of the closure volume graph (Figure 52) is similar to the graphs in the Scheepers (2012) discussion in Chapter 2 where the development of the maximum closure criterion is described. Even though the maximum closure criterion was successfully implemented at Mponeng Mine, using closure volume may be more appropriate and more easily updated or adapted for alternative rock types with different Young's Moduli.

Using the existing maximum closure criterion of 270 mm, the corresponding mining span of 164 m maximum for the quartzite footwall mining is read from the graph of maximum closure versus mining span in Figure 54. The associated closure volume of 9025 m³ at that mining span can be read from the graph of closure volume versus mining span in Figure 57 and the appropriate mining span of 152 m for mining on the shale footwall that would result in the same closure volume can be read from the same graph. This is significantly less conservative and more plausible than the 136 m maximum span for mining on the shale footwall determined before (using the maximum closure criterion). The maximum closure criterion should be reviewed and possible replaced with a closure volume criterion, and then adapted to accommodate different rock types (footwall lithology).

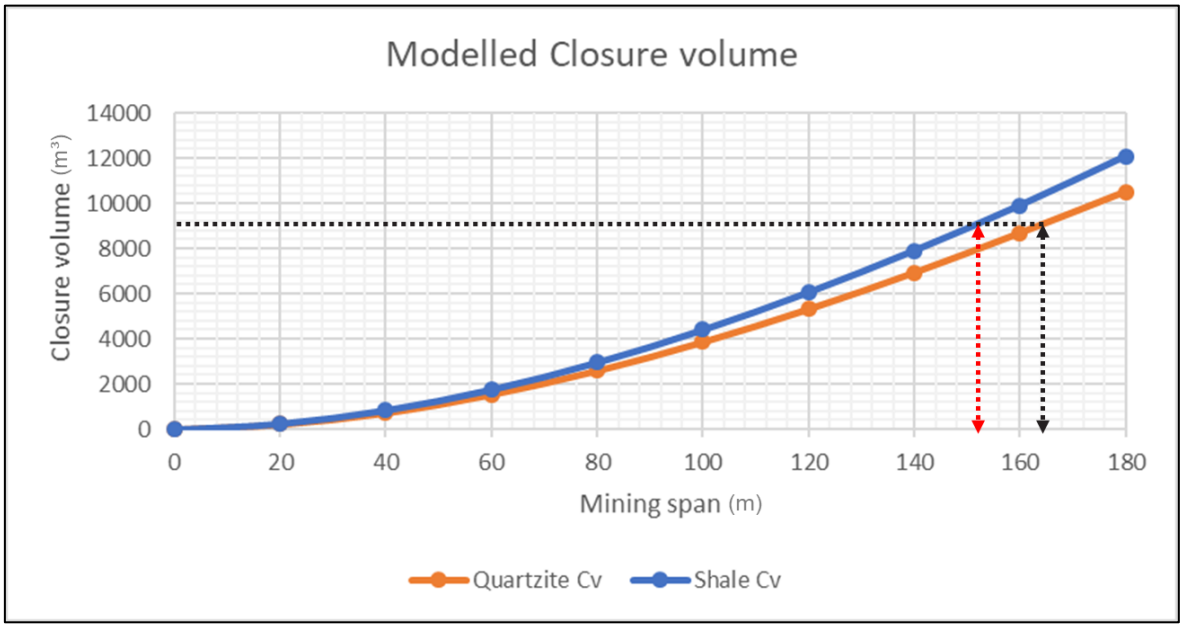

Figure 57. Modelled closure volume versus mining span with closure volume based mining limits for quartzie (black arrow) and shale (red arrow).

The current sequential grid mining strategy at Mponeng Mine includes regional stability pillars (30 m wide) on dip and strike. The designed strike mining span between dip pillars is 180 m. The dip mining span between strike pillars are determined using modelling and the maximum closure criterion of 0.27 m per m of stoping width. Typically the span is limited to approximately 150 m. The overall face shape design for the group of panels mined adjacent to each other between strike pillars is "overhand" (bottom panel leading) for panels mining in an eastern direction and "underhand" (top panel leading) for panels mining in a western direction. This is to optimise the approach angle onto the prominent joint set that is orientated northeast to southwest. The lead-lag distances between adjacent panels are controlled to 7 m minimum and 10 m maximum. This is done to prevent the creation of a long continuous mining abutment, thereby reducing the likelihood of large shear ruptures ahead of the mining abutment.

In spite of the implementation of this mining strategy, a large number of the large magnitude events recorded at Mponeng Mine are face related (based on the moment-tensor analysis, Chapter 3); that is shear through intact rock ahead of the mining front when the shear stress exceeds the shear strength of the intact rockmass. One of the factors to be considered is the fact that the virgin stress orientation (with σ_1 orthogonal to the reef plane, σ_2 in the direction of dip and σ_3 in the direction of strike) is such that it promotes fracture orientation in the direction of dip (σ_1-σ_2 plane, Chapter 2). The orientation of the overall mining fronts (overhand and underhand) are approximately 15° from this orientation (assuming on average 30 m long panels with 8 m lead/lag distances, Figure 58). It is possible that the similarity in the overall face orientation and the most likely fracture orientation (based on the virgin stress orientation) promotes face related seismicity. This effect is exacerbated when the dip pillars are formed as the panels are stopped in line with the overall face orientation parallel to the preferred fracture orientation (σ_1-σ_2 plane).

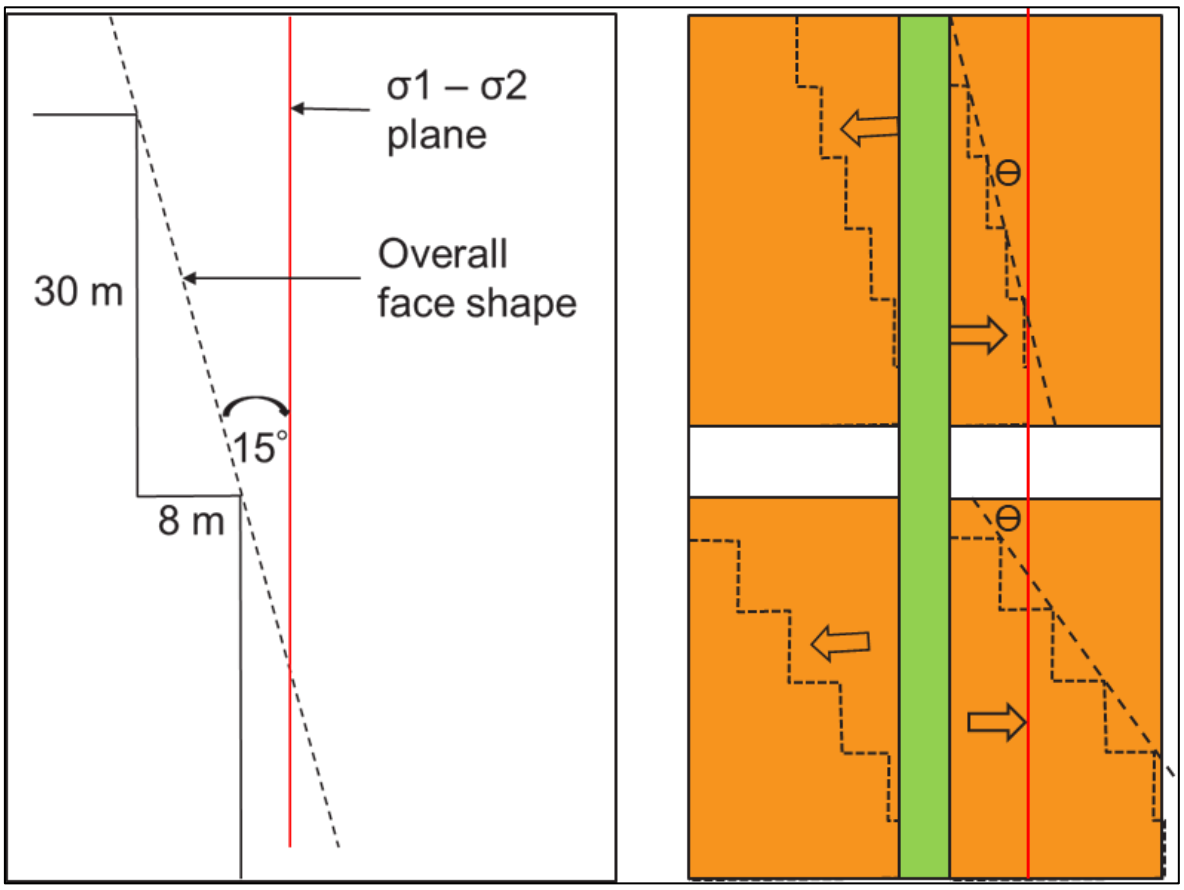

Figure 58. The angle between the overall face shape formed by a number of adjacent mining panels and the $\sigma_1 - \sigma_2$ plane.

It is suggested that the lead/lag strategy be reviewed to consider increased lead/lag distances (Figure 58, 21 m lead/lag distances will result in a 35° angle between the overall face orientation and the σ_1-σ_2 plane) and stopping the panels on this lead/lag configuration when reaching the dip pillar position rather than stopping the panels in line. This will reduce the likelihood of the overall face orientation coinciding with the most likely fracture orientation and therefore reduce the likelihood of large shear events ahead of the mining faces. Numerical modelling needs to be conducted to verify this hypothesis, but it is beyond the scope of this current study.

The average rock mass strength at the mining horizon can be calculated from the average of the lava hangingwall strength, the reef conglomerate strength and either the shale footwall

strength (eastern side of the mine) or the quartzite footwall strength (western side of the mine). The weaker shale on the eastern side of the mine reduces the average rock mass strength in that area. The rock mass with lower strength, more specifically with lower shear strength) will fail at lower stress levels compared to the areas where the average rock mass strength is higher.

The rock strengths would suggest that most events in the shale footwall area can be expected to occur in the footwall of the reef horizon (in the shale rock). However, a study of the location of the large events; hangingwall or footwall, revealed that most of the large events occurred in the strong lava hangingwall. This seems to contradict this postulation and disprove it. It is, however, possible that the failure in the shale in general occurs non-seismically (due to the weakness of the shale) and more events occur in the stronger lava hangingwall rock owing to the greater rock mass deformation. This may explain why the tendency for more events in the shale footwall area is increased, even though the events tend to occur in the stronger lava hangingwall.

CHAPTER 6 CONCLUSIONS

Mponeng Mine is the deepest mine in the world. The deepest stopes are on 127 Level at a depth of approximately 3700 m below surface. Scheepers (2018) describes the seismic hazard management practice for Mponeng Mine: The biggest rock-related hazard associated with mining at depth is rockbursts associated with mining induced seismicity. Stress changes in the rockmass are the drivers of mining induced seismicity. Typical sources of seismic events are faults, dykes, pillar abutments and mining abutments with stress changes at these sources, the driver and trigger of the events.

Two distinct areas based on the difference in footwall lithology can be identified for the Mponeng Mine VCR reef. On the eastern side of the mine the footwall is shale and on the western side the footwall is quartzite. The seismic hazard is higher when mining on the shale footwall compared to the mining on the quartzite footwall.

Careful seismic data selection was required to identify appropriate data sets for the different areas to compare the seismic response to mining for the shale footwall versus the quartzite footwall. In the process of data selection, all mining areas or time periods where a significant difference in mining depth, mining geometry and frequency of geological structures was identified, was not used for this study. Only the seismic data for the years 2016 to 2018 met the criteria for a comparative study of the two areas (shale footwall versus quartzite footwall), as during this time period mining on the shale footwall and the quartzite footwall occurred at similar depths, similar mining spans and the mining geometries were comparable. A similar frequency of geological structure intersections were also experienced.

The seismic response to mining for a similar mining volume and span illustrates a tendency for more of the large magnitude events to occur on the shale footwall than on the quartzite footwall. McGarr and Wiebols (1977) found that the seismic response to mining is proportional to the closure volume and it is hypothesised from this result that the closure rate is higher for the VCR with the shale footwall. The footwall lithology has a measurable influence on the seismic response to mining. Comparing the recorded number of events in different magnitude ranges for the two areas showed that for the shale footwall, fewer events in the smaller magnitude range, and more events in the larger magnitude range were recorded, compared to mining on the quartzite footwall.

By comparing the normalised seismic response to mining for the shale and quartzite footwall areas in terms of cumulative annual recorded potency divided by annual production, it was shown that the seismic response is higher (larger potency per m^2 mined) for the shale footwall than for the quartzite footwall.

Comparing the seismic hazard in terms of the b-slope of the GR graph for the two areas confirms that the seismic hazard associated with mining on the shale footwall is higher than for mining on the quartzite footwall as more events in the large magnitude range can be expected in the shale footwall area. This is also supported by the M_{Max} from the GR graph.

On Mponeng Mine, most of the seismic events in the large magnitude range are face related events. Considering the orientations of the moment tensor solutions (that are orientated with the overall mining abutments and virgin stress planes of maximum ESS), it is clear that the majority of seismic events in the magnitude range ML $\geq$ 1.5 are face related "Ortlepp shears". This is true for both the shale footwall area and the quartzite footwall area.

The difference in seismic response in the shale footwall area compared to the quartzite footwall area is most likely caused by the difference in Young's Modulus and average rock mass strength of the shale footwall area compared to the quartzite footwall area. The lower Young's Modulus (elastic modulus) of the shale rock probably allows for more closure and closure volume than in the quartzite area with higher Young's Modulus. This was

demonstrated with some preliminary elastic modelling. Underground measurements needs to be conducted to confirm this hypothesis.

Most of the larger events on Mponeng Mine are associated with “Ortlepp shears” ahead of the mining abutments and is not associated with slip on geological structures. The Moment-Tensor analyses showed that the majority of event orientations were similar to the overall orientations of mining fronts or mining abutments as well as the orientation of the most likely shear-failure plane associated with the virgin stress field. Few events were directly associated with geological structures. This indicate that the majority of large events (ML ≥ 1.5) are shear failures of the rock ahead of the mining abutments.

CHAPTER 7 RECOMENDATIONS AND FUTURE WORK

Based on the observation that the seismic hazard is different for the shale footwall area compared to the quartzite footwall area, it is recommended to develop mining strategies to manage the seismic hazard in the different areas and not only general strategies for the entire mine. The maximum closure criterion for mine design must be reviewed to distinguish between different footwall lithologies. It should be considered to use a closure volume-based criterion rather than a maximum closure-based criterion. Underground closure monitoring must be conducted in both the shale footwall and quartzite footwall area to quantify the actual differences in closure behaviour in the two areas. More information is also required on the actual mechanism of failure in the shale footwall area compared to the quartzite footwall area. This work needs to include underground observations and closure measurements and detailed numerical modelling of possible failure mechanisms.

Based in the observation that most of the seismic events are mining face related “Ortlepp shears” and based on the observation that the mining face orientation coincide with the most likely failure orientation associated with the prevailing stress field orientation, mining strategies should be developed to manage the occurrence of these large shear failures. Possible solutions are:

- Reduce the mining dip spans to a minimum, possibly by introducing micro longwalls with very small dip spans, consisting of two or three panels only (refer to Figure 43)

- Increase the lead/lag distances between adjacent mining panels to create an oblique angle between the overall mining face profile and the orientation of maximum ESS planes

Develop a new dip pillar design where the panels are not stopped in line to form the dip pillar, but rather stopped on the maximum lead/lag distance to form an echelon pillar.

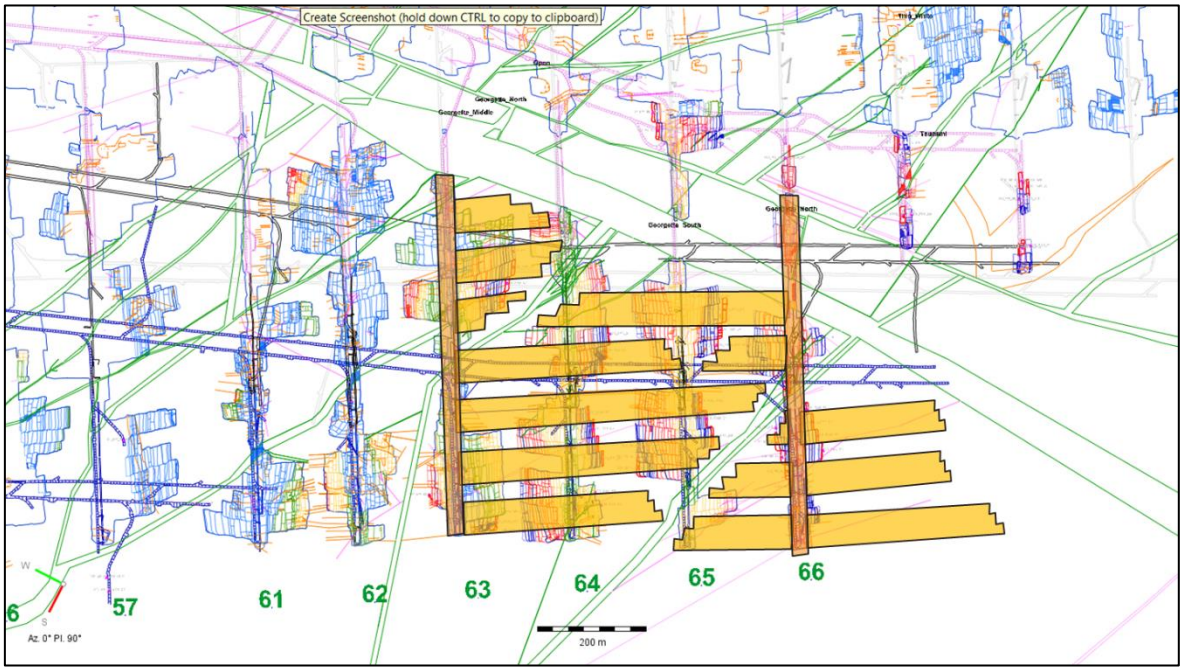

Figure 59. Proposed micro longwall mine design superimposed on the Mponeng eastern mining area and geology information.

REFERENCES

Andersen, L.M., 2001. A Relative Moment Tensor Inversion Technique applied to Seismicity Induced by Mining. *PhD Thesis*, University of the Witwatersrand, Johannesburg.

Andersen, L.M. and Spottiswoode, S.M., 2001. A hybrid relative moment tensor methodology. *Proc. 5th Int. Symp. on Rockbursts and Seismicity In Mines*, SAIMM, Johannesburg.

Blake, W., 1984. Rock preconditioning as a seismic control measure in mines. In: *Proc. 1st Int Cong. Rockbursts and Seismicity in Mines*, SAIMM Symposium Series No. 6, pp. 225 – 229.

Budavari, S. 1983. Rock Mechanics in Mining Practice. The South African Institute of Mining and Metallurgy, Monograph Series M5.

Cook, N.G.W., 1963. The basic mechanics of rockbursts. Journal of the Southern African Institute of Mining and Metallurgy. 64:71-81.

Cook, N.G.W., 1965. A note on rockbursts considered as a problem of stability, *Journal of the Southern African Institute of Mining and Metallurgy*, Volume 65, Issue 8, pp. 437 - 446

Cook, N.G.W., Hoek, E., Pretorius, J.P.G., Ortlepp, W.D., and Salamon, M.D.G. 1966. Rock mechanics applied to the study of rockbursts. *Journal of the Southern African Institute of Mining and Metallurgy*. vol. 66: 435–528.

Durrheim, R.J., 2010. Mitigating the risk of rockbursts in the deep hard rock mines of South African: 100 years of research. In: J. Brune (ed.), *Extracting the Science: A century of mining research*, Society for Mining, Metallurgy, and Exploration, Inc., pp. 156-171.

Gay, N.C., Spencer, D., Van Wyk, J.J., Van der Heever, P.K., 1984. The control of geological and mining parameters on seismicity in the Klerksdorp goldmining district. In:

Proc. 1st Int Cong. Rockbursts and Seismicity in Mines 1984, SAIMM Symposium Series No. 6, pp. 107 – 120.

Gay, N.C., Jager, A.J. and Piper, P.S., 1988. Quantitative evaluation of fill performance in South African gold mines. *Backfill in South African mines*. SAIMM, Johannesburg.

Handley, M.F., Selfe, D.A., Vieira, F.M.C.C., Maccelari, M.J. and Dede, T., 1997. Current position of strike stabilizing and bracket pillar design—Guidelines for deep level tabular orebodies. *Journal of the Southern African Institute of Mining and Metallurgy*, 97(3), pp. 103-117.

Han-Xiang, L., Qiang, X. and Yan-rong, L., 2014. Effect of lithology and structure on seismic response of steep slope in a shaking table test. *Journal of Mountain Science*, vol. 11, pp. 371–383.

Hedley, D.G.F., 1992. Rockburst Handbook for Ontario Hardrock Mines. Canmet Sp.Rep. SP92-1E.

Hofmann, G., Scheepers, L. and Ogasawara, H., 2013. Loading conditions of geological faults in deep level tabular mines, In: T Ito (ed.), *Proceeding of the Sixth International Symposium on In-Situ Rock Stress, Japanese Committee for Rock Mechanics*, Tokyo, pp. 558-580.

Jager A.J. and Ryder J.A. 1999. A handbook on Rock Engineering Practice for tabular hard rock mines, SIMRAC.

Jeppe, C.B., 1946. Gold Mining on the Witwatersrand Vol. I., The Transvaal Chamber of Mines. pp. 805-806.

Jooste, Y. and Malan, D.F., 2020. The need for improved layout design criteria for deep tabular stopes, *Journal of the Southern African Institute of Mining and Metallurgy*, vol. 120, no. 1, pp. 23-32.

Lenhardt, W. and Hagan, T.O., 1990. Observations and possible mechanisms of pillar-associated seismicity at great depth. *Proc. Technical Challenges in Deep Level Mining*, SAIMM, Johannesburg.

McGarr, A., and Wiebols, G.A., 1977. Influence of Mine Geometry and Closure Volume on Seismicity in a Deep-Level Mine. International Journal of Rock Mechanics and Mining Sciences & Geomechanics Abstracts, vol. 14, Issue 3, pp. 139-145.

Mendecki, A.J., 1997. Seismic Monitoring in Mines. Chapman & Hall, London.

Mendecki, A., 2016. Mine Seismology Reference Book - Seismic Hazard.

Mendecki, A., 2005. Persistence of Seismic Rock Mass Response to Mining. Rockbursts and Seismicity in Mines. In: Y Potvin and M Hudyma (eds.), *6th International Symposium*. ACG, Perth, Australia, pp. 97-106.

McGill, R.B., 2007. Strategies to manage seismicity in a deep VCR environment on Mponeng (1995-2003), In: Potvin, Y., Hadjigeorgiou, J., Stacey, D. (eds.) *Challenges in Deep and High Stress Mining*, Australian Centre for Geomechanics, pp. 217-223.

McCarthy, T.S., 2006. The Witwatersrand Supergroup. In: Johnson, M.R., Anhaeusser, C.R. and Thomas, R.J. (eds.), *The Geology of South Africa*, The Council of Geosciences, Pretoria, pp. 155 – 186.

Napier, J.A.L., 1987. The application of excess shear stress to the design of mine layouts, *Journal of the Southern African Institute of Mining and Metallurgy*, vol. 87, no. 12. pp. 397-405.

Ortlepp, W.D., 1984. Rockbursts in South African gold mines. A phenomenological view. In: *Proc. 1st Int Cong. Rockbursts and Seismicity in Mines*, SAIMM Symposium Series No. 6, pp. 165 – 178.

Ortlepp, W.D., 1997. Rock fracture and rockbursts – an illustrative study, The South African Institute of Mining and Metallurgy, Monograph Series M9.

Rademan, R., 2011. Mponeng Mine Key. AngloGold Ashanti internal media article.

Roberts, M.K.C., 1999. The Design of Stope Support Systems in South African Gold and Platinum Mines. Ph.D. Thesis, University of the Witwatersrand, Johannesburg.

Ryder J.A. and Jager A.J., 2002. A textbook on rock mechanics for tabular hard rock mines, SIMRAC.

Ryder, J.A. and Officer, N.C., 1964. An elastic analysis of strata movement observed in the vicinity of inclined excavations. *Journal of the Southern African Institute of Mining and Metallurgy*, 64(6), pp. 219-244.

Scheepers, L.J., Hofmann, G., Morkel, I.G., 2012. The study of seismic response to production for a grid mining layout. *Southern Hemisphere International Rock Mechanics Symposium SHIRMS 2012*.

Scheepers, L.J., 2007. Strategy Change in the 31 Line West on the VCR Horizon at Savuka Mine. AngloGold Ashanti Ltd internal report, South Africa.

Scheepers, L.J., 2018. Description of the Seismic Hazard Management Practice in AGA SAR. Internal report.

Spottiswoode, S.M. and Churcher, J.M., 1988. The effect of backfill on the transmission of seismic energy. *Backfill in South African mines*. Johannesburg, SAIMM, pp. 203-217.

Stacey, T.R. and Ortlepp, W.D., 2007. Yielding rock support – The capacities of different types of support, and matching support type to seismic demand. In Potvin, Y., Hadjigeorgiou, J., Stacey, D. (eds) Challenges in Deep and High Stress Mining, Australian Centre for Geomechanics, 407-411.

Tanton, J.H., McCarthy, T.F. and Hagan, T.O., 1984. The introduction of stabilising pillars to reduce rockbursts at Western Deep Levels, Limited, In: *Proc. 1st Int Cong. Rockbursts and Seismicity in Mines*, SAIMM Symposium Series No. 6, pp. 245 – 252.

Toper, A.Z., 2007. Destressing/Preconditioning to control rockbursts in South African deep-level gold mines. In: Potvin, Y., Hadjigeorgioud, J., Stacey, D. (eds.), *Challenges in Deep and High Stress Mining*, Australian Centre for Geomechanics, pp. 503-515.

Van Aswegen, G., 2013. Forensic Rock Mechanics, Ortlepp Shears and Other Mining Induced Structures - Institute of Mine Seismology, Stellenbosch, South Africa.

Wagner, H., 1984. Support requirements for rockburst conditions. In: Gay and Wainwright (eds.): *Proc. of the 1st Int. Cong. on Rockbursts and Seismicity in Mines*, SAIMM, Johannesburg, pp. 209 – 218.

Wiles, T., 2010. Map3D User's Manual, Mine Modelling Pty Ltd - www.map3d.com. Australia.

Wiles, T., 2002. Loading System Stiffness, A Parameter to Evaluate Rockburst Potential. Mine Modelling Pty Ltd, Australia.

APPENDICES

A.1 APPENDIX 1

DESCRIPTION OF THE SEISMIC HAZARD MANAGEMENT PRACTICE IN ANGLOGOLD ASHANTI SOUTH AFRICA REGION

In this document the seismic hazard management practice in the AngloGoldAshanti South Africa Region (AGA SAR) is described in non-technical terms for reference. The complete framework for managing rock related hazard is discussed with the mine design and seismic monitoring aspects discussed in more detail.

- **The Rock Related Challenge at AGA SAR (Mponeng Mine)**
  - Mining at depth - Rockbursts

    The biggest rock-related hazard associated with mining at depth is mining induced seismicity. Seismicity refers to seismic activity in the form of tremors or earthquakes and factors like frequency and magnitude of events are included. Induced seismicity refers to such tremors caused by human activity, including mining.

    Soon after mining started in the West Wits area, known as Western Deep Levels at the time, the workers reported that they hear and feel noises and bumps underground, and that damage is caused to underground excavations. Research into this phenomenon soon resulted in the installation of seismic networks underground to monitor the seismic hazard.

    A seismic event is a sudden inelastic (referring to permanent deformation) reduction of stress and release of stored strain energy in the rockmass. This is experienced as shaking of the ground as seismic waves, that radiate from the seismic source, interact with the rock.

A rockburst is a seismic event that causes damage to an excavation.

Typical sources of seismic events are faults, dykes, pillar abutments and mining abutments with stress changes at these sources the driver and trigger of the events.

The likelihood that a rockburst will occur is loosely related to the magnitude of the seismic event and more directly related to distance of the event from an excavation. Many events occur sufficiently far away or are sufficiently small in magnitude that no damage occurs and therefore they are not classified as rockbursts.

The likelihood of damage (vulnerability of an excavation) is proportional to the stress in the skin rock and the rockmass conditions in the excavation (rockmass response under seismic loading conditions). The extent of damage can be controlled (within limits) with rockburst resistant support. The most important property of rockburst resistant support is the fact that it can yield and therefore absorb energy.

As mentioned before, stress changes in the rockmass are the drivers of mining induced seismicity. Stress changes are associated with excavations underground. When you mine, the stress that was carried in the rock now being excavated is transferred to the unmined rock adjacent to the excavation leading to increased stress there. As the excavation span is increased with mining, more stress is transferred and cumulated adjacent to the excavation. This strains the rockmass and strain energy is stored in the rock.

Over-stressed rock can fail by controlled fracturing. The fractured rock carries lower stress and the stress is transferred deeper into the rockmass adjacent to the excavation.

Over-stressed rock can also fail violently, releasing the localised stored strain energy and resulting in a localised rockburst with relatively small magnitude, referred to as a strainburst. Typically small rock fragments are ejected from the skin rock into the excavation. The size of such rockbursts are typically limited to less than 10 m^3 of failed rock but in extreme cases can reach up to 100 m^3 of failed rock.

Where the stress changes associated with mining are superimposed onto a weak plane or fault, shear stress is induced on the plane. The shear stress tends to drive relative shear deformation on the contact plane. The cohesion plus shear friction (function of the normal stress and frictional properties of the fault plane) provide shear resistance to the driving stress, resulting in shear strain energy to be stored in the shear-strained rockmass forming the fault plane. When the shear driving stress exceeds the shear resistance, the contact surface will slip, releasing the stored energy. Slow slip is non-violent (slow energy release) and called creep. Violent slip results in sudden energy release; i.e. a seismic event. Where the slip occurs on a large area and where large amounts of stored energy is released, the result is a large magnitude seismic event with potentially devastating effects (>100m³ of failed rock).

Shear through intact rock is also possible. The stress changes adjacent to a mining excavation may not be superimposed onto a weak plane, but may be sufficient in shear stress magnitude that it exceeds the shear strength of the intact rockmass to cause a brittle shear fracture to form with the release of stored strain energy; i.e. a seismic event. This type of event is usually associated with long continuous and highly stressed mining abutments or long continuous regional pillars.

Another concept that needs to be addressed in parallel with the stress transfer due to mining is the concept of elastic closure. The rockmass reacts elastically within its elastic range; i.e. as stress is increased, the rockmass is strained. This can be explained at the hand of a laboratory scale experiment of a cylindrical rock sample in a press. The stress is increased by increasing the load on the ends of the sample in the axial direction. The sample deforms (strain) elastically and shortens in the direction of the applied load. Within the elastic range of the rock sample, if the load is removed, the sample will expand back to its original dimensions. If the sample is loaded beyond its elastic deformation range it will fail by forming fractures. Fractures are permanent and the rock sample no longer behaves elastically.

At depth, the rockmass is highly stressed due to the weight of the overburden and is therefore elastically strained. When an excavation is created, the strained rock will relax into the opening from all directions (hangingwall, footwall and sidewalls) as there is no resistance from the void. This will reduce the excavation dimensions (partially close up the excavation) from its original dimensions at the time of excavating it and is called elastic closure or

convergence. This convergence in the excavation will increase the strain in the already strained rockmass surrounding the excavation and strain energy is stored that can be released in the form of seismicity as explained above in the section on stress and stress changes. The magnitude of the closure is controlled by the extent of the mining span. As the horizontal mining span is increased, the vertical closure is increased and therefore the strain energy (and seismic hazard) in the rock adjacent to the excavation is increased. By limiting the maximum allowable mining span, the seismic hazard can be controlled.

Backfilling is the placing of rock material in the mining excavation. This backfill, when compacted sufficiently, can reduce the convergence and therefore based on the above discussion also reduces the seismic hazard.

Preconditioning is the practice of modifying the fracture zone directly ahead of mining panels to move the high stress zone deeper ahead of the panel faces. This reduces the likelihood of localised strain bursts and also reduce the panel vulnerability under seismic loading conditions by providing a de-stressed buffer zone directly ahead of the panels faces.

The second biggest rock related hazard is uncontrolled falls of ground, induced by gravity. Poor rockmass conditions may exist due to excessively fractured rock, or the intersection of adverse geological discontinuities. The rockmass surrounding mining excavations at depth will fracture on creation of the mining excavation due to the high stress. Mining practices that reduce the seismic hazard will also reduce the creation of excessive fracturing, but for the most part the gravity related fall of ground hazard is managed by the installation of support.

With this background in mind the hierarchy of controls or strategies for managing the rock related hazards associated with deep level mining can be discussed:

- Strategies for managing the rock related hazards

  A management system has been developed and employed to provide a framework for rock engineering related and production related efforts and controls in the process of eliminating falls of ground. This initiative is termed the Fall of Ground Management (FOGM) system. It is supplementary to and supports the AngloGold Ashanti strategic thrust in safety.

The five levels, foci or initiatives of the FOGM system are described in Table 1 and can be remembered as the "5 P's of FOGM.

Table 1: the FOGM framework

FOGM 1	FOGM 2	FOGM 3	FOGM 4	FOGM 5
Prevent poor ground conditions, reduce the likelihood of rockbursts	Protect against rock related hazards	Promote safe work practice and compliance to strategies in terms of the FOG hazards	Provide data on the rockmass response to mining; All rockmass related monitoring	Problem solving. Identify and fill knowledge gaps
Mine design; strategy layout configuration pillars conditioning	Support design Support standards	Organisational culture mind-set knowledge training and education communication compliance to standards Scrutiny meetings Planning meetings TARP	Seismic system design and operation data management data analysis data interpretation communication action plans	Incident/accident analysis to identify lack of knowledge Research Technology and innovation

The five strategic foci within the FOGM initiative are illustrated in Table 1. The FOGM framework provides a breakdown of the typical engineering design cycle (design – implementation – monitoring -redesign) as adapted for and implemented in AGA.

Planned mining needs to be designed with stability of excavations in mind (FOGM 1); i.e. the excavations needs to be stable for the life expectancy of such mining excavations. A wide range of factors needs to be considered in this design process and it is important to understand that no support can correct for a poor design.

Assuming a good design is well implemented, the residual risk needs to be managed with support (FOGM 2).

A good mine design and support strategy has no value unless properly implemented. FOGM 3 refers to the holistic approach that will ensure proper implementation of the design and support strategy.

Once implemented, it is important to measure and monitor the applicability and effectiveness of the design and support strategy (FOGM 4) so that improvements or a redesign can be done where required. A variety of rockmass monitoring tools and instrumentation is available to the mining industry, but the most important monitoring parameter for deep level mining is seismic monitoring. Analysis of the rockmass monitoring data provides insight into redesign requirements, or can highlight areas of insufficient understanding where research or technology and innovation is required. This is captured under FOGM 5.

- FOGM 1:

  Reduce the likelihood of a damaging event and poor ground conditions. This is the most important control to eliminate the rock related hazard and therefore is top in the hierarchy of controls. A lot of time and resources has been spent on the mine design for Mponeng Mine. The original strategy for Mponeng was the longwall mining method. Without mentioning detail, the redesign and implementation of the sequential grid mining method with partial extraction and limited mining spans resulted in a major improvement in terms

of the seismic hazard and associated rockburst related safety statistics on the mine. Further improvements include the introduction of inter panel lead/lag controls, bracket pillars on structures and additional strike stability pillars.

- Reduce closure by reducing the mining spans (place sufficiently large regional stability pillars); The maximum strike mining span at Mponeng Mine is 180 m, leaving 30 m wide dip stability pillars between the open mining spans. The mining spans and extraction ratio are further reduced by leaving strike pillars spaced approximately 120 m skin-to-skin on dip. The strike pillar spacing is continuously reviewed through numerical modelling and based on modelled closure rather than a fixed spacing.
- Reduce closure by installing backfill; At Mponeng Mine cyclone classified tailings (CCT) is placed as backfill to reduce the maximum closure. The backfill is hydraulically placed close to the mining face (4.5 m maximum) and more than 70% of the total area mined is filled.
- Limit mining near or in faults and dykes; i.e. leave bracket pillars on major structures; At Mponeng Mine 20 m wide bracket pillars are left both sides of significant geological structures (faults and dykes). The bracket pillar designs are reviewed and updated using numerical modelling.
- Where mining through structure is necessary, mine with the smallest practical mining span in the structure; raises through structures will be ledged only to ensure the stability of the raise.
- Reduce the vulnerability of panels through preconditioning; at Mponeng Mine, all mining panel faces are pre-conditioned by drilling 2.4 m deep holes, spaced 3 m apart, between and in addition to the shot holes for production.
- Reduce the vulnerability of service excavations
  - Do not place service excavations in highly stressed rock - Position service excavations away from mining abutments; At Mponeng Mine the Haulage and RAW pairs are placed minimum 90 m into the footwall (or hangingwall). Crosscuts are overstoped (de-stressed) early in the extraction sequence.

- FOGM 2:

  Support for residual seismic and rockfall hazard.

- Use support with high energy absorption capacity; i.e. yielding support. The Mponeng stoping support standards are the most stringent in the mining industry
- Backfill
- Pre-stressed yielding elongates'
- Packs (for gullies and breaker lines only)
- In-stope bolting
- Tunnel support is also designed to protect against seismic damage
- Yielding tendons
- Mesh and lacing to integrate support units into a support system

- FOGM 3:

  Promote safe work practice.

  FOGM 3 is mostly the realm of the line manager and supervisor

  Fostering an appropriate mind-set for workers to perform safely towards and within the optimised mining environment through education, training and influencing attitude of people within the organisation and providing the correct tools and equipment for safe work practice;

  - Monthly Production Manager scrutiny meeting
    - Get agreement on the FOGM 1 principles for all the working places
  - Monthly planning meetings
    - Follow the FOGM structure to direct the planning meeting and to ensure that the appropriate issues are discussed and addressed at the planning meeting
  - Waiting place communication
  - Training
    - Ensure that supervisors on all levels understand FOGM and their role in each of the FOGM foci
    - Promote knowledge so that workers understand the need to work to standard
    - Promote training for all employees who work underground to be able to recognise hazards that lead to falls of ground
    - Promote training for all employees who work underground to be able to deal effectively with potential falls of ground

- Promote training so that within their area of control employees who work underground are capable of minimising the occurrence of hazards that contribute to falls of ground

- FOGM 4:

  Provide monitoring data.

  Monitoring the rock mass response to mining through instrumentation and measurements, including seismic networks. FOGM 4 is mostly the realm of the rock engineer, but also the engineering technical service team to maintain the seismic systems

  - Development and maintenance of monitoring systems to:
  - Check effectiveness of mining layout and associated designs, and to modify as required
  - Identify rock mass characteristic behaviour in different ground control districts and design accordingly
  - Other geotechnical monitoring
  - Closure instruments
  - Extensometers

  Seismic monitoring and procedures have evolved significantly over time since the installation of the seismic networks underground. Where the recording and processing of seismic events is a reactive process, the understanding that is gained from analysing and interpreting the data in terms of the rockmass response to mining has shaped mining strategies significantly over time to proactively implement mining strategies with the aim of reducing the overall seismic hazard. The research conducted twenty years ago also led mine seismologist to believe that, in time, individual seismic events will be predicted in time and space to some acceptable accuracy level. Prediction is still a research topic today and no tool is available that can consistently and to any level of accuracy predict individual events in space and time. AGA do support continued research towards prediction and is a patron to the IMS research fund.

  Whilst prediction may seem like the ultimate goal in mine seismology and safety, prediction on its own is insufficient to support the long-term objectives of the mining

industry. It is important to use the seismic data to improve the mine design for the long-term stability of the mine and safety of mine workers; i.e. design the seismic hazard/risk down. Then prediction could add additional value by potentially saving lives where the mine design failed to prevent the occurrence of the event.

At Mponeng Mine, the seismic system has been active since 1996 and able to locate seismic events accurately (within 60 m error) and providing an estimate of the magnitudes of the events. A full event catalogue is maintained since then.

The current seismic system at Mponeng consists of 42 seismic sensors, coupled to 30 seismometer boxes, several underground modems and cabling spread over the mine to form a network. The data is recorded and communicated to a surface seismic server in real time and communicated to IMS (Integrated Seismic Systems – the seismic service provider to AGA SAR) for processing. Event locations and magnitude estimations are provided back to AGA within minutes of the event happening.

The cost of this seismic system is in the order of six million rand for the equipment only. The cost of installation of the seismic network is dominated by the drilling cost (the sensors are installed into purpose-drilled seismic holes) and is in the order of four and a half million rand bringing the overall cost of the network installation in excess of ten million rand.

As mining progress further away from the shaft, the seismic network is expanded and maintained on an on-going basis. The associated cost is in the order of ten million rand per annum.

AGA SAR employs a centralised technical team to direct seismic hazard management in the SAR. The team currently consist of a mine seismologist, a seismic system specialist and a stress modelling expert. The centralised team reports directly the Senior Rock Engineering Manager and provides a service to the operations. The annual budget for the centralised service is approximately ten million rand.

AGA SAR contracts Integrated Mine Seismology (IMS) for seismic event processing, data management and reporting through a comprehensive contract. The main output

from this work is a well-maintained detail event catalogue available for analysis and research work, three short-term hazard assessment reports every working day, monthly seismic hazard assessment reports and monthly stress modelling reports as well as on-going technical support. Ad-hoc services includes special event reports and investigations on request. The cost of this service is in the order five million rand per annum for Mponeng Mine.

IMS does seismic-related research on behalf of the industry internationally, including AGA SAR. To fund this research work, money is gained from so-called research patrons, including AGA. The patronage fee paid by AGA amounts to approximately R 750 000 per annum. AGA SAR has a chair on the research patrons committee, gets research reports and a vote on research projects for the next year. One of the on-going research projects is the continuous improvement of the short-term seismic hazard rating system.

The current and recently updated short-term seismic hazard rating system at Mponeng Mine;

In order to improve the effectiveness of the short-term seismic hazard assessment system, it was decided to change the short-term seismic hazard rating system to a robot rating system where green, orange and red ratings will mean different and increasing levels of hazard and will trigger different reactions to be completed in the mining panels.

Implementation of an additional response is also required in panels where events with local magnitude greater or equal to 1.0 have been recorded.

The short-term hazard assessment is done by IMS (an outsourced seismic service provider) and is communicated to the mines by e-mail in the form of a daily hazard rating (including a plot and listing of events with magnitude of 1.0 and above). If communication problems result in the e-mail not sent successfully, the ratings are phoned through. Currently the ratings range between 0 and 10 with 0 indicating the lowest possible hazard and 10 being the highest possible hazard (for an A-polygon with the Rock Engineering factor set to 1.0).

The day-shift (daily) rating is done by a seismologist by reviewing certain seismic parameters and its trends over time. This rating is completed and communicated to the mine in the morning before 12:00 (as per contract). The rating is reviewed and automatically adjusted where required for nightshift after the blast and communicated to the mine by shaft specific agreed times. This time may move later if the blast was set off late, but this is communicated on an ad hoc basis. This rating is again reviewed and adjusted automatically early in the morning and communicated to the mine by approximately 04:00 in the morning. This is the rating that day-shift reacts to before entering into their working places.

When the morning shift or nightshift automatic update turns a rating to red, the seismologist is notified and the red rating is reviewed manually.

The procedure for providing the daily rating must allow for a robot system where ratings 0 to 4 is coloured green and represent a low hazard rating, ratings greater than 4 and less than 6 are coloured orange and represent an intermediate hazard rating, ratings of 6 and greater are coloured red and represent a high hazard rating.

Every miner must know the rating of the panel where he plans to work for the day before entering that panel. The mine must have a system in place to confirm that the miner has received his rating before entering his panel.

Summary of the robot rating system for the management of the short-term seismic hazard ratings provided by IMS

Seismic hazard rating	Miner	Shift Overseer	Mine Overseer	Section Manager	Rock Engineer
Rating ≤ 4	No additional action	No additional action	No additional action	No additional action	No additional action
4<rating<6	Miner to complete the hazard rating checklist	Review the hazard rating checklist	Review and file the hazard rating checklist	No additional action	Review the hazard rating checklist
Rating ≥ 6	Ensure no person enter reef horizon. This remains in place until red rating uplifted (shift Overseer communication)	Attend meeting with section manager and rock engineer. Accompany ASCO or SCO on 3rd party audit (red rating checklist)	Attend meeting with section manager and rock engineer Arrange 3rd party audit by ASCO or SCO (hazard rating checklist)	Hold meeting with rock engineering officer to determine any additional recommendations. Shift Overseer and Mine Overseer to attend.	Verify the rating with seismologist and attend meeting with the section manager. Notify control room about rating. Arrange and review 3rd party audit by ASCO or SCO (hazard rating checklist)

An additional hazard assessment tool, based on the TARP-principle, is implemented (this is separate and in addition to the robot rating system and the required actions are in addition to those required by the procedure regarding yellow and red ratings). The intension is that the miner will complete an audit, based on the increased seismic hazard checklist, when a magnitude 1.0 or larger event has been recorded in his working place. The miner will be notified of the occurrence of a 1.0 and larger seismic event through one of two systems:

When the miner gets the robot rating for his working place polygon, included in the ratings report is an event listing of Magnitude 1.0 and larger events. When he signs for his rating, he also signs for the events listing to be aware of the occurrence of magnitude 1.0 and larger events at his working place polygon.

The IMS system sends an sms-notification to all on the sms list (including the Shift Boss, Mine Overseer, Section Manager, Senior Rock Engineering Officer and Rock Engineering Manager) with the event detail; Working Place name and distance to the nearest working place, date and time of event, event magnitude and location coordinates. An e-mail also goes to the control room.

When a miner feels a seismic event underground, he must phone the control room to find out where the event was and what magnitude. The control room operator will also try to

phone the miner and notify him of the occurrence of the event and share the event detail. The control room operator must keep minutes of the discussion with the miner.

At any time when the miner is notified of a magnitude 1.0 or larger seismic event that occurred in the polygon where one or more of his crews are mining, the following actions must be complied with for all the panels in that polygon:

The miner must immediately stop all normal mining activity and withdraw his crew from the mining face (Zone 3).

The miner must, starting at the waiting place, examine the workplace according to the entry examination procedure.

The miner must complete the audit process with checklist as described for orange ratings. Normal mining activity cannot continue until all sub-standards identified during the audit has rectified.

The Miner must discuss the outcome from the audit with his Shift Boss and hand the checklist to the Shift Boss. The Shift Boss must ensure that all non-compliances have been rectified. The Shift Boss must discuss it with his Mine Overseer and hand the checklist to the Mine Overseer to file.

Once a day, before the Shift Overseer completes his shift, he must reconcile the number of panels where audits were required according to this procedure with the number of checklists he received back from his miners and follow up where miners are not complying.

Once a week the Mine Overseer must reconcile the number of panels where audits were required according to this procedure with the number of checklists received and filed. He must follow up where miners and Shift Bosses are not complying.

Once a month at the planning meeting or the Production Manager scrutiny meeting the Rock Engineering Manager and Section Manager must reconcile the number of panels where audits were required according to this procedure with the number of checklists received and filed and follow up where Mine Overseers (and their sections) are not complying.

As part of continued research, a new rating system, called STAT (Short-term activity tracker) was tested for Mponeng Mine, in parallel with the current rating system and comparing with the current rating system.

Short-term seismic hazard assessment in South African mines is currently performed according to the so-called hazard rating method developed during the 1990s. The corresponding hazard rating (a number between 0 and 10) is generally used as an indicator of rockmass instability, but the relationship between the hazard rating and the probability of occurrence of a large (and possibly damaging) seismic event is not well understood, and the associated stability parameters (such as Energy Index and Schmidt Number) are often not sufficiently robust for routine, day-to-day analysis.

In this regard, the Institute of Mine Seismology (IMS) has developed the Short-Term Activity Tracker (STAT): STAT is a simple, activity-based method for short term seismic hazard assessment that has been successfully implemented as a re-entry protocol at several Australian mines. STAT supports continuous ground motion parameters, triggers and associated seismic events, and the results can be analysed in real-time via IMS Ticker 3D. The proposed Short-Term Seismic Hazard Assessment project will calibrate the input parameters of STAT for Mponeng Mine and compare the success rate of STAT and the current hazard rating method.

STAT was proven not to be a viable short-term rating system for the Mponeng environment and therefore not implemented at Mponeng to replace the current rating system. IMS feels that currently more research still needs to be done on the Short-term-activity-tracker (STAT) in the South African environment. AGA will continue to support research into improving the short-term seismic hazard assessment tools and programs.

- FOGM 5:

  Problem solving.

  From continuous evaluations and audits of successes and failures, address knowledge gaps through research and development of appropriate technology. FOGM-A is the rockburst investigation form and FOGM-B the fall of ground investigation form.

  FOGM 5 is mostly the realm of the rock engineer and research agencies.

  - Research, development and implementation of appropriate technologies to:

- support key prevention and protection strategies based on the requirements derived from monitoring the progress and success of the designed layout and support strategies
- identify and ratify research and development projects, timing, specific outcomes and budgets
- track progress and ratify of project continuance
- promote technology transfer and implementation